

MASTER THESIS

Quantifying cerebral blood flow of both the micro- and macrovascular system using perfusion computed tomography

Sytse de Jong

Technical Medicine

19-08-2015

Graduation Committee:

Chairman:

Prof. dr. ir. C.H. Slump

Medical Supervisor:

Dr. C. Hoedemaekers

Technical Supervisor (Radboud UMC):

Dr. ir. R. Manniesing

Technical Supervisor (UT):

Prof. dr. ir. C.H. Slump

Supervisor profession behavior:

Drs. P.A. van Katwijk

External member:

Dr.ir. T. Heida

Radboudumc

UNIVERSITY OF TWENTE.

Preface

The past seven years I have been a technical medicine student. This master thesis is the result of just the last of those seven years. But all the things I have learned and all experiences of that amazing time are included in this piece of work. I liked almost every aspect of the study. This made it very hard to choose the right master track. I choose medical sensing and stimulation, but now, three years later I will graduate with a study about an imaging technique for which I needed more image processing tools than I ever needed medical signaling tools.

The graduation position was offered to me by Astrid Hoedemaekers. I want to thank you for your dedication to this project. You were always interested in the progress of the study and you were always available for help. Even with the page count increasing every day, you didn't hesitate to check it and reply comments within a few days.

The technological part of the results could not have been realized without the effort of Rashindra Manniesing. Thank you for the informative discussions we had while enjoying a cup of supreme freshly grounded coffee. I enjoyed watching the way your attitude towards technical medicine students adjusted during the year.

Next, I would like to thank Kees Slump for visiting Nijmegen every now and then and for your advice on the scientific and technological aspects of the study. And I would like to thank Bernard Geurts and Christophe Brune for the thoughts we shared about my study. Thanks go to Ciska Heida for being external member in my graduation committee.

Furthermore, I would like to thank Tessa Kappers and Trudy van Ruiten for our useful meetings that gave me more confidence to finish this year successfully. I would like to thank Paul van Katwijk for asking the right questions at the moments I hated them most.

Erik Koers and Willem Jan van der Woude, thanks for getting out of your bed at 6.30 on a Saturday morning to help a student put a flow phantom in a CT scanner. Erik, thanks for exciting me to become a clinical perfusionist.

I would like to thank Eline Vinke for being good company and for your support. Thanks for arranging most of the meetings we had with supervisors.

Finally, I would like to thank my family and friends for being a big support during my seven years of study.

A special thanks to Suzanne, for listening to all boring stories about blood flow and CT scanners. Thanks for checking my thesis and for your many great ideas for improvement of this thesis.

Contents

Preface.....	3
Abbreviations	6
Abstract	7
1. Introduction.....	9
1.1 Cerebral Blood Flow	9
1.1.1 Control of CBF.....	10
1.1.1 Optimal CBF.....	13
1.1.2 Requirements of cerebral blood flow measurement.....	14
1.1.3 Cerebral blood flow velocity.....	15
1.2 Perfusion Computed Tomography	16
1.2.1 CTP data acquisition	17
1.2.2 CTP processing steps	17
1.2.3 Mathematical background of the maximum slope model and the deconvolution model 22	
1.2.4 Validity of CTP.....	25
1.2.5 Clinical Application	27
1.3 Potential of quantitative use of CTP.....	29
1.3.1 Macrovascular system.....	29
1.3.2 Microvascular system.....	30
1.4 Study Objectives.....	31
1.4.1 Quantifying cerebral <i>macrovascular</i> bloodflow using CTP: the direct flow model.....	31
1.4.2 Establishing normal values of CBF, MTT and CBV in the <i>microvascular</i> system	32
2. Quantifying cerebral <i>macrovascular</i> blood flow using CT perfusion: the direct-flow model.....	33
2.1 Method.....	33
2.1.1 Developing the direct-flow model.....	33
2.1.2 Validating the direct-flow model.....	36
2.2 Results	43
2.2.1 Developing the direct-flow model.....	43
2.2.2 Validating the direct-flow model.....	45
2.3 Discussion	56
2.4 Limitations	60
2.5 Recommendations.....	61
2.6 Conclusion	62

3.	Establishing normal values of perfusion in the <i>microvascular</i> system using CT perfusion.....	63
3.1	Method	63
3.1.1	Population	63
3.1.2	Main study endpoint	65
3.1.3	Secondary study endpoints	65
3.1.4	Study protocol	65
3.1.5	Data analysis.....	66
3.1.6	Repeatability of ROI selection	68
3.1.7	Ethical considerations.....	68
3.2	Results	69
3.2.1	Population	69
3.2.2	Deriving normal values of CBF, MTT and CBV in healthy subjects per brain region	69
3.2.3	Comparing normal values to perfusion values in TIA and ischemic stroke patients.....	71
3.2.4	Intraobserver repeatability	74
3.3	Discussion	75
3.3.1	Deriving normal values.....	75
3.3.2	Comparison to perfusion values of TIA patients and ischemic stroke patients	76
3.3.3	Repeatability.....	77
3.4	Limitations	77
3.5	Recommendations.....	78
3.6	Conclusion	80
	References.....	81
	Appendix.....	89

Abbreviations

ΔL	Distance between laminae
ΔP	Pressure difference between laminae
ABI	Acute Brain Injury
ACA	Anterior Cerebral Artery
AIF	Arterial Input Function
amp	amplitude of time-density curve
AVDO ₂	Arterio-Venous Differences of Oxygen
AVM	Arteriovenous Malformations
CA	Cerebral Pressure Autoregulation
CBF	Cerebral Blood Flow
CBFv	Cerebral Blood Flow velocity
CBV	Cerebral Blood Volume
CMRO ₂	Cerebral Metabolic Rate of Oxygen consumption
CoG	Center of gravity
CoV	Coefficient of Variation
CPP	Cerebral Perfusion Pressure
CTA	CT Angiography
CTP	CT Perfusion
CVR	Cerebral Vascular Resistance
d	distance between skeletons
fs	sample frequency
HU	Hounsfield Unit
ICA	Internal Carotid Artery
ICP	Intracranial Pressure
IQR	Interquartile Ranges
L	Tube Length
MAP	Mean Arterial Pressure
MCA	Medial Cerebral Artery
mRS	modified Rankin Scale
MTT	Mean Transit Time
η	Fluid Viscosity
NIHSS	National Institute of Health Stroke Scale
P _a CO ₂	partial Pressure of Carbon dioxide
P _a O ₂	partial Pressure of Oxygen
PCA	Posterior Cerebral Artery
PET	Positron Emission Tomography
r	Radius
ROI	Region of Interest
S _{n,x}	Coordinate of skeleton _{n, number, axis}
SAH	SubArachnoid Hemorrhage
SD	Standard Deviation
SNR	Signal-to-Noise Ratio
(b/o/s)SVD	(block-circulant/oscillating/standard) Singular Value Decomposition
TBI	Traumatic Brain Injury
TCD	Transcranial Doppler
td	time delay
TDC	Time-density Curve
TIA	Transient Ischemic Attack

Abstract

Introduction: Patients with acute brain injury (ABI) may have insufficient cerebral blood flow (CBF), with the CBF deficit varying per brain region. The brain is very sensitive to hypoxic and ischemic states and therefore it is of great importance to monitor the CBF. Currently, no valid modality is available for that purpose. CT perfusion (CTP) is promising, but solely used qualitatively to distinguish ischemic and infarcted tissue from healthy tissue.

Study aim: The primary goal of this study was to enhance and improve the current quantitative analysis possibilities of CTP in both the macro- and the microvascular system.

Methods: This was achieved by 1) the development of the direct-flow model to calculate CBF velocity (CBFv) in the macrovascular system. This model was based on the principle that CBFv is the quotient of the distance between points in a vessel and the time delay of bolus arrival between those points. 2) The model was validated by conducting three short studies. Digital simulation data was used to determine CTP properties required to use the model; a flow phantom was used to test the model in a controlled setting; and the reliability was studied with *in vivo* data. For the microvascular system 3) normal values were derived of the perfusion parameters CBF, cerebral blood volume (CBV) and mean transit time (MTT) in the anterior, medial, posterior and basal ganglia flow territory in grey and white matter. Normal values were derived from subjects with an indication for CTP, but without the diagnosis of TIA or stroke. CTP data was acquired according to the best combination of processing steps. 4) The normal values were compared to perfusion values of patients with TIA and ischemic stroke.

Results: 1) the direct flow principle was developed successfully, but 2) was not reliable. The flow phantom showed severe overestimation of the true flow velocity and *in vivo* data revealed negative CBFv. 3) Normal values were derived successfully, but showed large variance. 4) A significant difference was found between the MTT in the medial flow territory of normal subjects and ischemic stroke patients.

Conclusion: CTP has the perspective to become a reliable tool to monitor CBF quantitatively in both the macro- and the microvascular system. However, the direct-flow model should be improved before introduction in clinical practice. To establish reliable normal values sample sizes should be enlarged and CTP data processing should be optimized.

1. Introduction

Sufficient cerebral blood flow (CBF) is an important factor that influences the disease course in patients suffering from acute brain injuries (ABI) such as stroke, cerebral hemorrhage and traumatic brain injury (TBI). In 2011, 21.000 TBI patients and 26.000 stroke patients were admitted in Dutch hospitals. Of these patients 1017 and respectively 8500 died because of their ABI.¹ Many of the patients with ABI are admitted to the neurocritical care unit, in which maintaining sufficient CBF is of great importance. This requires accurate monitoring of CBF. However, the techniques currently available can only monitor a limited part of the brain, while the CBF may be heterogeneously distributed throughout the brain. To stimulate CBF guided treatment a technique that measures the CBF in the complete brain is required. CT perfusion (CTP) has the potential to monitor the CBF quantitatively in both the macro- and the microvascular system. Therefore, this study is aimed at enhancing and improving the current quantitative analysis possibilities of CTP.

1.1 Cerebral Blood Flow

Cerebral blood flow (CBF) is the amount of blood that passes a certain part of the brain per time. In contrast to other organs that have oxygen storages and glucose reserves, the brain is very sensitive to hypoxic states. Therefore it should be continuously supplied by a sufficient amount of oxygen and nutrients to function adequately.² Insufficient supply of oxygen by blood may be caused by inadequate substrate, such as malfunctioning diffusion after hypoxia, inadequate carrying capacity, or inadequate delivery.² Insufficient CBF is one of the main factors in the pathophysiology of Acute Brain Injury (ABI) resulting in neuronal loss with subsequent disability and is associated with poor outcome and a high mortality.³ A distinction can be made between primary and secondary brain damage. In ABI the primary brain damage is directly caused by an injury such as cerebral hemorrhage, infarction or traumatic brain injury (TBI). Secondary brain damage arises after compromise of cerebral tissue oxygenation and metabolism due to insufficient CBF that is induced by the primary brain damage. States causing secondary brain damage are vasospasm, cerebral hypoperfusion, arterial hypotension, hypoxemia, flow-metabolism uncoupling, inflammation and reperfusion hyperemia.⁴ Alternatively, insufficient CBF may be the cause of primary brain damage resulting in ABI such as acute stroke.² Concluding, CBF should be monitored in patients with ABI because of the damage that can be caused by insufficient CBF to the brain.

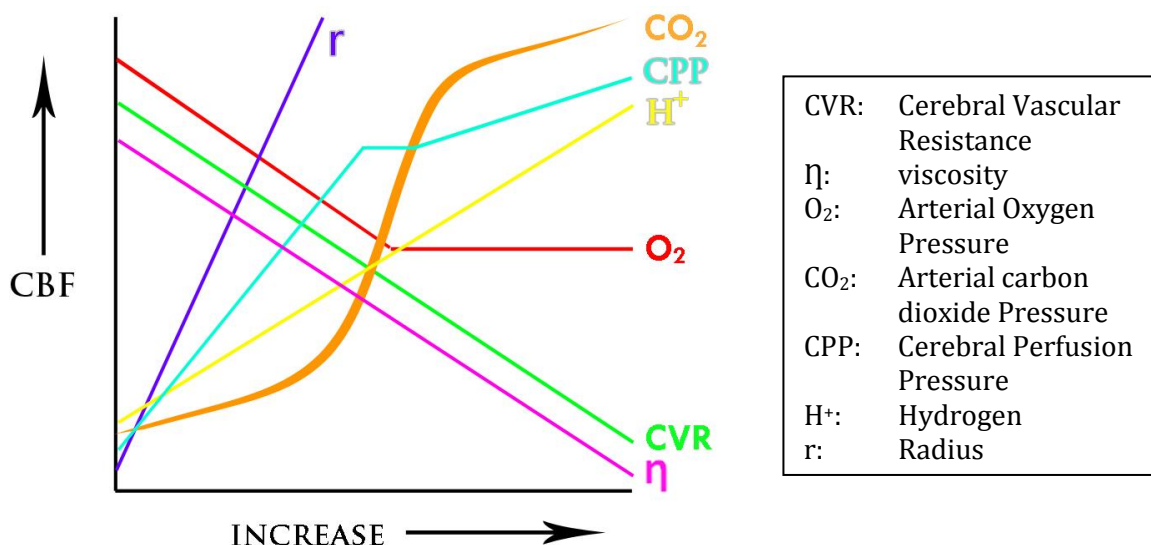


Figure 1. Schematic diagram showing the effect of several hemodynamic factors on CBF.

1.1.1 Control of CBF

CBF is controlled by four main mechanisms which are discussed below: 1) Cerebral pressure autoregulation; 2) blood gasses; 3) the autonomic nervous system; and 4) flow-metabolism coupling. The control of the CBF is complex and difficult to assess clinically, because different control systems interact. Figure 1 shows the effect of the most important CBF influencing factors.

Cerebral pressure autoregulation

Firstly, CBF is controlled by the cerebral pressure autoregulation (CA), which is a mechanism that attempts to maintain CBF constant over a range of cerebral perfusion pressure (CPP). If the CBF is too low, the cerebral arterioles dilate in order to decrease cerebral vascular resistance (CVR) and allow the inflow of more oxygenated blood. Contrarily, if CBF is too high the arterioles will contract and increase CVR, resulting in a decrease of CBF.² The CBF is determined by both CPP and CVR according to equation 1²:

$$CBF = \frac{CPP}{CVR} \quad 1$$

CPP is the difference between the MAP and the Intracranial Pressure (ICP) as shown in equation 2:

$$CPP = MAP - ICP \quad 2$$

Perfusion pressure is usually determined by the difference between the arterial and the venous pressure, but since the ICP is usually larger than the cerebral venous pressure, the CPP is determined by ICP. From equations 1 and 2 can be deduced that an increase in ICP leads to a decrease in CBF. Therefore, the brain aims to maintain low ICP when volume within the skull increases (e.g. due to cerebral edema).

Equation 1 shows that that the CVR is inversely proportional to CBF. Poiseuille's equation can further clarify this relation between flow and resistance. It states that resistance (*CVR*) to flow (assuming an incompressible fluid undergoing laminar flow) is proportional to the length of the tube (*L*) and the viscosity of the fluid (η) and is inversely proportional to the radius of the tube (*r*) raised to the fourth power^{2,5}:

$$CVR = \frac{\eta L}{r^4} \quad 3$$

Equation 3 shows that a small change in vessel radius has a large impact on the CVR and thus CBF. Therefore, changes in vessel radius (i.e. vasoconstriction and vasodilatation) play an important role in the control of adequate CBF. The CVR is altered by changes in vessel diameter; vasoconstriction and vasodilatation prevent hyperemia and ischemia, respectively. The precapillary arterioles are considered to be the main contributors to the fine CVR adjustment⁶ and it is thought that the large arteries of the brain may form a first line defense against large pressure changes.⁷

Viscosity of the cerebral blood influences CVR as well, as can be seen from equation 3. Viscosity of the blood increases with a decrease in shear rate, which depends mainly on hematocrit. Inflammatory proteins also increase viscosity to a smaller extent by aggregating forces on blood cells. This effect is stronger with low shear rate⁸, which is present with low blood flow velocity as frequently seen in ABI patients. Inflammation is a major factor in the secondary brain injury after ABI, possibly contributing to increased viscosity with subsequent CVR increase and CBF decrease

(equations 3 and 2).⁹ Increase in viscosity may delay vasodilatation after an ischemic stimulus resulting in a higher risk for infarction.¹⁰

The classical idea is that CA works as a CBF buffer and can keep it constant for a CPP from 50 mmHg to 150 mmHg.¹¹ If CPP rises or falls beyond the limits of autoregulation, flow varies directly with pressure and causes, respectively, hyperemia based on forced dilatation or ischemia based on vascular collapse.² However, this concept is challenged by the introduction of blood pressure and CBF quantification with a high temporal resolution.⁷ Recent data indicate a smaller plateau region, with a steeper slope in the hypotensive range than in the hypertensive range, as shown in figure 2.¹² A steep slope means that a change in mean arterial pressure (MAP) leads to a large change in CBF, and vice versa. Thus, the flatter slope in the hypertensive range indicates that the buffering capacities of CA can better compensate for hypertension than for hypotension.

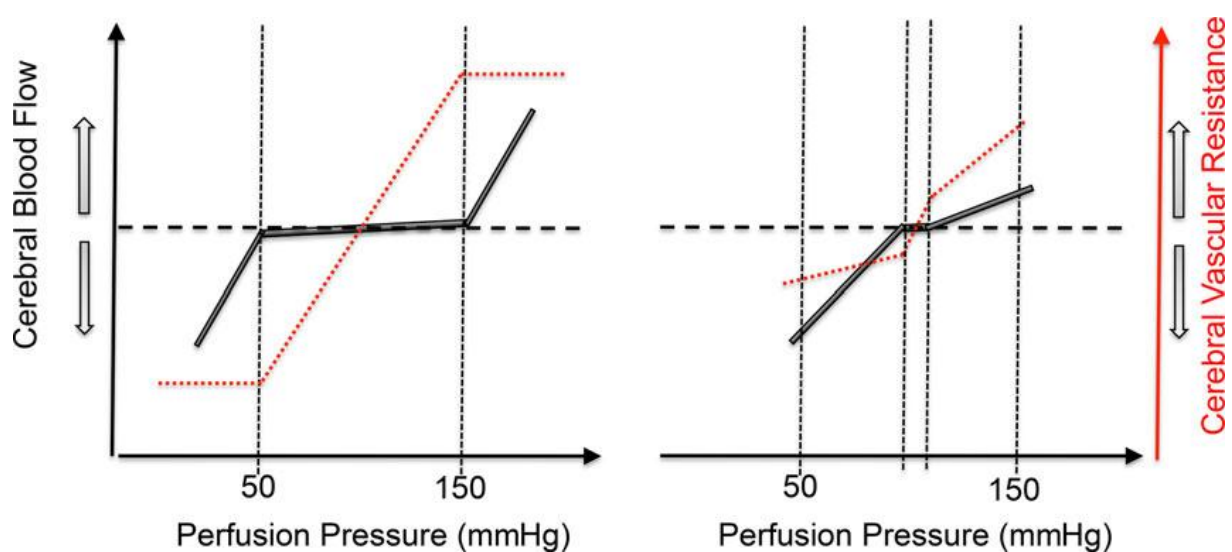


Figure 2. Diagrams showing the relation between CBF (solid black line), CPP (indicated as Perfusion Pressure) and CVR (dotted red line). The left panel presents the classical view on the cerebral autoregulation of pressure. It was thought that CBF could be kept constant over a large range of CPP, and that it was proportional with CPP beyond the limits of that range. The right panel shows the relationship between CPP and CBF based on data indicating a small plateau and a steeper slope for hypotension than for hypertension.¹² Image obtained from Willie *et al.*⁷

Blood gases

Another mechanism regulating CBF is that of the arterial blood gases. Changes in partial pressure of carbon dioxide (P_aCO_2) have a high impact on brain perfusion.⁷ A P_aCO_2 increase of 1 mmHg leads to an increase in CBF of 3-6%.^{13,14} The vascular response to P_aCO_2 is unique for the cerebral vasculature, no other organ is equally sensitive to P_aCO_2 changes.¹⁵ The response to P_aCO_2 occurs mainly in the pial arterioles, but is present throughout the whole cerebral vasculature, even in the large vessels.⁷ Increase of P_aCO_2 from 15 to 65 mmHg leads to a linear increase of Internal Carotid Artery (ICA) diameter of 20%.¹³ Beyond that range the P_aCO_2 vs CBF curve is sigmoidal.^{16,17} The effect of P_aCO_2 to CBF is related to the extravascular pH, which can alter smooth muscle tone. Hypercapnia in combination with extravascular acidification and hypocapnia with an extravascular alkaline homeostasis leads to CBF increase and decrease, respectively. The net CBF response is a balance between the effects of P_aCO_2 and extravascular pH.⁷

The CBF is also sensitive to changes in partial pressure of oxygen (P_aO_2), but only below a P_aO_2 of 50 mmHg. Reduction of P_aO_2 below that threshold leads to increase of the CBF. This effect is dependent on P_aCO_2 : hypercapnia increases and hypocapnia decreases sensitivity to P_aO_2 .¹⁸ The effect resulting from P_aO_2 changes affects both the micro- and the macrovascular system.

Vascular innervation

A third CBF influencing factor is the vascular innervation. The extracerebral vasculature is extensively innervated by the autonomic nerve system, which controls the smooth muscle of the artery. The precise role of the cerebral vasomotor nerves is poorly understood, but is presumed to play an important role in the functioning of pressure autoregulation, especially in the large vessels where it acts to buffer changes in perfusion pressure.⁷ The smaller intracerebral vessels lack smooth muscle and consequently its innervation. Yet, they are connected to neurons that are part of the neurovascular unit and may control contractile pericytes.¹⁹ Unified vasomotion is very important for the cerebral homeostasis, because the pressure in the microvascular system can be kept constant during flow adjustment this way. Figure 3 clarifies the innervation of smooth muscle surrounding vessels and the neurovascular unit. The sympathetic nervous system is, according to data from animal experiments, involved in the maintenance of flow in the larger vessels during changes in blood pressure. Human studies show that denervation by ganglionectomy universally increases CBF and impairs CA, suggesting a role of the sympathetic nerves in CBF regulation and CA.⁷ The competence of the sympathetic nervous system in restraining large increases in CBF after severe hypercapnia or hypoxia has never been studied well, but low evidence signs exist.¹³ Knowledge of the role of the parasympathetic system is even more limited, but it is known that the intracranial vessels are distributed richly with cholinergic nerve terminals, indicating some parasympathetic participation. Moreover, a study in healthy humans using transfer function coherence between MAP and CBF suggests an impaired CA after cholinergic blockade, but the physiological meaning of transfer function metrics is questioned.^{7,20} Concluding, both the sympathetic and parasympathetic nervous systems play a role in CBF control, but the exact working mechanisms are not well understood.

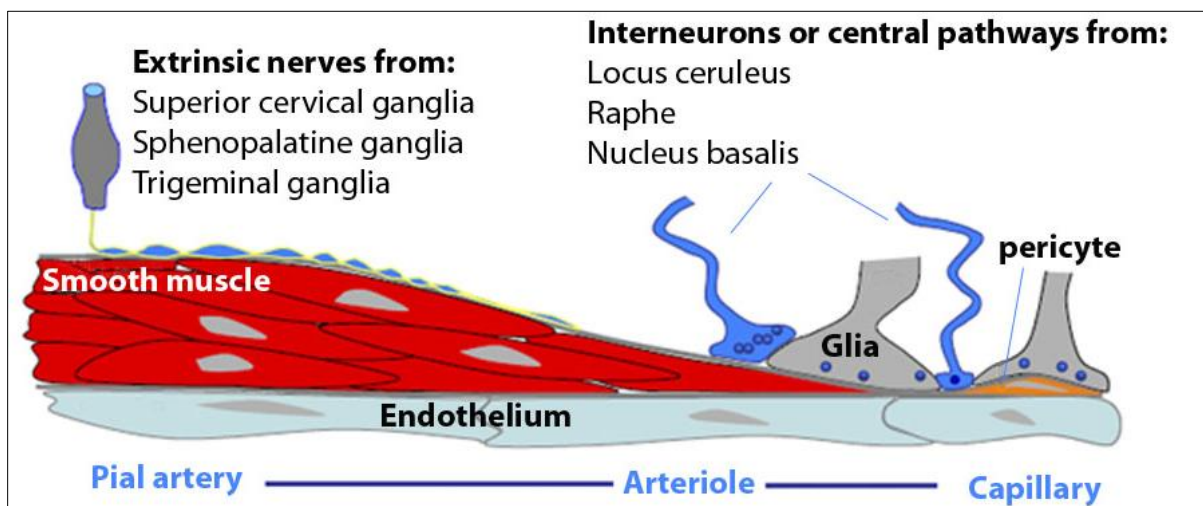


Figure 3. Structures related to the cerebral vasculature. The autonomic nervous system innervates the smooth muscle surrounding pial arteries and arterioles. The smooth muscle is absent around the capillaries and the innervations is provided by neurons of the neurovascular unit.

Flow-metabolism Coupling

Lastly, the level of CBF is regulated to meet the metabolic demand of the brain, as expressed in the Fick equation:

$$CMRO_2 = CBF \times AVDO_2 \quad 4$$

The cerebral metabolic rate of oxygen consumption ($CMRO_2$) is equal to the product of the CBF and the amount of oxygen extracted from the arterial blood (expressed as arterio-venous differences of oxygen ($AVDO_2$)).² Local alterations in neuronal electrical activity induce similar alterations in local metabolism, which in turn cause alterations in CBF. Thus, activation of the brain increases the CBF or the $AVDO_2$ in order to satisfy the demanded $CMRO_2$. For example, structures having high metabolic rates such as grey matter tend to have a high CBF and structures having low metabolic rates such as white matter tend to have a low CBF. CBF increase seems to be the primary parameter to satisfy the increased demand, but if the required $CMRO_2$ cannot be reached by an increase in CBF, a compensatory increase in oxygen extraction can occur.⁴ Since the metabolic demand is proportional to the level of neuronal activation per region and therefore is distributed heterogeneously throughout the brain, the CBF may vary throughout the brain as well.^{21,22} The flow-metabolism coupling may be regulated by metabolites, K^+ or H^+ ions and NO, because their extracellular concentration increases after an increase in metabolism. One of the metabolites playing a role in the flow-metabolism coupling is adenosine. During neuronal activity the extracellular adenosine levels rise, which causes vasodilatation and thus CBF increase in the microvascular system. A similar effect is caused by ions such as K^+ and H^+ .²³ The flow-metabolism coupling may be the clinically most relevant CBF influencing mechanism, because if the flow does not meet the metabolic demand it may cause damage immediately.²³

1.1.1 Optimal CBF

The required level of CBF is dependent on the individual demand of oxygen and nutrients, the region within the brain, the current state of the patient and the treatment the patient receives. Therefore no single value can be defined as the optimal CBF. The CBF is sufficient if a balance between the metabolic demand and the blood supply is established. Disturbance of this balance is undesirable; CBF shortage leads to brain damage, while an overdose of CBF leads to hyperemia, which may result in edema, ICP increase and subsequently brain damage. As this balance differs per patient, the optimal CBF has to be determined for every individual patient.

Normal CBF is estimated at 50 ml/100g/min². However, for gray matter this is higher (80 ml/100g/min) than for white matter (20 ml/100g/min). Regions with a shortage of supply may show, within certain limits, a compensatory increase in oxygen extraction.^{2,4} The severity of tissue ischemia is expressed in two classes; irreversible and reversible damage. The first refers to an infarct and the latter is known as penumbral tissue. Regions of penumbra are salvageable, but will proceed to infarction if the CBF is not restored quickly. Frequently, ischemic regions contain an infarct core and a penumbral border zone. The penumbra may be saved from infarction using thrombolytic agents. For clinical reasons the distinction between infarcted and salvageable tissue is of great importance as it will guide therapy. Thresholds for penumbral and infarcted CBF are approximated at 20 ml/100g/min and 8 ml/100g/min, respectively.²⁴

1.1.2 Requirements of cerebral blood flow measurement

Direct measurement of CBF in the macro- and microvascular system of all brain regions provides a good insight in the localization and extent of the brain tissue at risk. This gives the best chance to avoid secondary brain damage in the ABI patient. Knowledge about the CBF in the macrovascular system is needed because it is the first line of defense against blood pressure changes. The CBF in the microvascular system is important because it truly reflects the flow that reaches the tissue and should be in balance with the metabolic demand. A low CBF in the tissue may indicate a problem with blood supply as well as a decreased metabolic demand of the tissue. The microvascular CBF reflects the extent and severity of the brain tissue ischemia in case of stroke and it is helpful in the evaluation of benefits of thrombolytic therapy.^{25,26}

Several aspects are important for a CBF measurement technique, as summarized in table 1. The first property is the possibility to gain quantitative measures.²⁷ This is needed to be able to distinguish different levels of CBF, perform serial measurements in time, and compare results within patients and between patients. Moreover, a technique that provides quantitative results could be used as a validation method for other CBF measurement techniques. Second, CBF should be measured directly, because this lowers the risk of measurement errors and minimizes the influence of possible confounding factors. Furthermore, the technique should have a high spatial resolution to ensure distinctions between multiple brain regions and to differentiate between vessels and tissue.⁴ Likewise, it should have a high temporal resolution, or preferably, it should be able to measure CBF continuously.^{4,27} In addition, a patient-friendly technique is required.⁴ It should be non-invasive, without the need to burden the patient with unacceptable amounts of radiation or adverse effects and the procedure should be quick. A bedside technique is preferred to avoid a transfer to a radiologic department, which may be harmful to the patient since it causes stress and the safe environment of the neurocritical care unit has to be abandoned. Most patients that qualify for CBF measurement are very weak and may experience severe disadvantage from laborious measurements. Moreover, the results should be repeatable, a steep learning curve for physicians would stimulate this.⁴ The technique should be readily available too. Mostly CBF measurement is required instantaneous and delay may have severe consequences on the patient's prognosis. Finally, the CBF measurement technique should be cost-effective.⁴

A CBF technique that fulfills most of the requirements presented in table 1 is computed tomography perfusion (CTP). Currently, CTP is mainly used to perform qualitative analysis to CBF of the microvascular system²⁸, but also quantitative measures of the microvascular system already can be obtained already²⁹ and it has the theoretical perspective to acquire quantitative CBF data of the macrovascular system. CTP has a high spatial resolution of 0.5 mm, is non-invasive, relatively easy to perform, fast and cost-effective. However, CTP is not bedside, not continuous and the patient receives radiation and contrast agents. The working mechanism of CTP and its advantages and drawbacks will be discussed in more detail in section 1.2.

Table 1. CBF measurement technique requirements.

CBF measurement technique requirements
Quantitative
Direct
Macro- and microvascular information
High spatial resolution
Continuous (high temporal resolution)
Patient friendly (Non-invasive, no radiation burden, no adverse effects, quick procedure)
Bedside
Repeatable
Good availability
Cost-effective

1.1.3 Cerebral blood flow velocity

A derivative of CBF that is frequently measured is cerebral blood flow velocity (CBFv). CBFv is not directly translatable to CBF, but according to Brauer *et al.*³⁰ CBFv is correlated to CBF. They used 32 patients with intracranial pathology and showed a positive correlation between CBF and CBFv, however the strength of the correlation differed per pathology. Therefore, CBFv should be interpreted as an indication of CBF, but not as a quantified measure.

CBFv is regulated by the CBF and the cross section of the vessels, as specified in equation 5. Increase of CBF in a vessel with constant cross section will lead to increase of CBFv and vice versa. Every time a vessel branches, the summed cross section of the two branches is larger than the cross section of the primary vessel, assuming no local vasoconstriction occurs. Therefore the total blood volume is higher in the branches compared to the primary vessel. The total CBF of the branches will remain the same as in the primary vessel, so the CBFv will be lower in the branching vessels.

$$CBFv = \frac{CBF \text{ (branching level)}}{\text{aggregate cross sectional area}} \quad 5$$

This mechanism applies to all vascular systems in the human body. The blood flow velocity is highest in the aorta and decreases towards the capillaries. Capillaries are very small (internal radius $\pm 3\mu\text{m}$), but the human body has approximately 1×10^{10} capillaries. They have an aggregate cross-sectional area of $\pm 2827 \text{ cm}^2$, which is about 700 times larger compared to the aorta. Therefore the velocity in the capillaries can be 700 times lower than in the aorta, which facilitates the exchange oxygen, carbon dioxide and nutrients.³¹

CBFv is heterogeneous within the blood vessel, with increasing velocities towards the center of the vessel, assuming laminar flow in a viscous fluid. Blood flow is assumed to be laminar in larger straight branchless vessels. This principle is derived from Newton's definitions of viscosity, which states that the shear stress required to produce a particular shear rate is the viscosity of a fluid. The shear rate is the velocity gradient between two moving planes and the shear stress is the force needed to make the second plane moving faster than the first one. If a pressure is applied to a volume of blood in a vessel, each lamina of blood will move parallel to the long axis of the tube. A small layer of blood at the vessel wall cannot move because of cohesive forces. The layer of blood next to it will move faster than the outer layer, but slower than the layer next to it, and so on. A higher viscosity will lead to a larger shear stress and therefore a lower velocity gradient between the laminae. The function of the velocity profile as a function of radius and its relation to viscosity is presented in equation 6³¹:

$$CBFv(r) = \frac{\Delta P}{4\eta\Delta L} (r^2 - R^2) \quad 6$$

With r indicating the radius of the vessel; R the distance between the center of the vessel and the lamina of concern; ΔL the distance between two laminae; ΔP the pressure difference between the laminae and η the viscosity. This equation indicates a quadratic decrease of velocity towards the border of the vessel and shows that a higher viscosity leads to a lower CBFv. The equation also makes clear that CBFv is 0 at the vessel wall, because $R^2 - r^2 = 0$.

The velocity also varies within the vessel according to the shear stress and the cardiac cycle. Therefore, the most frequently used velocity parameter is mean CBFv. The measurement of CBFv is

performed using transcranial Doppler (TCD), which is repeatable, images in real time and can be used bedside. Major drawbacks of TCD are its operator dependency, failure to provide flow measurements in all vessels and the insufficiency of the temporal bone window in a significant number of patients.³²

Table 2. Overview of studies that measured CBFv. All studies used transcranial Doppler. CBFv indicates cerebral blood flow velocity; TBI, traumatic brain injury.

Study	Patient status	Mean CBFv (cm/s)
Aaslid <i>et al.</i> ³³ 1982	Healthy	62 +- 12
Kelley <i>et al.</i> ³⁴ 1992	Healthy (rest)	60/59
	Healthy (cognitive activity)	65/67
Newell <i>et al.</i> ³⁵ 1994	Healthy	41
Ferrara <i>et al.</i> ³⁶ 1995	Hypertensive	59.8
	Healthy	58.1
Nakae <i>et al.</i> ³⁷ 2011	Cerebral Ischemia	104
	Healthy	78
Pase <i>et al.</i> ³⁸ 2012	Healthy	57
Haubrich <i>et al.</i> ³⁹ 2014	TBI (day 1) (left/right)	60/56
	TBI (day 4) (left/right)	66/58
Pase <i>et al.</i> ⁴⁰ 2014	Healthy	58
Droste <i>et al.</i> ⁴¹ 2014	Atherosclerosis (peak)	89 (peak)
	Atherosclerosis (peak-enddiastolic)	35 (peak-enddiastolic)
Serber <i>et al.</i> ⁴² 2014	Healthy	53

Normal values of CBFv

A number of different techniques have been used to measure blood flow velocities in different parts of the body. Boulpaep *et al.*³¹ found the highest mean blood flow velocity in the aorta, with a velocity of 21 cm/s. The velocity is decreased with increased branching, with 1.3 cm/s in the small arteries, 0.6 cm/s in the arterioles and 0.03 cm/s in the capillaries. Most studies regarding the cerebral vasculature found higher velocity values. As shown in table 2, studies using TCD to measure mean CBFv in the middle cerebral artery (MCA) in healthy subjects measured CBFv between 41 to 78 cm/s.^{33–37,40,42} Velocities found with TCD in healthy subjects for the internal carotid artery (ICA) and the anterior cerebral artery (ACA) vary from 32 to 37 cm/s,^{33,36} and 47 to 51 cm/s,^{33,34} respectively.

1.2 Perfusion Computed Tomography

CTP is an imaging technique to gain insight in brain perfusion and cerebral hemodynamics. It can make a distinction between normal perfused brain tissue, ischemic brain tissue and infarcted brain tissue, based on qualitative analysis. Patients undergoing CTP are intravenously injected with a bolus of contrast agent that travels within 7 seconds to the brain. Multiple iterative CT scans are produced, resulting in a per-voxel time-density curve (TDC) of the first passage of the contrast bolus through the brain. Because there is a direct linear relation between the amount of contrast agent and enhancement on the CTP, the level of enhancement is a measure for cerebral perfusion. Various analysis techniques are available to determine parameters of the cerebral perfusion. The most frequently used flow parameters are CBF, cerebral blood volume (CBV) and mean transit time (MTT). This section discusses the acquisition of CTP data and CTP processing steps, it goes deeper into the mathematical background of CTP analysis models and it discusses the assumptions and challenges that are associated with CTP.

1.2.1 CTP data acquisition

A CT scanner consists of a radiator and a set of detectors. The radiator sends radiation in the direction of a panel of detectors, which detects the intensity level of the arriving radiation. The radiation may be absorbed by structures it meets on the way from radiator to detector. Denser structures such as bone will absorb more radiation than less dense structures such as muscles or fluids. The more radiation absorbed, the less will arrive at the detector. The amount of radiation arriving at the detector will be saved as an intensity value. The combination of radiator and detector can rotate very fast and can create intensity projections from all angles. The CT scanner creates a CT image by back projecting the individual created projections.⁴³

CTP can be performed on any spiral CT scanner that is capable of cine mode scans in combination with an automatic injector.²⁸ In most studies regarding CTP the anatomical coverage is limited, since only a slice of the brain could be analyzed. Recently, 320-detector-row CT scanners are developed which are, depending on the slice thickness, able to scan approximately 160 mm along the craniocaudal axis in a single rotation and are thus able to scan the whole brain.⁴⁴ These scanners present a complete overview and reduce the risk of missing pathologies.

1.2.2 CTP processing steps

The result of a CTP scan is converted to perfusion parameters by a number of processing steps, of which an overview is given in figure 4. Different algorithms and protocols can influence the CTP result and may contribute to the variety of results obtained by CTP. All processing steps have to be considered carefully in order to gain valid results.

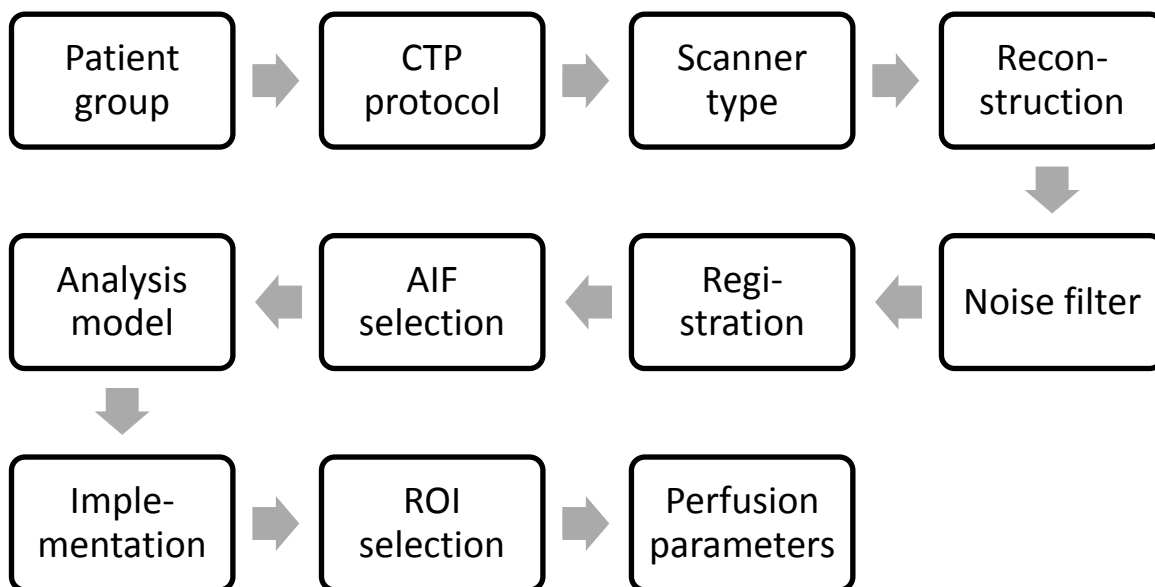


Figure 4. Overview of factors influencing the values of the perfusion parameters. Every block in this overview represents a choice or selection that has to be made in order to obtain the final result and with every step new uncertainties are introduced in the data analysis. AIF indicates arterial input function and ROI, region of interest.

Patient group

Firstly, the type of patient influences the CTP results that can be expected. For example, a patient with a stroke may present a lower CBF than a healthy subject.

CTP protocol

Every CTP scan is performed according to a certain protocol including settings such as the injection rate and amount of contrast agent, duration of scanning, intensity of scanning, scan frequency and slice thickness. The choice of scanning protocol is a compromise of image quality and potentially harmful radiation dose. The contrast agent is a nonionic iodinated fluid (300-370 mg%) that attenuates radiation. It is injected in an antecubital vein at a flow rate of 4-10 ml/s, with a higher injection rate serving better spatial resolution.^{45,46} Scanning starts with a delay of 5-7 seconds in order to let the contrast bolus approach the cerebral perfusion. The CT scanner creates, depending on the settings, an image every 0.5 to 4 seconds for almost a minute. A higher image frequency improves temporal resolution, but increases radiation dose. Wintermark *et al.*⁴⁷ showed that it is possible to reduce the radiation dose, by using scanning intervals greater than 1 second, without altering the accuracy of the results. The tube voltage and tube current may vary between 80-120 kVp and 50-200 mA, respectively.⁴⁶ For these settings a comparable consideration has to be made: higher kVp or mA results in an improved signal-to-noise ratio (SNR), but increases radiation dose as well. Most scanning protocols tend to measure the first-pass of the bolus, which may take maximally 50 seconds after injection.⁴⁶ For some purposes, such as the measurement of the blood brain barrier permeability, longer acquisition times may be used.⁴⁸ A typical radiation dose found in CTP studies of a limited volume of brain is 2-4 mSv.⁴⁶ As a reference, the average American citizen receives this amount of radiation every year from natural background radiation, an ordinary X-thorax radiates 0.1 mSv and a positron emission tomography (PET)-CT scan delivers 25 mSv to a patient. The dose received from CTP has a low additional lifetime risk of fatal cancer.⁴⁹ The influence of radiation dose on the CBF is studied by Manniesing *et al.*⁵⁰ They used 20 patients with ischemic stroke to create CTP maps and constructed digital perfusion phantoms to simulate the same scanning protocol at a varying dose (0.5-5.0 mSv, with steps of 0.5 mSv). 5.0 mSv is the standard radiation dose used, but Manniesing *et al* found that the results of CTP were comparable, for doses between 5.0-2.5 mSv, but deteriorated with lower radiation doses.

Scanner type

Several different CT scanner brands and types exist. Every scanner may contain different hardware and will produce slightly different results. For example, the CT scanner used for this study is part of a Toshiba CT scanner family in which every member varies in detector size, number of slices per rotation, rotation speed and generator power.⁵¹ So even within this family of a single manufacturer variations exist, let alone if different manufacturers are compared.

Reconstruction

The CT images are reconstructed from raw projection data. The result of the reconstruction is among other things based on the number of projections used and the angles of the projection data. Moreover, the method of reconstructing the projection data may influence the value of perfusion parameters. However, Lin *et al.*⁵² used 'filtered back projection' and 'iterative reconstruction' and did not find significant differences in CBF, CBV and MTT. They advocate for the iterative reconstruction because it is applicable using a lower dose and only slightly lower signal-to-noise ratio. Another factor is the slice thickness chosen, as studied by Martinez-de-Alegria *et al.*⁵³ They performed CTP in 18 oncologic patients with different types of cancer and reconstructed the data into slices with three different thicknesses. They found a significant difference in CBF, CBV and MTT between the different thicknesses. A smaller slice thickness ensures a better spatial resolution, but is at the cost of a worse SNR.

Noise filter

Another important preprocessing step is noise filtering. Reduction of the dose of radiation received by a patient undergoing CTP goes at the cost of noise increase. Noise may influence the deconvolution algorithm in a way that the resulting TDC has a shape completely different from the true TDC.⁵⁴ In order to keep the amount of radiation low and the resulting perfusion parameters correct, the noise filter should be chosen with great care. Mendrik *et al.*⁵⁵ performed CTP in 15 acute stroke patients and applied different noise filters to process the data. They found that the TIPS bilateral filtering method produces higher quality CBF maps than Gaussian, 3D bilateral or 4D bilateral filters. The TIPS filter resulted in more realistic mean values with a smaller standard deviation and therefore higher signal-to-noise ratios.

Registration

Severe deterioration of CTP analysis accuracy may occur as a result of patient motion.⁵⁶ An option to correct for patient motion is a registration algorithm. Several registration algorithms are available of varying quality. Fahmi *et al.*⁵⁷ used 35 CTP datasets that were classified as defective due to head movement to study the quality of a 3D rigid registration method. They used the unenhanced CT as a reference for registration, while others use the first time point of CTP. Fahmi *et al.* found that the registered CTP correlated better to follow-up scans and found that 63% of CTP improved after registration. The same author described another, more standard commercially available, technique that may correct for motion angles up to 1, 2 and 7 degrees for, respectively, pitch, roll and yaw movement. Larger angles caused major flaws in the CTP analysis, especially in the z-direction. Motion of more than 1 or 2 degrees occurred frequently.⁵⁶

Selection of arterial input function

Furthermore, the accuracy of CTP may depend on the correct placement of the arterial input function (AIF). The AIF serves as a reference to other TDC, as explained in section 1.2.3. The AIF location should be a voxel lying completely inside an artery. In theory, the artery supplying the region of interest (ROI) should be selected as the AIF, but this is not possible in practice. Moreover, it is shown that the selection of a contralateral AIF produces similar results or even improves results when the ipsilateral AIF is faced with problems such as stenoses.²⁸ The selection of AIF can be performed manually or automatically by most commercially available CTP software. From our own experience, it is clear that the automatic selection of AIF by the software package PMA ASIST (Acute Stroke Imaging Standardization Group [ASIST], Japan, <http://asist.umin.jp/index-e.htm>)^{58,59} does not function well. Frequently, the AIF are not located in a main artery, but in bone or in smaller arteries with the risk of partial volume averaging, resulting in overestimation of perfusion parameters. Niesten *et al.*⁶⁰ studied the effect of AIF location in CTP data of 44 acute ischemic stroke patients. They selected AIF in the ACA, MCA, ICA and basilar artery and found the AIF in the ICA to have the highest area under the curve and the lowest CBF. The authors claim that these results show that the ICA is the best location for AIF selection. Zaro-Weber *et al.*⁶¹ studied the influence of AIF location in perfusion weighted imaging data of 22 patients with acute stroke. They placed the AIF at 7 (intra-arterial) sites and found that the AIF selection significantly influences penumbral flow values. They found AIF placement in the proximal segment of the contralateral MCA preferable for perfusion parameter quantification. More research has been done to AIF selection in CTP recommending the selection of the AIF as close to the ROI as possible⁶² or to take the ACA for the AIF⁶³. Another reference curve used for CTP analysis is the venous output function (VOF). The VOF is selected in a vein, which is usually larger than an artery and therefore has a lower chance to be subject of partial

volume averaging.⁶⁰ However, nowadays whole brain CTP is performed including the arteries that are large enough for AIF selection without partial volume averaging, such as the proximal MCA. The added value of VOF is therefore questioned; some researchers found improved perfusion values using a VOF⁶⁰, but others do not recommend usage of a VOF because of scaling problems during the process.^{60,64} Concluding, the AIF should be selected in the largest unaffected artery present, because this results in the biggest TDC. A VOF is not necessary if the AIF is completely intra-arterial.

Perfusion analysis model

Many different perfusion analysis models are available with varying quality and complexity. The most frequently used models are the maximum slope model and the deconvolution model, which will both be discussed in more detail in section 1.2.3. The maximum slope model is fast and easy to perform, but needs a high injection rate and is sensitive to small disturbances.⁶⁵ The deconvolution model is robust to noise and has a high accuracy, but is complex and wrong selection of AIF may result in errors.²⁹ Other possible perfusion analysis models are the Patlak model, which is suitable for blood brain barrier permeability analysis.⁶⁶ Deconvolution can be implemented in several ways, all with its own advantages and disadvantages. Block circulant SVD (bSVD) deconvolution is used frequently, but also Bayesian methods are promising and increasingly used⁶⁷. The choice of perfusion analysis models has a large impact on perfusion parameter values, but also on algorithm complexity and computation time. Abels *et al.*⁶⁵ compared the maximum slope method to a deconvolution method and found comparable qualitative and quantitative results. However, several studies showed that CTP correlates better to PET and Xenon-CT when deconvolution is used instead of the maximum slope model.^{68,69,70} Boutelier *et al.*⁶⁷ invented a deconvolution model based on Bayesian statistics and compared it to an oscillating SVD (oSVD) deconvolution model using a digital flow phantom. They found that their Bayesian model outperforms the oSVD model on goodness-of-fit, linearity and statistical and systemic errors on all parameters. However, their model is not commercially available yet. Concluding, the choice of perfusion analysis model is a balance of accuracy on one side and complexity and computation time on the other side.

Implementation

All the previously mentioned preprocessing steps have to be implemented in a software package somehow. Many different software packages are available, mostly provided by CT scanner manufacturers, but also developed in house by several research groups. Different software packages use different algorithms to produce CTP results and have different user definable settings. Kudo *et al.*⁷¹ used a phantom data set for CTP to compare 13 algorithms including five commercial vendors and two academic programs. They found good correlation between software packages for CBV ($r > 0.9$ in 12 algorithms), but not for CBF and MTT ($r > 0.9$ in 7 and 4 algorithms, respectively). As of relevance for this study, the bSVD algorithm of the software developed by PMA is one of the algorithms showing good correlation between the true values and the measured values for all perfusion parameters. Fahmi *et al.*⁷² found large differences between two software packages when they compared the size of infarct core and penumbra in 26 patients with acute ischemic stroke. These results clearly indicate that the software chosen influences the results of perfusion analysis.

Region of interest selection

Depending on the purpose of the CBF analysis, regions of interest (ROI) can be selected. The ROI can be used to acquire quantitative perfusion parameter values. The selection of ROI is performed manually and is therefore sensitive for inter- and intraobserver variability. Sanelli *et al.*⁷³ assessed the

interobserver variability using six observers and 20 CTP datasets. The observers (neuroradiology attending physician, neurology attending physician, neuroradiology fellow, radiology resident physician, senior and junior CT technologists) placed 10 ROIs on the cortex after a short training session. They found a low degree of variability in the CBF, CBV and MTT values among the observers, ranging from 3.55 to 13.66%. Only one observer showed significant differences in mean CBF and CBV. Sanelli *et al.* concluded that the overall quantitative differences between observers in the study would not necessarily affect quality of the perfusion analysis. Moreover they state that the analysis can be performed by observers with various levels of skill and experience when a uniform and standard technique is used.

Perfusion parameters

The value of the perfusion parameters is the outcome of interest. The most commonly used perfusion parameters are CBF, MTT and CBV. CBF varies between patient groups, but may also vary within patient groups or within a group of healthy subjects. It is not clear what a normal value of CBF should be. This is caused by the many factors that play a role in the CTP analysis algorithms. Every study uses other variables, resulting in incomparable study outcomes. Some of the literature available regarding perfusion values is presented as an overview in table 3. Sase *et al.*⁷⁰ compared CBF obtained by CTP to CBF obtained by Xenon-enhanced CT in 7 normal subjects. They found a significant lower value of CBF using CTP in ROIs created in tissue in ACA, PCA and MCA flow territories and found higher values in the thalamus and putamen compared to Xenon CT. They found

Table 3. Overview of studies acquiring perfusion parameter values in healthy or healthy subjects. CBF is given in ml/100g/min; MTT in s and CBV in ml/100g. WM indicates white matter; GM, grey matter.

Study	Year	Patients	Values			
			CBF WM	CBF GM	MTT GM	CBV GM
Sase <i>et al.</i>⁷⁰	2005	7 Normal subjects		30-45		
Waaiker <i>et al.</i>⁷⁴	2007	20 Symptomatic unilateral carotid artery stenosis (unaffected side)		50-71	4.7-5.6	3.9-5.3
Ziegelitz <i>et al.</i>⁷⁵	2009	20 neurologically healthy elderly subjects	13	42		
Gruner <i>et al.</i>⁷⁶	2011	12 healthy subjects	21.8	71.8		
Wang <i>et al.</i>⁷⁷	2014	8 healthy patients	23-29	44-50		

mean CBF values between 30 and 45 ml/100g/min for the ACA, MCA and PCA territories and found mean values between 65 and 75 ml/100g/min for the thalamus and putamen. Waaiker *et al.*⁷⁴ used 20 patients with symptomatic unilateral carotid artery stenosis to study intraobserver and interobserver variability and a possible improvement of reproducibility when ratios of healthy vs unhealthy tissue are used instead of solely the quantitative values. They found MTT more reproducible than CBF and CBV and an improvement in measurement variability when CTP ratios are used. They found mean CBF values of the asymptomatic side varying between 50 and 71 ml/100g/min for ACA, MCA, basal ganglia, and PCA territories. They found mean values for CBV and MTT varying between 3,9 and 5,3 ml/100g and between 4,7 and 5,6 s, respectively. Gruner *et al.*⁷⁶ compared CTP to ¹⁵O-H₂O PET in 12 healthy subjects. They found a large systemic overestimation of CTP and they conclude that PET performs better than CTP in quantifying brain perfusion. They found white matter and grey matter CBF values of 21.8 and 71.8 ml/100g/min respectively. Wang *et al.*⁷⁷ studied quantitative CTP values in patients with depression and in 8 healthy patients. They found CBF

of grey matter between 44 and 50 ml/100g/min and CBF of white matter between 23 and 29 ml/100g/min. These results clearly indicate that the range of perfusion values found differs per study. The differences may be caused by differences in study protocols. These studies show a variability of normal values for CTP of the brain, which is probably caused by differences in study protocol. For CTP choices have to be made regarding both pre-processing and post-processing. For example, the study by Wang et al. is the only one using whole brain scans, the others use only a few slices. In some of the studies healthy subjects are used, while the study of Waaijer *et al.*⁷⁴ uses patients with a perfusion deficit. Also the method of AIF and ROI selection and localization differs: some studies use automatic AIF and ROI selection, others use manual selection.

1.2.3 Mathematical background of the maximum slope model and the deconvolution model

The basis of the analysis of CTP is the ‘tracer-kinetic’ model.⁷⁸ This model assumes that the ROI is supplied with contrast-mixed blood by a single artery, that the blood passes through the capillary network of the ROI and that it flows out through a single vein, as is schematically presented in figure 5. Blood cells can take various paths through the capillary network, with varying transit times. The concentration of contrast agent in the arterial and venous vessel is measured as well as the average concentration in the tissue of the ROI.

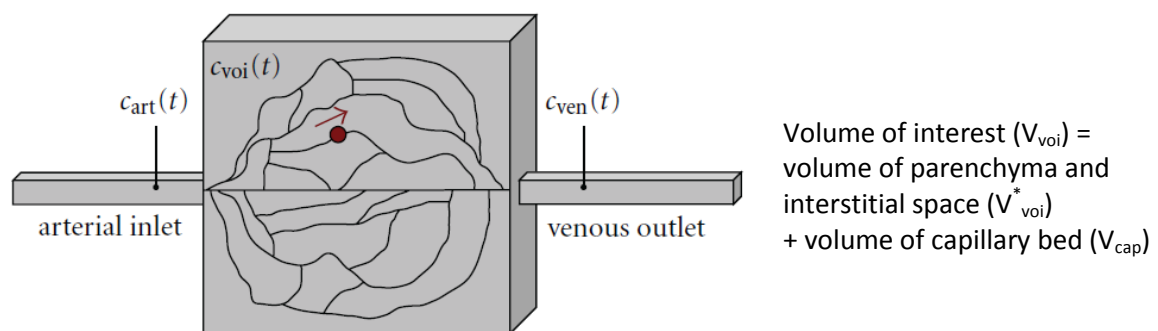


Figure 5. Representation of the ‘tracer-kinetic model’. This model supposes that the amount of contrast agent within a region of interest (ROI) entered the ROI via a single artery and leaves the ROI via a single vein. Image taken from Fieselmann *et al.*²⁹ ROI indicates region of interest; VOI, ROI; c_{art} , arterial contrast concentration; c_{ven} , venous contrast concentration and c_{voi} , contrast concentration within VOI.

Next, the calculation of cerebral perfusion parameters is performed by measuring the amount of contrast present per voxel, which is graphically presented in a TDC, see figure 6. The analysis of these TDC can be done in several ways differing in complexity and quality of results. None of these ways are without limitations and all methods are estimations of the true cerebral hemodynamics. In the next sections, the basic methods are explained and some frequently used implementation methods are discussed.

Maximum slope method

An easy method to determine cerebral perfusion parameters is the maximum slope method. This method uses the Fick principle. In this method the CBV is approximated as the area under the TDC. The CBF is estimated as the maximum slope of the TDC and the MTT of blood between the arterial input and the venous outflow is approximated according to the central volume theorem, represented by equation 7²⁸:

$$CBF = \frac{CBV}{MTT} \quad 7$$

This method is accurate under very strict assumptions and is very sensitive to small disturbances.²⁸ One of these assumptions is that no venous outflow occurs during arterial inflow. To meet this assumption a very narrow TDC is needed which is achieved by very high contrast injection rates which increases the risk of nausea among patients.⁴⁶

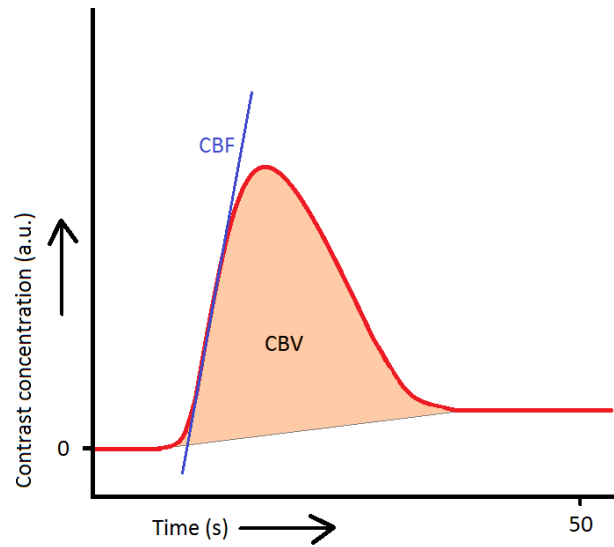


Figure 6. Example of time-density curve (TDC). The curve should ideally rise steeply and decrease to the ground level within 50 seconds. The true ground level will not be reached due to recirculation and dispersion of contrast agent. The maximum slope model uses parameters derived directly from the TDC. The CBV is calculated as the area under the curve, the CBF is approximated as the maximum slope of the TDC and the MTT is derived via the central volume theorem: $MTT = CBV/CBF$.

Deconvolution method

Deconvolution is a more precise but complex method to calculate the perfusion. The deconvolution method requires an AIF, which is the TDC of an artery. This is then compared to a TDC of parenchymal tissue to correct for bolus dispersion and tracer-arrival time delay, as explained in figure 7.

The measured $AIF(t)$ is related to the tissue $TDC(t)$ by convolution with the flow scaled impulse residue function, $F \cdot R(t)$, as shown in equation 8⁵⁴:

$$TDC(t) = AIF(t) \otimes [F \cdot R(t)] = F \cdot \int_0^t AIF(t-t') \cdot R(t') \cdot dt' \quad 8$$

$F \cdot R(t)$ contains information about the perfusion parameters desired as follows. The CBF can be calculated as:

$$CBF = \frac{1}{\rho_{voi}} \cdot \max(F \cdot R(t)) \quad 9$$

With ρ_{voi} the density of the volume of interest and $\max(F \cdot R(t))$ the maximum value of the function $F \cdot R(t)$. The CBV can be calculated as:

$$CBV = \frac{1}{\rho_{voi}} \cdot \int_0^{\infty} F \cdot R(\tau) d\tau \quad 10$$

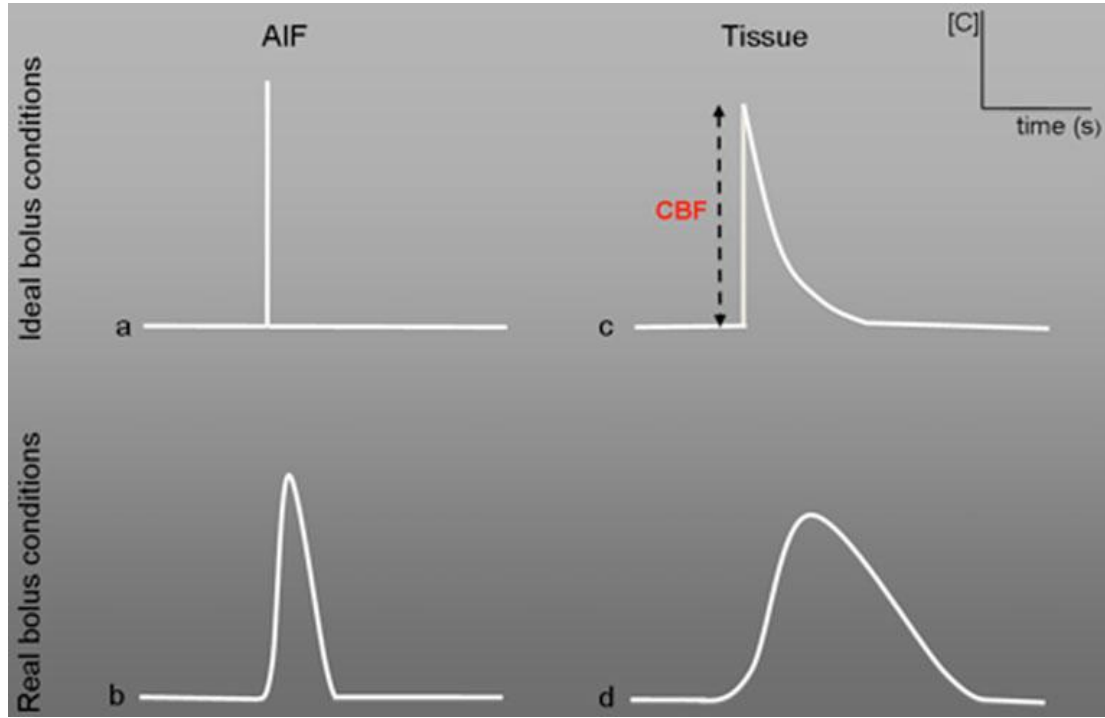


Figure 7. Four time-density curves (TDC) with time on the x-axis and contrast concentration (c) on the y-axis are shown. The upper row reflects an idealized situation: the contrast bolus passes the artery, enters the tissue instantaneously and its enhancement falls gradually in the tissue (a,c). The result is called the residue function (c), since it reflects the remaining contrast in the tissue. The CBF of the tissue is then represented by the peak of the residue function. The lower row represents a more real situation. Due to dispersion and time-delay of the contrast agent the arrival of contrast agent is gradually (b). The shape of the residue function (d) is now dependent on both CBF and the shape of the AIF. In order to derive the CBF and other parameters the effects of the dispersion within the AIF on the tissue concentration must be removed, which can be done using 'deconvolution'. Image taken from Leiva-Salinas *et al.*⁷⁹

Using equation 10 the MTT can be calculated as:

$$MTT = \frac{1}{\max(F \cdot R(t))} \cdot \int_0^{\infty} F \cdot R(\tau) d\tau \quad 11$$

$F \cdot R(t)$ can be obtained by deconvolution of equation 11. Deconvolution is complex because it has no single right solution and the different solutions do not necessarily have to be similar. However, with effective noise suppression, $F \cdot R(t)$ can be obtained validly by deconvolution.⁵⁴ The basis of deconvolution consists of a few steps. First, the above mentioned equation is discretized and written in matrix notation. Next, to find an estimate of $F \cdot R(t)$, an estimate of $AIF(t)$ is found such that the difference with the real $AIF(t)$ is minimized. Then the generalized (pseudo) inverse artery matrix AIF^{-1} is found. Combining these steps gives us an estimation of $F \cdot R(t)$, $\tilde{F} \cdot \tilde{R}$, as following:

$$\tilde{F} \cdot \tilde{R} = \frac{1}{\Delta t} \cdot AIF^{-1} \cdot TDC \quad 12$$

With $\tilde{F} \cdot \tilde{R}$ an estimation of $F \cdot R(t)$ and Δt the time step used for discretization. This deconvolution method leads to an estimation of the residue function, but it contains large oscillations due to the instability of the method. To avoid these oscillations, some more complex steps have to be included. The instability can be avoided by finding a decomposition of the AIF matrix in terms of orthogonal matrices, as in equation 13:

$$AIF = U \cdot S \cdot V^T \quad 13$$

With the matrix S containing the singular values of the matrix AIF . Therefore equation 13 is called the singular value decomposition (SVD). The pseudo inverse AIF^{-1} is found again and now an estimate of $F \cdot R(t)$ is as following:

$$\tilde{F} \cdot \tilde{R} = \frac{1}{\Delta t} \cdot V^T \cdot S^{-1} \cdot U \cdot TDC \quad 14$$

This standard SVD method (sSVD) leads to improved impulse residue functions, but still contains disturbing oscillations. These oscillations can be controlled by the incorporation of some constraints. Hereby, the impulse residual function is imposed to some characteristics that are known to be true in general, for example that the impulse residue function should be smooth. Smoothing the curve may reduce the amount of oscillations, but the estimate may differ more from the true $F \cdot R(t)$. This method is called the constrained deconvolution method. By minimizing Δ^2 in equation 14 a compromise has to be found between minimizing the residual and smoothness of the curve:

$$\Delta^2 = \|r\|^2 + \lambda \cdot \|D_2R\|^2 \quad 15$$

With r the difference between the estimated $TDC(t)$, \widehat{TDC} , and the real $TDC(t)$; λ the multiplier which controls the weight placed on the smoothness of the estimate of $F \cdot R(t)$ relative to the weight on the estimate residue; and D_2R the second difference of the impulse residual function. A small λ will lead to the same result as with the unconstrained deconvolution and a large λ will lead to a smoothed estimate that may deviate from the true impulse residue function.

Concluding, the deconvolution models use complex algorithms, in which estimating plays a role, but they are more accurate than the maximum slope model. However, both models use assumptions that may be too much of a simplification of reality. The assumptions are discussed in the next section.

1.2.4 Validity of CTP

Assumptions

Several assumptions regarding blood flow and CTP have to be made in order to be able to use the calculation methods as described. The assumptions made are 1) intact blood brain barrier, 2) perfect mix of contrast agent in blood, 3) validity of the tracer kinetic model, 4) no time delay or dispersion, 5) correctness of the equation: 1 Hounsfield Unit (HU) = 1 gram of blood per ml tissue and 6) no hematocrit differences.

- 1) Firstly, it is assumed that the contrast agent does not pass the BBB. The enhancement of contrast is transient, meaning that all contrast agent entering the arterial inlet will eventually flow through the venous outlet. In cases of a breakdown of the BBB, the estimates achieved with the methods described may become inaccurate.²⁹ In reality a small amount of contrast will always leak through the blood brain barrier, which may influence the perfusion parameters. However, the most important part of the TDC is the rising part and the amount of blood brain barrier leakage is negligible then.

- 2) Next, it is supposed that the contrast agent mixes perfectly with the blood. Thereby, it is assumed that the contrast agent does not influence the behavior and physical properties of the blood.²⁹ The contrast agent and blood are stirred by the double passage through the heart so the assumption seems plausible.
- 3) Furthermore, as mentioned before, the tracer-kinetic model contains one capillary bed, one inlet and one outlet. However, a voxel as measured by CTP contains numerous capillary beds as well as arterioles and venules that supply and drain these capillary beds. Thus, the concentration of contrast agent measured in a voxel is a combination of contrast present in capillary beds and in arterial and venous vessels. Therefore, the calculated perfusion parameters are not true representatives of the state of the cerebral perfusion, instead it is an average perfusion of the voxel.²⁹
- 4) Moreover, the AIF measured does not truly represent the arterial inlet of a ROI. Instead, it is accepted to acquire a global AIF from a large arterial vessel, such as the anterior cerebral artery. This adaptation has two consequences: a time delay between the AIF and the tissue function appears and bolus dispersion occurs. Time delay and bolus dispersion may lead to an underestimation of CBF.⁸⁰
- 5) It is assumed that image enhancement of 1 HU corresponds to 1 gram of blood per ml of tissue.
- 6) Finally, the method does not take into account hematocrit differences. However, the hematocrit value in the capillaries is lower than the hematocrit value in the arteries, thus the concentration of red blood cells is lower in the capillaries. Since the contrast agent solutes solely in plasma, the concentration of contrast will be overestimated in tissue. A correction for this underestimation is proposed. It is found that the hematocrit of the capillaries differ a factor 0.73 from the hematocrit of the arteries.⁶⁹

Comparison to other CBF measurement techniques

The accuracy of CTP has been validated against other CBF measurement techniques, of which some results are presented in table 4. Cenic *et al.* compared dynamic CT to a microsphere method in rabbits and found good correlation between both measurements. Kudo *et al.*⁶⁹ performed both CTP and PET to five healthy volunteers using the deconvolution method and vascular pixel elimination for CTP. They found a good correlation between both if the vascular pixel elimination method was optimized. Grüner *et al.* compared CTP to ¹⁵O-H₂O-PET in 12 healthy subjects and found a significant and systematic overestimation of regional CBF in both white and grey matter using CTP. The overestimation of CBF for grey matter, which is highly perfused, is with 47% unacceptably high.⁸¹ Bisdas *et al.*⁸² developed a distributed parameter tracer kinetics model to derive CTP values and validated it with PET. They found significant correlation between the mean flow values of both techniques. Koenig *et al.*⁸³ studied the validity of CTP related to SPECT. They performed both techniques in 16 stroke patients and found good correlation in 13 of 16 patients, but the remaining 3 patients had an infarct outside the CTP scanning range that was missed. Furukawa *et al.*⁸⁴ showed that CBF obtained from CTP correlates well with CBF obtained from Xenon-CT. Wintermark *et al.*⁶⁸ also showed good correlation between CBF obtained from CTP and CBF obtained from Xenon-CT, but mentioned that the appropriate choice of the artery for the AIF may influence the result and is therefore very important.

Table 4. Overview of studies comparing CTP to some other modality. The studies by Cenic, Wintermark and Kudo present a good correlation between CTP and the other modality (with some constraints), but Grüner found a large overestimation of CBF. sSVD indicates deconvolution using standard singular value decomposition and LMS, deconvolution using least mean squares; VPE, vascular pixel elimination and rCBF, regional CBF.

CENIC 1999⁸⁵	Dynamic CT		Microsphere
Whole brain	73.3 (31.5)		74.3 (31.6)
WINTERMARK 2001⁶⁸	CTP sSVD	CTP LMS	XENON-CT
Whole brain VPE	46 (24)	47 (26)	49 (25)
Gray matter VPE	68 (13)	69 (17)	71 (15)
White matter VPE	26 (10)	25 (9)	28 (10)
Whole brain no VPE	70 (14)	100 (23)	54 (27)
Pathological parenchyma	14 (10)	15 (11)	14 (9)
KUDO 2003⁶⁹	CTP without VPE	CTP with VPE	PET
Whole section	59.01	45.56	47.17
Grey matter	66.73	52.75	51.37
White matter	42.53	30.38	37.86
BISDAS 2007⁸⁶	CTP model		PET
ACA territory	27.7 (8.5)		29.4 (7.9)
MCA territory	42.6 (11.8)		40.6 (11.3)
PCA territory	43.3 (6.6)		36.8 (6.6)
GRÜNER 2011⁷⁶	CTP rCBF with VPE		PET
Anterior white right	18.9 (5.2)		17.6 (3.0)
Frontal grey right	74.4 (9.1)		49.4 (6.8)
Posterior white right	22.5 (4.2)		18.0 (2.5)
Parietal grey right	72.0 (8.5)		45.0 (6.7)

1.2.5 Clinical Application

CTP is currently used to detect or control ABI with qualitative methods. CTP is also used in other occasions such as cerebral tumors or with a balloon occlusion test, though these indications are beyond the scope of this thesis and are therefore not discussed.

Stroke

CTP is widely used in the diagnosis and treatment of acute stroke. Using the deconvolution method, regions that are potentially reversibly ischemic (the 'penumbra') can be distinguished from regions that are irreversibly damaged.²⁵ The presence of penumbra supports treatment with thrombolytics, while thrombolytics are contra-indicated when large infarctions are present, because of the increased risk of hemorrhage.²⁸ The distinction of penumbra and infarction from healthy tissue can be made by combining the CBF-, CBV- and MTT-maps. As given in table 5, penumbra will show decreased CBF, normal or elevated CBV and delayed MTT. Yet infarcted areas will show the same change in CBF and MTT, combined with a decreased CBV. Recently some studies have been done into the additional value of CTP in the treatment of stroke patients. Van der Hoeven *et al.*⁸⁷ showed that CTP has significant additional diagnostic values to noncontrast CT and CT angiography (CTA) for detecting ischemia in patients suspected of acute posterior circulation stroke. Biesbroek *et al.* performed a systematic review and meta-analysis of published reports regarding detection of ischemic stroke using CTP. They included 15 studies performed between 1998 and 2010 with a total

of 1107 patients and found that ischemic stroke could be detected with a sensitivity of 80% and a specificity of 95%. Almost two third of the false negatives were because of small lacunar infarcts and the remaining was mostly due to limited coverage or motion artefacts. They conclude that the sensitivity and specificity are very high and that the amount of false negatives can be reduced by whole-brain scanning and by optimization of CTP techniques.

Table 5. Consequences of circulatory impairment on perfusion pressure, MTT, CBV and CBF. CBV seems to be the most logical parameter to distinguish penumbra from irreversible damaged tissue. Table obtained from Miles *et al.*⁸⁸ MTT indicates mean transit time; CBV, cerebral blood volume; and CBF, cerebral blood flow.

Circulatory impairment	Perfusion pressure	MTT	CBV	CBF
Mild	↓	↑	↑	Normal
Moderate (penumbra)	↓↓	↑↑	↑	↓
Severe (irreversible)	↓↓↓	↑↑↑	↓	↓↓

Traumatic brain injury

CTP outperforms conventional CT in the detection of TBI patients who are at risk of delayed hemorrhage due to hypoperfusion of non-hemorrhagic contusion.⁸⁹ A finding of hypoperfusion may indicate disturbed cerebral autoregulation, which is a predictor of cerebral edema and consequently a bad prognosis.⁹⁰ Bendinelli *et al.*⁹¹ performed CTP in 30 patients with severe traumatic brain injury as an addition to unenhanced CT. They found additional deficits on the CTP in 60% of the patients which had therapeutic consequences in 10% of the patients. These are high numbers that suggest that CTP is a useful addition in traumatic brain injury management.

Cerebral hemorrhage

Patients with cerebral hemorrhage benefit from CTP because a lower mean CBF may indicate vasospasm and the risk of delayed infarction.⁹² Severe vasospasm may be represented by delayed MTT and decreased CBF.⁹³ Cremers *et al.*⁹⁴ studied the benefits of CTP during delayed cerebral ischemia after subarachnoid hemorrhage (SAH). They included 33 patients with acute SAH and delayed cerebral ischemia and performed CTP. They did qualitative analysis and found that presence of a perfusion deficit had a positive predictive value (PPV) of 71% and a negative predictive value (NPV) of 83% for infarction on follow-up. They also used a CBF threshold of 17.7 ml/100g/min which had a PPV of 63% and a NPV of 78% for infarction. They concluded that qualitative evaluation performs marginally better than quantitative analysis. CTP should probably be combined with some other modality to improve the validity to detect delayed cerebral ischemia in acute SAH patients. Cremers *et al.* also performed a systematic review and a meta-analysis to the utility of CTP in patients with delayed cerebral ischemia in aneurismal SAH. They included 11 studies totaling 570 patients and found no on-admission differences in CBF, MTT and CBV between patients who did and did not develop delayed cerebral ischemia. However, they found CBF decrease and MTT increase in the delayed cerebral ischemia time-window (4-14 days after SAH). They concluded that CTP can be used in the diagnosis, but not in the prediction of delayed cerebral ischemia.

1.3 Potential of quantitative use of CTP

The previous sections introduced and outlined the current use of CBF and CTP. This section will focus on the wide application potential of CTP that this study aims to examine. As shown before, CTP is a promising technique in the treatment of ABI and can be used to acquire additional information regarding the cerebral hemodynamics, but currently only qualitative information regarding the microvascular system is used. The quantitative microvascular results and the information regarding the macrovascular system are barely used due to a lack of knowledge and research on these topics. Next, the issues concerning macro- and microvascular system will be discussed separately.

1.3.1 Macrovascular system

Currently, CTP is aimed at microvascular perfusion and not at the flow in the macrovascular system. This is understandable, since ischemia affects the micro- and not the macrovascular system. At the moment, the only technique used in clinical practice that reveals any information regarding the macrovascular blood flow is TCD. However, this technique has severe limitations. There are especially two main problems with TCD. First, TCD provides indirect measurement of CBF. It only takes into account CBFv, without knowledge of the actual amount of blood that passes through. The second problem is low spatial resolution; it only measures CBF at a single location in time. With CTP, CBF can be measured more directly, because it takes both CBFv and vessel radius into account. These two factors together can more accurately calculate CBF. In addition, CTP offers the opportunity to detect the CBF in all cerebral vessels, offering high spatial resolution. More accurate quantification of the cerebral blood flow (CBF) in the macrovascular system would be greatly beneficial for both current research and patients suffering from insufficient CBF. Nevertheless, CTP is never used for CBF analysis in the macrovascular system, because there is no algorithm to quantitatively analyze the CTP data. Therefore, the first part of this study focuses on the development of a model, including such an algorithm.

An algorithm for the detection of absolute values of CBF in the macrovascular system would have large benefits. First, it would create the possibility to measure the CBF before and after therapy and would therefore give an indication of the efficacy of the therapy. Next, comparison of flow between different groups of patients will enable the determination of threshold values requiring intervention. Furthermore, it would provide the opportunity to follow the progress of CBF and to quickly detect improvements or deteriorations. In addition, a valid technique that measures CBF in the macrovascular system is valuable for further research because it may function as a reference technique.

The development of a model to measure CBF in the larger vessels can also have practical advantages. Firstly, no complex mathematical procedures such as deconvolution should be required to acquire the perfusion parameters. The method should be transparent, not a black-box. Furthermore, vessels are easy to recognize and hardly border any structures with similar intensity values, such as cartilage and bone, which should make extraction of vessel data easier.

After the model is developed, it needs to be validated to evaluate the quality of the model. The second part of this study focuses on the validation of the model, using three methods: digital simulation data, flow phantom data and in vivo data. First, the behavior of the principle was roughly tested using digital simulations.⁹⁵ Next, the results of the simulation were used to prepare a flow

phantom to test the principle in a real but controlled environment.⁹⁶ Finally, in vivo data was acquired based on findings from the simulation and flow phantom measurement.⁹⁷

1.3.2 Microvascular system

Nowadays, the clinical practice uses only qualitative measures of CTP to diagnose ABI. Qualitative analysis of CTP is based on visual interpretation of perfusion maps.⁹⁸ Regions with reduced perfusion can be detected by comparison to surrounding tissue or to the contralateral hemisphere. In combination with clinical symptoms or other imaging modalities a diagnosis of ABI could be confirmed. Qualitative analysis is easy to perform compared to the quantitative analysis, but the results are less specific since a difference in perfusion does not necessarily indicate a perfusion deficit.⁹⁸ Quantitative CTP results can be obtained as well,²⁸ and have the potential to be more specific.

According to Boutelier *et al.*⁶⁷, quantitative analysis can be performed using a pixel-by-pixel analysis or using averages which can be calculated using the selection of regions of interest (ROI). The pixel-by-pixel method could be used in case of stroke to distinguish unrecoverable infarcted tissue from potential salvageable tissue using threshold values. The ROI averaging method can be used to calculate the average CBF of an anatomical structure. ROIs can eventually be mirrored to compare it to the contralateral hemisphere.⁷⁴ Despite its potential, these methods are rarely used in clinical practice, probably because normal values of perfusion are unknown.

The quantitative values of the microvascular system obtained with CTP have been a frequent topic of discussion. Limited literature is available on quantitative values of brain CTP and these results were obtained as a secondary outcome in a study with a specific group of patients.^{70,74,76,77} In literature, normal CBF values range from 13 to 72, this range is far too wide to distinguish healthy subjects from ABI patients. Therefore, quantitative CTP analysis is useless. The wide range of perfusion values may be caused by the numerous processing steps that affect CTP results, as described in section 1.2.2. There are many choices to be made among these factors, which makes it very difficult to establish the optimal combination of choices. To obtain reliable values, the processing steps have to be performed with great care. For example, the selection of AIF and ROI is operator-dependent and influences the CTP values. Also the inclusion of large vessels and parts of the brain image that are not tissue, such as fissures, may influence the values of CTP. These factors create a large variability in CTP values amongst stroke patients.⁹⁸

The derivation of true normal values will be of great value. First, reliable normal values facilitate diagnosis of the nature and severity of the injury and will therefore improve treatment of ABI patients. For example, it can guide physicians in the management of treatment of patients with a variability of neurological and cardiovascular diseases affecting the brain. The perfusion parameters of a new patient can be compared to the normal values, which may confirm or reject a diagnosis. Second, normal values of CTP may be a reference for future research in both patient care and CTP or other quantitative perfusion imaging modalities.

The third part of this study focuses on the derivation of normal values of CBF, cerebral blood volume (CBV) and mean transit time (MTT) obtained by CTP in several different brain regions. In order to do so, the best possible combination of CTP processing factors will be used. The fourth part of this study involves a comparison between the resulting normal values and values in patients with transient ischemic attack (TIA) or ischemic stroke in both the affected and the unaffected cerebral area.

1.4 Study Objectives

The primary goal of this study is to enhance and improve the current quantitative analysis possibilities of CTP. As shown in the previous section, for quantitative micro- and macrovascular imaging to be accepted in clinical practice, reliable analysis algorithms have to be developed. Therefore, this study focuses on the development and validation of quantitative analysis algorithms for both macro- and microvascular systems, as is presented in flowchart 1.

To ensure a clear study structure, the study has two distinct research topics segregating the macro- and microvascular systems.

RT1) Quantifying cerebral *macrovascular* blood flow using CTP: the direct flow model

RT2) Establishing normal values of CBF, MTT and CBV in the *microvascular* system

1.4.1 Quantifying cerebral *macrovascular* bloodflow using CTP: the direct flow model

In order to quantify cerebral macrovascular bloodflow, a model for CBF calculation will be developed. Subsequently, this model will be validated to ensure reliable analysis algorithms. These goals are captured by study objectives 1 and 2.

- 1) Developing the model for the calculation of macrovascular CBF using the *direct-flow principle*
- 2) Validating the direct-flow model with simulation data, a flow phantom and in vivo data

To meet study objective 1, an algorithm is developed to measure CBF in the macrovascular system. The algorithm is based on the assumption that the contrast bolus administered during CTP passes regions of interest (ROI) in a vessel with a constant speed and with a constant shape of the time-density curve (TDC). It is assumed that the only difference in the TDCs is a time shift. The algorithm developed extracts this information from the CTP and transforms it into CBF values. The flow is calculated directly from the CTP data without complex mathematical procedures, therefore the algorithm is called the 'direct flow model'.

To meet study objective 2, the direct-flow model will be validated by means of three short studies called *digital simulation*, *flow phantom* and *In vivo*. While the main objective of all three studies is the validation of the direct-flow model, their objectives also differ on some grounds.

Digital simulation. This study aims to obtain an indication of the required parameter settings. The simulation will show whether a CBF measurement in the macrovascular system is possible using the direct-flow model and parameter settings that are feasible for both data acquirement and data analysis. The simulation can reveal the complexity of CTP data and can give an indication of the required properties of the CTP data for CBF calculation.

Flow phantom. The aim of the study with the flow phantom is to determine the influence of the flow velocity, tube radius, bifurcations and pulsating flow on the results of the direct-flow model. It is assumed that the shape of the TDC may be influenced by the mentioned parameters. The influence of the parameters on both the direct-flow model and the TDC shape can be investigated in a controlled setting. The results may be useful to optimize the direct-flow model.

In vivo data. The aim of the study using *in vivo* data is to evaluate whether the direct-flow model is feasible using this type of real data. The model may be valid in digitally created simulation data or

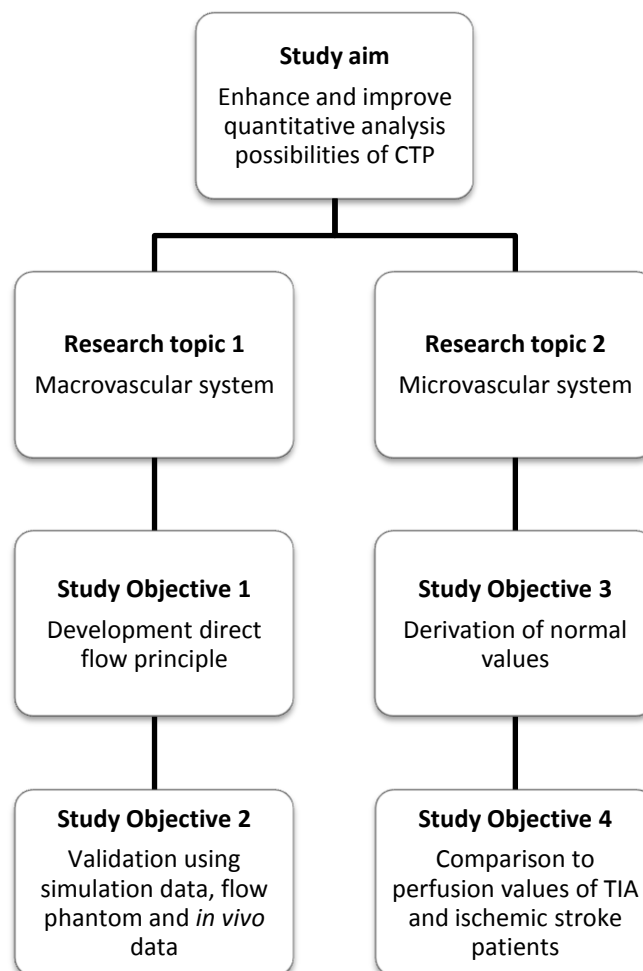
flow phantoms, but those are simplifications of reality. With *in vivo* data, more parameters can be encountered that have an unknown effect on the results.

1.4.2 Establishing normal values of CBF, MTT and CBV in the *microvascular* system

For the microvascular research topic, normal values will be established for CBF, MTT and CBV in the microvascular system. Next, these normal values will be compared with perfusion values of patients with TIA and ischemic stroke. This is captured by study objectives 3 and 4.

- 3) Determining normal values of CBF, MTT and CBV in healthy subjects for several different brain regions
- 4) Comparing normal values to perfusion values of patients with TIA and ischemic stroke

Flowchart 1 represents the study structure, including the research topics and study objectives. The next chapter contains the methods, results and discussion for research topic one. It is followed by a separate chapter covering research topic two.



Flowchart 1. Flowchart presenting the study aim, research topics and study objectives. The research topics are treated in separated chapters.

2. Quantifying cerebral *macrovascular* blood flow using CT perfusion: the direct-flow model

This chapter describes the method, results and discussion of the study objectives related to the first research topic, which was introduced in the previous section.

RT1) Quantifying cerebral *macrovascular* blood flow using CTP: the direct-flow model

First, the procedure to develop the direct-flow model for the calculation of macrovascular CBF will be explained. This will be followed by the procedures for validation of the resulting model.

2.1 Method

2.1.1 Developing the direct-flow model

This section describes the procedure that was used to attain the first study objective.

Developing the model for the calculation of macrovascular CBF using the direct-flow principle.

The development of the model started with the rather general notion that velocity could be calculated by the quotient of distance and the time it took to travel that distance. In the present study, within the context of CBF, this was called the *direct-flow principle*.

The basics of the direct-flow principle

First, the basic idea of the direct-flow model was constructed: the direct-flow principle. The direct-flow principle used the assumption that the TDC that passed a proximal ROI also passed a distal ROI with the same shape but with some time-delay, revealing ascending bolus arrival times along the vessel. Using the direct-flow principle the cerebral blood flow velocity (CBFv) was calculated as the quotient of the geodesic distance between two in-series connected ROIs in a vessel and the time delay of bolus arrival, as shown in equation 16.

$$CBFv = \frac{\text{geodesic distance}}{\text{time delay}} \quad 16$$

Geodesic indicates the distance over the true path that the blood cells followed to flow between two ROI. The geodesic distance was used instead of the straight distance between the ROI. CBFv was transformed to CBF by multiplying it with the cross-sectional area of the vessel, which was calculated using the (mean) radius (r) of the part of the vessel between the two points, as shown in equation 17.

$$CBF = CBFv * \pi r^2 \quad 17$$

ROI selection

Next, a method to define ROI was developed. With the direct-flow model, ROI had to be selected manually. In order to do that, the CT acquisition that was performed at peak intensity was loaded into ITK-SNAP⁹⁹ software (www.itksnap.org). In this software, a voxel could be selected that was located in both the center of the vessel and the desired ROI. Next, the software marked the particular voxel and voxels that lay closely to the selected voxel with a comparative intensity value. Multiple voxels could be selected until a total of exactly 100 voxels was marked. Partial volume averaging should be avoided and checked for visually. The marked voxels together formed a ROI. The

marking of voxels should be iterated at five homogeneously distributed locations in a vessel to form five ROI.

Time delay calculation

Subsequently, an algorithm to calculate time delay of contrast arrival between ROI was created using MATLAB (MATLAB R2013b, The MathWorks Inc., Natick, MA, 2013). The algorithm derived the time delay between ROI using the calculation of the center of gravity (CoG) of the TDC of all ROI. The difference in CoG corresponded to the time delay of contrast bolus arrival. The CoG was the point at which a stand should be placed to keep the area under a curve (in this case the TDC) balanced. A TDC from a point where the contrast bolus would arrive later would have a higher CoG. The CoG could be calculated according to the following equation, with N indicating the number of time points:

$$CoG = \frac{\sum_{t=a}^b t * tdc(t)}{\sum_{t=a}^b tdc(t)} \quad 0 \leq a < b \leq N \quad 18$$

With a and b indicating the last time point before the first moment of contrast arrival and the first time point after the bench point at which most contrast had left the vessel, respectively, and with N indicating the number of time points.

Then, a method to extract the TDC from the CTP data was developed. The direct-flow model extracted the TDC of the voxels in the ROI using MATLAB. CTP data could be loaded into MATLAB and the intensity values of the voxels within the ROI could be saved for every time point. The TDC should be created per voxel by plotting the time points versus the intensity. The average TDC of all voxels in a ROI should be calculated and this could be used for time delay calculation.

Distance calculation

After that, an algorithm to calculate the distance between ROI was constructed. In order to do that, first, a method to distinguish the vessel from the surrounding tissue was needed. Segmentation of blood vessels could be performed using a region growing algorithm offered by MeVisLab software (MeVisLab 2.6.1, MeVis Medical Solutions AG and Fraunhofer MEVIS in Bremen, Germany). Using that algorithm the user put a marker on a voxel in a vessel. If the marked voxel had an intensity value within a patient and session dependent range, the voxel got a positive value in the segmentation mask. Next, the intensity of the direct neighboring voxels was analyzed automatically by the algorithm. The neighbors with an intensity value within the specified range also got a positive value in the segmentation mask. The algorithm was finished when no more neighbors with an intensity value in the specified range could be found. As a result, the positive valued voxels in the segmentation mask represented the structure of interest, in this case (a part of) the vessel tree, as shown in figure 8.

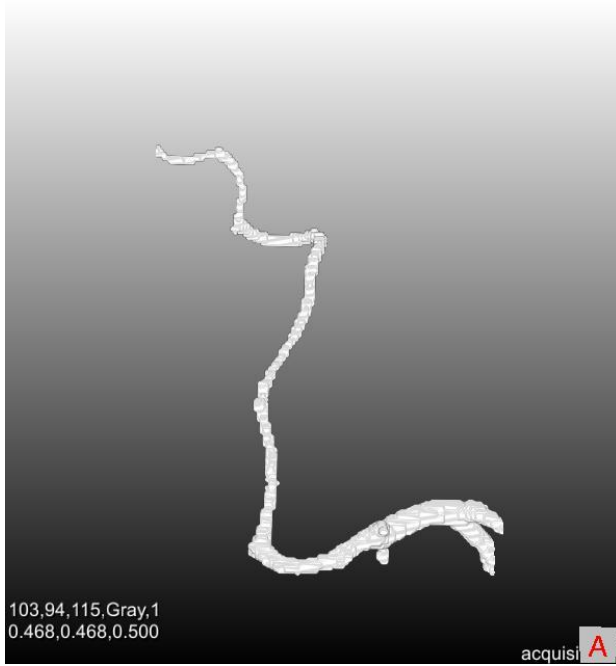


Figure 8. Segmentation of the right medial cerebral artery using the region growing algorithm.



Figure 9. Skeleton of a segmented left medial cerebral artery using the skeletonization algorithm.

Then, a method to transform the segmented vessel to a skeleton was used. A skeletonization algorithm was developed using MeVisLab software. The skeletonization algorithm resulted in a centerline of the segmented vessel (figure 9) obtained with the region growing algorithm. The centerline followed the path with the highest intensity, which was the path with the highest blood flow. This usually corresponded to the center of the vessel, but at vessel curves or pathological deficits such as stenoses, the centerline might deviate from the center. Nevertheless, the centerline still followed the path that the major part of the blood travelled, so the distance calculated was the distance the blood truly travelled. The centerline branched when the segmentation branched and stopped when the segmentation stopped. The centerline consisted of many connections between neighboring voxels, which were called skeletons. The voxels at which the centerline bifurcated was called a node and the set of skeletons between two nodes was called an edge, see figure 10. The straight distance d between two skeletons s_1 and s_2 could be calculated using a Pythagorean method:

$$d = \sqrt{(s_{1,x} - s_{2,x})^2 + (s_{1,y} - s_{2,y})^2 + (s_{1,z} - s_{2,z})^2} \quad 19$$

Subsequently, the length of the edges was determined by summation of the distances d between the skeletons present in that edge. Next, the total vessel length could be calculated by summation of the length of the edges that were part of the centerline. Now, a method was invented to extract the right part of the total vessel length. As described before, the ROI should be manually selected in the vessel of interest and did not necessarily represent points on the centerline. Therefore an algorithm was constructed to find the point on the centerline that is located the closest to the ROI. This point was found for the second ROI as well. Then, the distance between ROI was calculated as the distance between the two points on the centerline. The algorithm was implemented in MATLAB and explained below as a roadmap.

1. The CT scan created at peak contrast enhancement was loaded. The ROIs were selected and the region growing and skeletonization algorithms were performed.
2. The distance between all neighboring skeletons was calculated.
3. The length of the edges were calculated as the distance between nodes by the sum of the distances d (equation 19) between skeletons that lay between the nodes.
4. The distance between the coordinates of the ROI and skeleton were calculated for every skeleton and were recorded.
5. The skeleton with the smallest distance to the ROI was recorded. The edge it belonged to was also recorded. A distance less than 0.5 cm was correct; a larger distance indicated that the ROI and centerline were not selected in the same vessel.
6. The distance between the recorded skeleton and the first node in the direction of the second ROI was calculated by the sum of the distances d between the skeletons between the node and the recorded skeleton.
7. Performed steps 1 to 6 for the second ROI
8. The distance between ROI was calculated as the sum of the complete edges between the ROI and the two incomplete edges at both tails of the centerline.

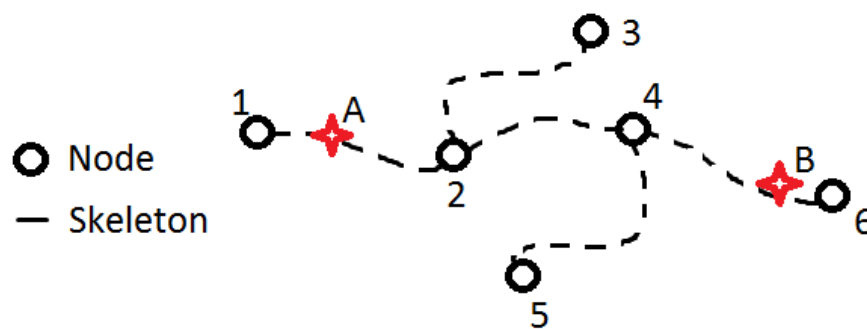


Figure 10. Schematic representation of the skeletonization of a vessel and the calculation of the distance between two regions of interest. First, the skeleton closest to the regions of interest (A and B) was calculated. Next, the distance to the closest node in the direction of the other region of interest was determined (2 and 4). Subsequently, the total distance between the ROIs was calculated by summation of the edge parts and the edges in between (edge between nodes 2 and 4). Concluding, the distance between ROI A and B was calculated as the sum of the distances between A and 2, 2 and 4 and 4 and B. Nodes 3 and 5 did not lay on the centerline and were therefore ignored. Node 1 and 6 were located outside the range that the ROI were selected in.

2.1.2 Validating the direct-flow model

This section describes the method to reach the second study objective.

Validating the direct-flow model with simulation data, a flow phantom and in vivo data

The direct-flow model (figure 13) is shown in the results section 2.2.1. Three studies were conducted to validate this model, working towards validation of *in vivo* data. Below, the study procedures regarding the simulation, the flow phantom and the *in vivo* data are described. The first step towards *in vivo* validation was the application of the direct-flow model to simulated data.

Simulation data

Study protocol

TDC were digitally created using MATLAB. For every simulation two TDC were created that represented the TDC of a proximal and distal ROI. They had a time delay that was calculated using physiologically reasonable parameters. The variable parameters of the simulation were the amplitude, time delay, ROI distance, CBFv, sample frequency and signal-to-noise ratio (SNR). Different combinations of parameter settings were used to detect the limits where reliable results could still be obtained.

The digitally created TDC were based on a sine wave and were adjusted to a real-TDC mimicking curve, according to equation 20.

$$time\ density\ curve = w + amp * \sin\left(\frac{3}{2}\pi - \frac{t - td}{\pi}\right) + amp \quad 20$$

For time t from 0 to 19,8s with steps according to $\frac{1}{fs}$. w indicated white noise; amp , amplitude; fs , sample frequency in Hz and td , time delay in s.

Adequate time delay was calculated with the quotient of a physiologically reasonable distance between ROI and CBFv:

$$td = \frac{ROI\ distance}{CBFv} \quad 21$$

td indicated time delay; ROI distance, distance between ROI in a vessel and CBFv, cerebral blood flow velocity.

The TDC were multiplied with white noise to mimic TDC that may be present in *in vivo* data. Noise was called 'white' when no correlation between time points existed and the only constraint was the range of the values. Noise was added to the TDC and was created using the MATLAB function 'rand'. The amplitude of the noise was chosen according to the signal-to-noise ratio (SNR) of *in vivo* data. The SNR was estimated using the red wiggle at $t = 6s$ in figure 24. There, the local maximum seemed to overestimate the intensity about 20 Houndsfield units (HU), corresponding to 10% of the maximum intensity of the most distal ROI, resulting in a signal-to-noise ratio of 10:1. The proximal ROI showed larger amplitudes and therefore the SNR was approximately 5%. Therefore noise amplitude was chosen 5-10% of amp , which corresponded to an SNR of 5% for proximal ROI and 10% for distal ROI.

Simulation settings

The first simulation was performed with the parameters set to the value most frequently found in *in vivo* data, i.e. true CBFv = 50 cm/s; distance between ROI = 10 cm; amplitude TDC2 = $\frac{1}{2}$ amp TDC1, $fs = 2$ Hz and SNR = 5% for TDC1 and 10% for TDC2. According to equation 21, the time delay between TDC was 0.2 s. The simulation was iterated 100 times to investigate the repeatability. The simulation was performed with both complete TDC and incomplete TDC that only included the first 12 seconds, because for some *in vivo* data only half of the TDC was available. The results are presented in boxplots and graphs with the TDC.

Next, the simulation parameters were altered in a range that was physiologically or technically possible, as presented in table 6. The distance between ROI was altered to 20 cm and the scanning frequency was improved to 10 Hz. Moreover, the CBFv was increased incrementally to 200 cm/s to simulate flow in a pathological narrowed vessel. Several combinations of changes were applied. The SNR, amplitudes and number of iterations were kept constant.

Table 6 Overview of simulation sessions. fs indicates sample frequency (Hz); CBFv, cerebral blood flow velocity (cm/s); distance, distance between ROI (cm) and SNR, signal-to-noise ratio (%).

Session	fs (Hz)	Distance (cm)	True CBFv (cm/s)	SNR (%)	Iterations
1	2	10	50	5-10	100
2	2	20	50	5-10	100
3	10	10	50	5-10	100
4	10	20	50	5-10	100
5	10	20	60	5-10	100
6	10	20	75	5-10	100
7	10	20	100	5-10	100
8	10	20	150	5-10	100
9	10	20	200	5-10	100

Data analysis

The time delay of contrast arrival between ROI was calculated according to the direct-flow model, as presented in figure 13. The distance between ROI was preset. The CBFv was calculated as the quotient of the distance between ROI and the time delay of contrast arrival. A result was considered satisfying when it showed a CBFv that was similar to the CBFv that was used as input parameter.

Flow phantom

The next step towards in vivo data was the application of the direct flow model to measurements in a fully controlled setting. Using a phantom, a large set of variables such as tube radius and fluid flow could be controlled, that were not controllable in a human subject. The phantom served as a simplification of the human cerebral macrovascular system.

Phantom

The phantom was created in the Radboud UMC using materials that were destined for extracorporeal membrane oxygenation (ECMO). It consisted of a centrifugal pump (mimicking the heart) connected to a network of tubes (mimicking the larger vessels of the brain), as schematically drawn in figure 11a. The pump and network were connected to a heart-lung machine that was able to control the pump. The pump was able to generate flows up to 8 l/min and could create a pulsatile flow. The tubes were transparent and a bit compliant. The network existed of tubes with radii varying from 3/8 inch to 3/16 inch (0.476 cm to 0.635 cm) and contained multiple bifurcations. To select specific regions to where the fluid should flow, the network could be closed everywhere using clips. Furthermore, the phantom contained a 3-way tap to administer the contrast agent and a fluid reservoir to deal with the increasing volume at contrast injection. A second advantage of the fluid reservoir was that it enlarged the total volume of the system which prevented contrast recirculation during CT scanning.

Study protocol

The CT scanner used in the Radboud UMC was a Toshiba Aquilion One, which created 900 projections per rotation in 0.275 seconds. The CT scanner had a detector consisting of 320 rows with 0.5 mm slice thickness, which resulted in a 512x512x320 matrix with voxels of 0.5x0.5x0.5 mm, covering 16 cm. Since the radiation would not be dampened by the phantom, the tube current and tube voltage were kept low. The scanning frequency was set to continuous scanning, resulting in 3.63 scans per second. The CT scanner also offered the possibility to use projection data to calculate higher frequencies. Total scanning time was 15 seconds. The contrast agent was a nonionic iodinated fluid (300-370 mg%) that was diluted 1:10 using 0,9%NaCl. The contrast agent dilution was injected at a rate of 5 ml/s during 5 seconds, followed by a 2 ml/s flush bolus using 0,9%NaCl during 2 seconds. Scanning was started 10 seconds after the start of contrast injection.

Four consecutive scan sessions were performed, according to table 7. The content of the phantom was refreshed after every scan to erase all contrast from the phantom. Several parts of the phantom were scanned during the same session to save materials. The first scanning session was aimed at setting a baseline and consisted of a straight tube and the thick bifurcation, as shown in figure 11b. The branch to the small bifurcation was clipped. The flow from the pump was set to 1000 ml/min, which resulted in a flow velocity of 53 cm/s in the straight tube and a flow velocity of 26 cm/s in both branches of the thick bifurcation. The second session consisted of the straight tube, which was curled in the scanner zone to increase tube length, and the small bifurcation. The branch to the thick bifurcation was clipped. The flow from the pump was 1000 ml/min, which resulted in a flow velocity in the straight tube of 53 cm/s and a flow velocity of 31 cm/s in both branches after the small bifurcation. The third session was aimed at comparing flow velocity and consisted of the curled straight tube and both bifurcations. No parts of the phantom were clipped. The flow from the pump was increased to 2000 ml/min, which resulted in a flow velocity of 105 cm/s in the straight tube, 36 cm/s in the branches after the thick bifurcation and 30 cm/s in the branches after the thin bifurcation. The final scanning session was aimed at comparing continuous and pulsating flow and consisted of the curled straight tube and the thin bifurcation. The branched of the thick bifurcation were clipped. The pump produced a pulsating flow of 1000 ml/min. The velocities in the tubes could not be determined.

Table 7. Overview of flow phantom scanning sessions. Radius comparison was performed using tubes with two different radii. Flow and velocity was compared using different flows from the pump and different radii. Pulsating flow was compared to continuous flow using the pulsating function of the pump. Thick indicates the tube with a diameter of 0.635 cm; thin, the thin tube with a diameter of 0.476 cm and bif, bifurcation.

Scan session	Aim	Included tubes	Flow (from pump; ml/s)	Velocity (per tube; cm/s)
1	Set baseline, influence of bifurcation	Bifurcation of thick tube	1000	thick: 52 thick bif: 26
2	Radius comparison	Bifurcation of thin tube	1000	thick: 53 thin bif: 31
3	Flow and velocity comparison	All	2000	thick: 105 thick bif: 36 thin bif: 30
4	Influence of pulsating flow	Bifurcation of thin tube	1000	Unknown

Data analysis

After the image acquisition the data passed a noise filter. Next, the scans were reconstructed twice using scanning frequencies of 2 Hz and 10 Hz, respectively. Subsequently, the direct-flow model was used to calculate flow velocity and flow. For every scanning session, five ROI were placed in the straight tube, six ROI were placed around the bifurcation and 5 ROI were placed in one of the branches after the bifurcation.

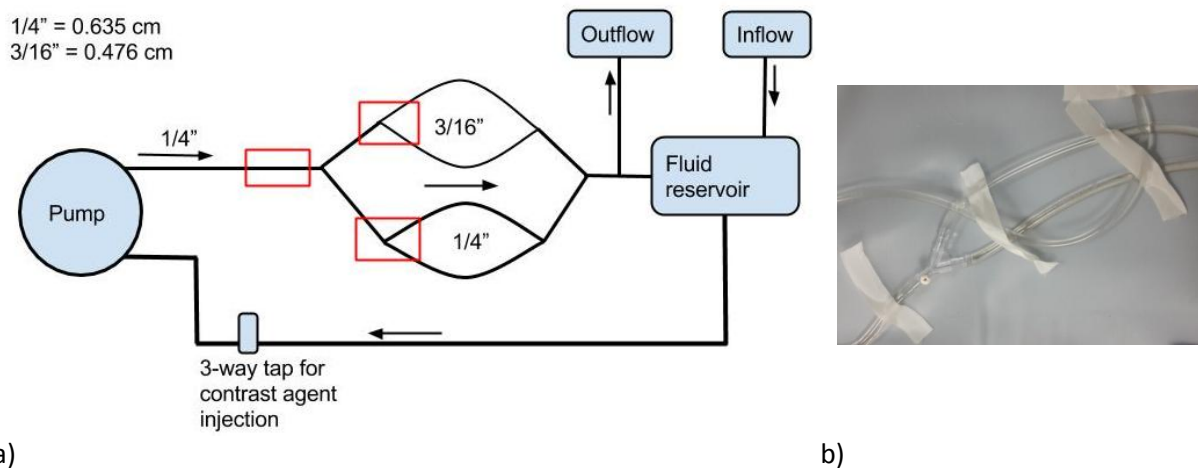


Figure 11. a) Schematic representation of the flow phantom. A pump was connected to a network of tubes with radii of $\frac{1}{4}$ " and $\frac{3}{16}$ " (0.635 cm and 0.476 cm) and two bifurcations. The fluid reservoir was used to increase phantom volume and to handle the volume increase after contrast injection, the 3-way tap was used for the contrast injection and the inflow and outflow were used to refresh the phantom in between measurements. The red squares indicate sides that were of interest for the CTP measurement. b) Photo of the placing of the phantom during session 1, with the straight tube and the thick bifurcation. The tape was used to fix the tubes to the scanning table.

In vivo data

Population

The direct-flow model was tested in *in vivo* data of healthy subjects and arteriovenous malformation (AVM) patients. The healthy subjects were used because it might be assumed that their cerebral hemodynamics were normal. This was required to compare the results to CBFv values found in other studies. However, the CT scanning frequency applied to healthy subjects was 0,5 Hz. In order to obtain data fulfilling the, according to the digital simulation results, required CT scanning frequency, results from AVM patients were used. The definition of AVM is 'an abnormal tangle of vessels that results in arteriovenous shunting'.¹⁰⁰ The perfusion CT was indicated to detect possible shunts from an artery to a vein. The disadvantage of AVM patient data was that only the rising part of the TDC was needed for clinical practice. Therefore, to limit the radiation dose, the scanning was stopped a few seconds after the peak intensity was reached and thus only the half TDC was measured.

Patients were identified from a database containing all CTPs performed between January 2014 and June 2015. General indications for a CTP were clinical signs and symptoms of stroke or AVM.

General inclusion criteria

- CTP of adequate quality for quantitative analysis, without clips, coils or drainage tubes or other imaging artefacts in the region of interest
- CT perfusion within 9 hours after onset of symptoms

- Stable vital signs
- Age > 17 years

Healthy subjects

- No signs compatible with recent ischemia on CT or CT angiography (CTA), and no perfusion defects on CTP
- Other identified, non-vascular cause of the clinical symptoms and signs
- No other concomitant neurological disease, known to compromise cerebral blood flow

AVM patients

- Diagnosed with AVM
- CT sample frequency of 2 Hz
- Availability of projection data

General exclusion criteria

Patients meeting one or more of the following criteria were excluded from the study:

- Stroke based on or accompanied by hemorrhage
- Presence of tumor lesions, other pathologic malformations in the brain
- Unstable vital signs, requiring support by using airway devices, supply of > 5 l O₂/min, or any hemodynamic support.

In this study one healthy subject and two AVM patients were included.

Study protocol

For this study two different scanning protocols were used. Firstly, for the healthy subject the stroke protocol was used, in which a baseline scan was performed after 4 s. This was followed by 13 scans every 2 seconds covering the arterial part of the TDC, and 5 scans every 5 seconds to cover the venous outflow (figure 12). The total scanning time was 60 seconds. Five seconds prior to the scan, a bolus of 50 ml nonionic contrast agent (300 mg iodine/ml Iomerol 300) was injected into an antecubital vein at a rate of 5 ml/s followed by a 40 ml saline flush at the same rate. The CTP acquisitions were registered to correct for patient motion.

Secondly, for the AVM patients the CTP protocol for AVM was used. First, 50 ml nonionic contrast agent was injected at a rate of 5 ml/s. After 5 seconds, an acquisition was created every 0.5 second until the TDC peak was reached, after which the protocol was stopped. For the 2 AVM patients 25 and 21 acquisitions were created, respectively.

Data analysis

The direct-flow model was used to calculate CBF_v in all data sets. The vessels of interest were the left and right MCA. In both vessels 5 homogeneously distributed ROI were selected distal from the circle of Willis. Care was taken that the voxels were completely included in the vessel. Each ROI consisted of 100 voxels.

For the healthy subject the time delay between the internal carotid artery (ICA) and the jugular vein was calculated. From literature it was known that blood flow through a capillary bed might take about 10 seconds,³¹ so it should be possible to acquire this time delay with a low time resolution.

ROIs were created in bilateral ICA, basilar artery and bilateral jugular veins to acquire the time delay. Intensity values were extracted for every time point and TDCs were created. It was not possible to calculate the distance between these ROI, because the skeletonization algorithm was not applicable to capillaries. Therefore it was not possible to calculate the CBFv or the CBF.

Repeatability

The study repeatability of the direct-flow model was iterated five times for the left MCA using the projection data of the AVM patient. The only difference between analyses was the location of the ROI. The ROI of the iterations were shifted distally in such a way that the ROI of iterations were connected, but not overlapping. A repeatable mode would show similar CoG trends between the iterations and similar distances between the ROI.

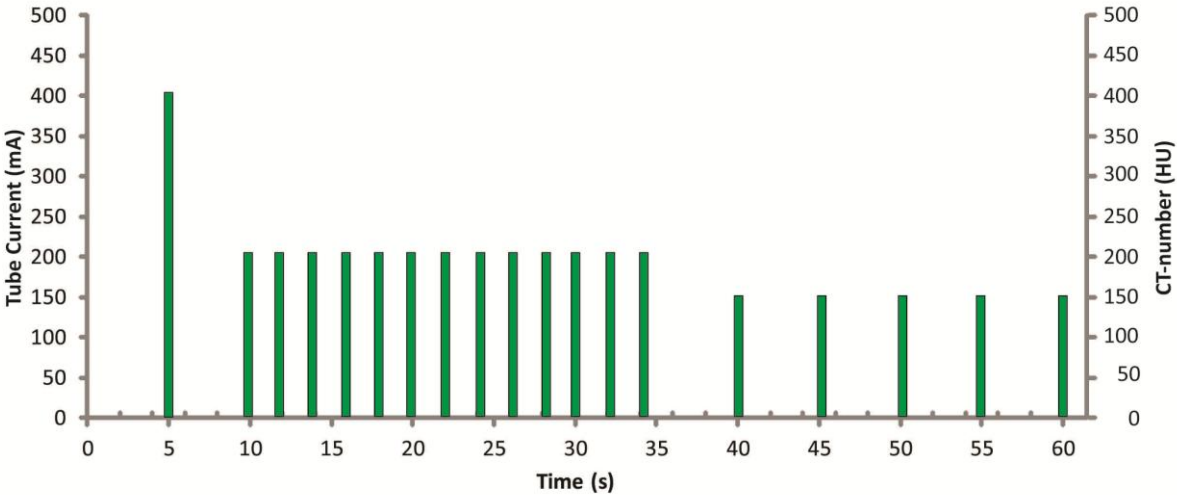


Figure 12. CT perfusion stroke protocol. Five seconds after contrast agent bolus administration an unenhanced CT image was created. Followed by 13 CT scans every 2 seconds to cover the flow of contrast through the arterial system and 5 CT scans every 5 seconds to cover the flow of contrast through the venous system. The sample frequency of this protocol was 0.5 Hz for the flow through the arterial system.

2.2 Results

2.2.1 Developing the direct-flow model

In this section the results of the first study objective are presented.

Developing the model for the calculation of macrovascular CBF using the direct-flow principle

The direct-flow model was developed and is presented as workflow in figure 13. The input in the workflow should be preprocessed CTP data. Preprocessing included at least registration of the acquisitions. Next, to obtain the CBF, ROI should be selected and both the distance between ROI and the time delay of contrast arrival between ROI should be calculated. The calculation of the distance between ROI and the time delay of contrast arrival between ROI both covered a branch of the workflow. The branches finally reunited when calculation of CBFv could be performed. If the CBFv value was reliable, it was used to calculate CBF, using the average radius of the vessel. The workflow also presents the software in which the steps are executed.

Direct-flow model

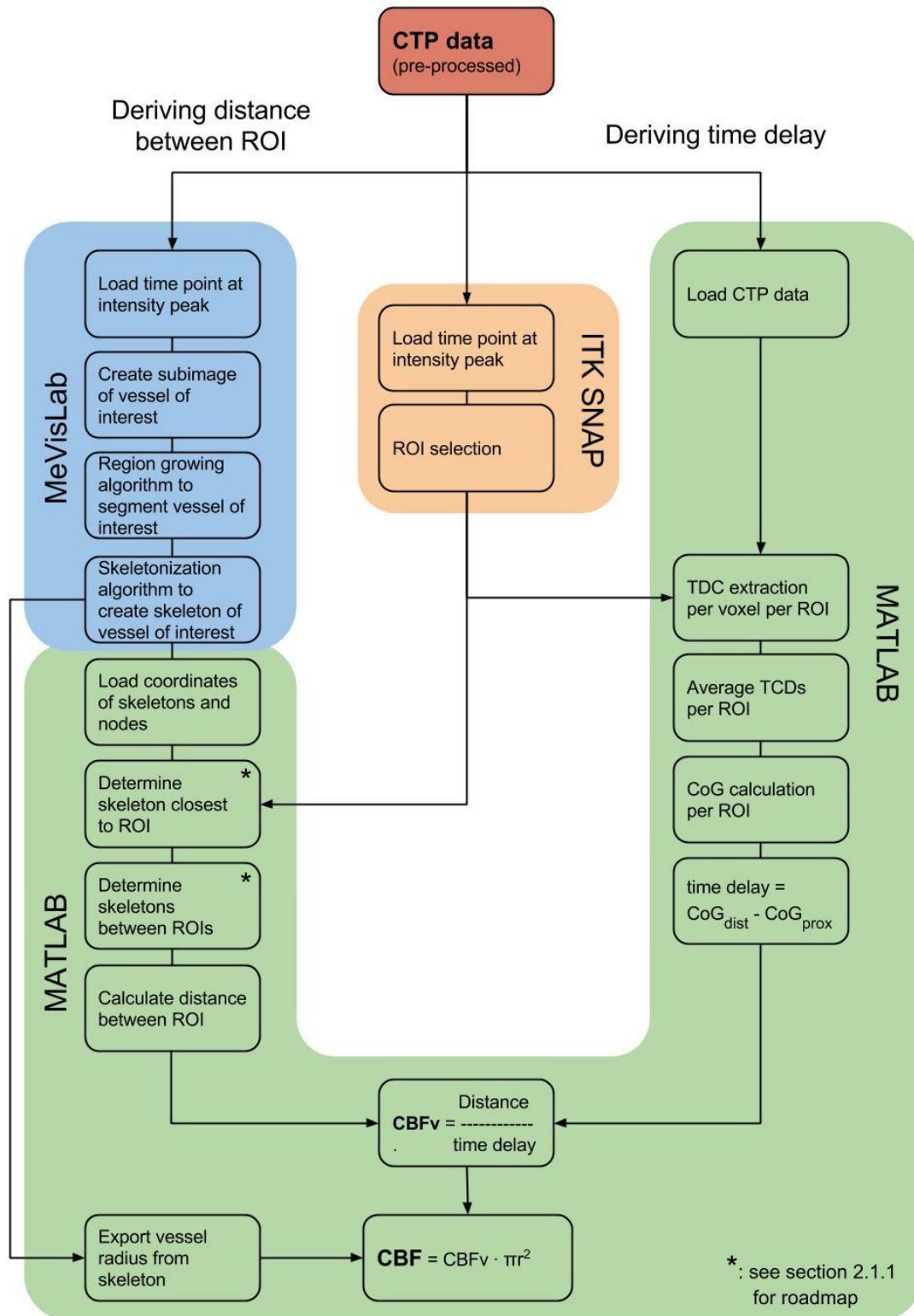


Figure 13. Workflow of the direct-flow model. The model used the direct-flow principle, which stated that CBF_v could be calculated using the quotient of the distance between ROI and time delay of contrast arrival. Both the distance between ROI and the delay of contrast arrival covered a branch of the workflow and reunited to calculate CBF_v and subsequently CBF. ROI indicates region of interest; CoG_{dist} , center of gravity (s) of distal ROI and CoG_{prox} , center of gravity of proximal ROI.

2.2.2 Validating the direct-flow model

In this section the results of the second study objective are presented.

Validating the direct-flow model with simulation data, a flow phantom and in vivo data

Consecutively the results of the simulation, the flow phantom and the *in vivo* data are described. To obtain the results of the three validation studies, the workflow that resulted from the first study objective was used. The workflow is presented in figure 13.

Simulation data

Application of equation 20 resulted in TDC that mimicked true TDC, as shown for both TDC with and without noise in figure 14. The time delay between the TDC without noise was small, but visible and the difference between CoG of both TDC was approximately the true time delay of 0.20s. The time delay between the noisy TDC was not visible, but the difference in CoG revealed that the time delay was present and was 0.18s, which was close to the true time delay of 0.20s.

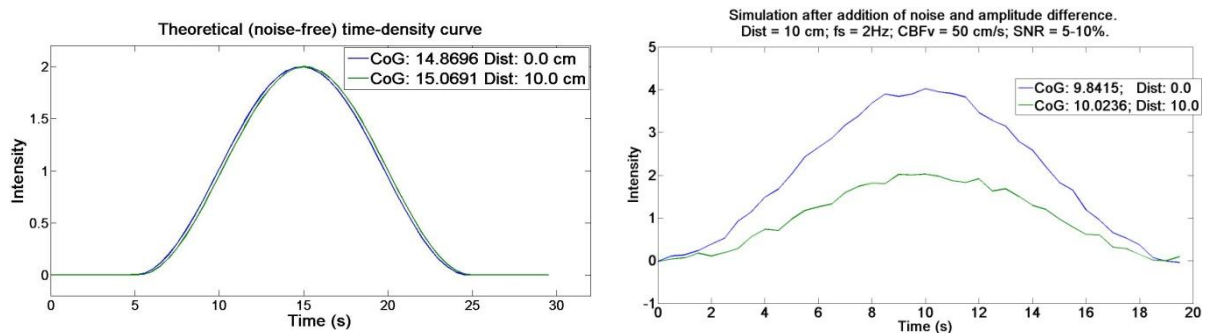
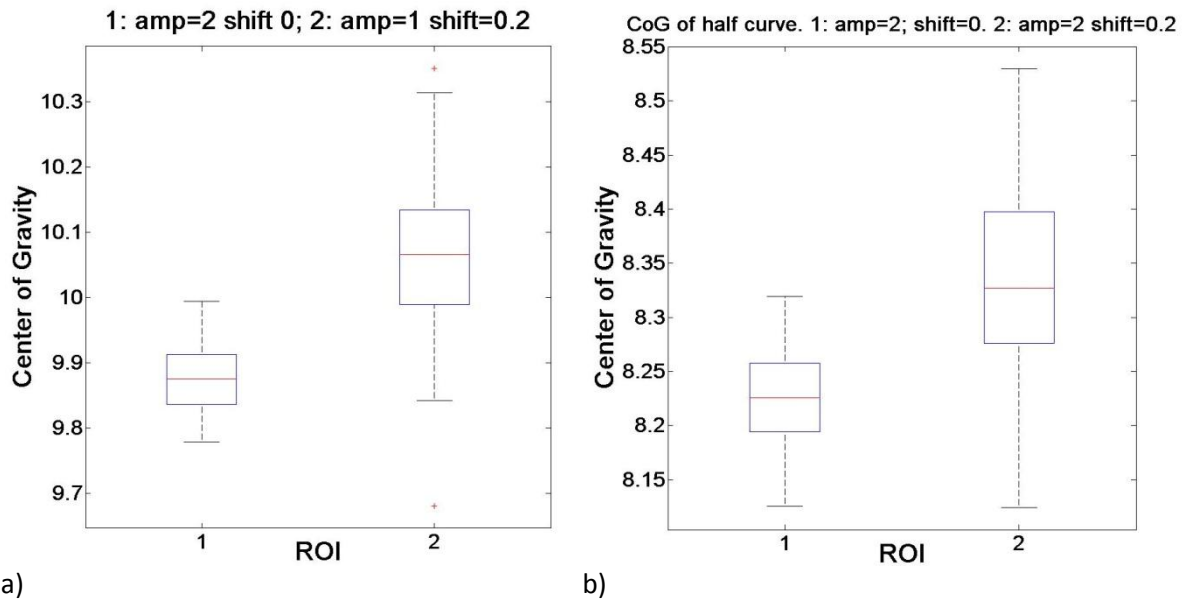


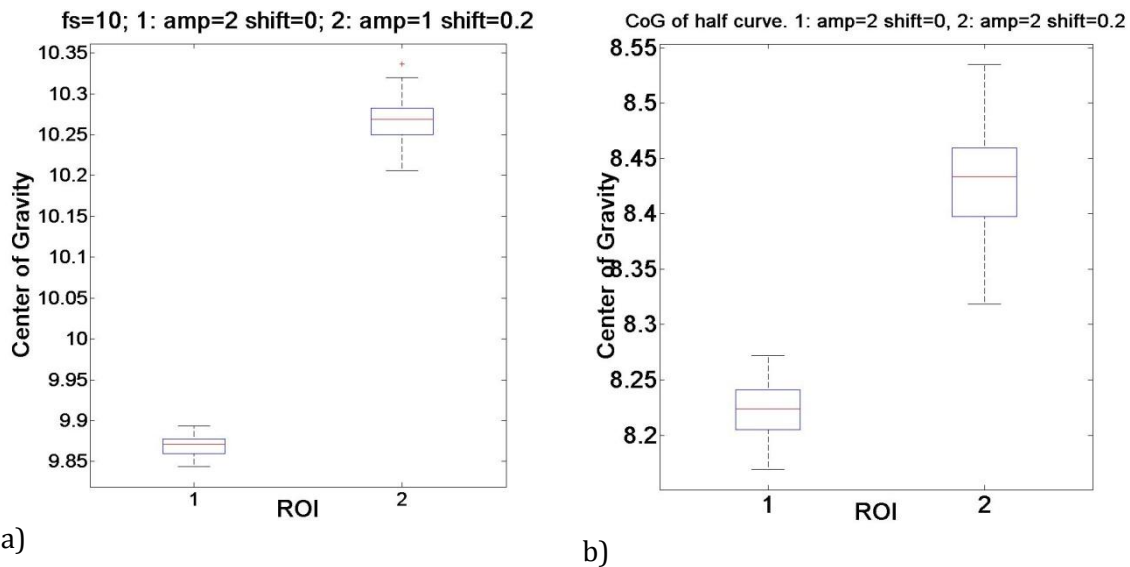
Figure 14. Simulation data. a) Simulations without noise and without amplitude variance showed the perspective of the direct flow principle. Despite a bad time resolution the time delay between the ROI could be calculated using CoG. b) The time delay was visually absent after addition of noise and amplitude variance, but the CoG was still showing a time delay corresponding to the true time delay. CoG indicates center of gravity (s); fs, sample frequency; SNR, signal-to-noise ratio and dist, distance (mm).

The resulting boxplots for the first simulation are shown in figure 15. For both the complete and incomplete TDC the CoG of the distal TDC were higher than the CoG of the proximal TDC. However, the boxplots overlapped, suggesting that a large deviation from the true time delay was possible and that even a negative time-delay and therefore negative CBFv could have occurred. The overlap of boxplots increased for the CoGs based on in-complete TDC. These results showed that the direct flow principle was not applicable with the parameters as set for this simulation.

Alteration of the simulation parameters improved the results. The distance between the ROIs was doubled to 20 cm and the scanning frequency was increased to 10 Hz. Except from the changes mentioned, the same simulation was executed. The resulting boxplots, presented in figure 16, showed less variation in CoG and did not overlap for both the complete and the in-complete TDC. The difference between CoG of both TDC was close to the true time delay.



a) b)
Figure 15. a) Boxplots for the first simulation with TDC with parameter values of respectively: amplitude = 2 for TDC1 and 1 for TDC2; time delay=0.2s; SNR=5% for TDC1 and 10% for TDC2; fs=2Hz; N=100 and the full TDC was used for CoG calculation. The boxplots showed a higher CoG for TDC2, representing the distal ROI. This difference was not significant and it was possible that the second ROI has a lower CoG than the first row, resulting in a negative CBFv. b) Boxplots of TDC with the same parameter values as in figure a, but with less time points causing a calculation of CoG using only the first half of the TDC. The CoG of the distal ROI was still higher, but the difference was decreased. The parameters used were not reliable for CBF measurements. CoG indicates center of gravity (s); amp, amplitude; shift, time shift (s) and ROI, region of interest.



a) b)
Figure 16. Boxplots presenting the results of the simulation with improved parameter values. The distance between ROI was doubled to 20 cm and the scanning frequency was improved to 10 Hz. The remaining parameters were kept constant. a) Boxplots presenting the CoG using the complete TDC. The boxplots did not overlap and showed an average CoG difference of 0.4s, which corresponded to the true time delay. b) Boxplots presenting the CoG using the first half of the TDC. The boxplots were not overlapping. CoG indicates center of gravity (s); amp, amplitude; shift, time shift (s); fs, sample frequency (Hz) and ROI, region of interest.

The results of the iterative simulation of several combinations of parameter settings are presented in table 8. The difference in CoG between the TDC was converted to CBFv. An increase in distance between ROI showed an improvement of mean velocity calculation if the complete TDC was used. Improvement of the scanning frequency improved CBFv results. A combination of distance and scanning frequency alteration showed a CBFv that matched best with the input CBFv. Increase of the

input CBFv resulted in adequate calculations of the CBFv up to 100 cm/s. Input CBFv of 150 and 200 cm/s showed large SD that might influence CBF calculation largely. Use of incomplete TDC resulted in overestimation of CBFv values and large SD.

Table 8. Results of simulation data analysis with varying settings of parameter values. Every session 100 iterations are performed. The SNR was 10% for the proximal ROI and 5% for the distal ROI. The results for both the full TDC analysis as for the half TDC analysis are given. Results are presented as mean (SD). N indicates number of iterations; fs, sample frequency (Hz); CBFv, cerebral blood flow velocity (cm/s); SNR, signal-to-noise ratio (%); SD, standard deviation and half, half time-density curve.

Settings				Results	
Session	fs (Hz)	Distance (cm)	True CBFv (cm/s)	Mean measured CBFv (cm/s)	Mean measured CBFv half (cm/s)
1	2	10	50	54 (16)	80 (395)
2	2	20	50	52 (7)	109 (33)
3	10	10	50	50 (6)	104 (29)
4	10	20	50	50 (3)	102 (10)
5	10	20	60	60 (5)	121 (17)
6	10	20	75	75 (8)	155 (28)
7	10	20	100	102 (13)	216 (55)
8	10	20	150	154 (29)	343 (157)
9	10	20	200	212 (60)	713 (2194)

Flow phantom

The direct-flow principle was successfully applied to the different parts of the phantom. All ROI presented a TDC with a steep intensity increase at contrast bolus arrival, followed by a less steep intensity decrease at contrast outflow, of which an indication is given in figure 17. Some of the TDC presented a jerky curve, while others were smooth. No differences were found between the data obtained by the 2 Hz and 10 Hz, therefore the results obtained with the 10 Hz data are presented. The results regarding the flow and flow velocity comparison is presented in table 9. The results regarding the continuous and pulsating flow are presented in table 10.

Table 9. Results of flow velocity calculation using the direct-flow principle for varying tube radii, ROI distance, flow and therewith flow velocity. The calculated flow velocities showed a large overestimation of the true flow velocities. CoG indicates center of gravity (s) and ROI, region of interest.

Settings					Results		
Session	Tube diameter (cm)	True flow (ml/min; x10 ³)	True flow velocity (cm/s)	ROI distance (cm)	Time delay CoG (s)	Direct-flow principle velocity (cm/s)	Relative velocity (% of true velocity)
1	0.635	1,00	53	25	0.24	104	200
1	0.635	0,50	26	17	0.27	55	212
2	0.635	1,00	53	65	0.57	114	219
2	0.476	0,50	31	13	0.18	72	232
3	0.635	2,00	105	81	0.34	237	226
3	0.635	0,69	36	20	0.33	60	167
3	0.476	0,32	30	18	0.24	73	243

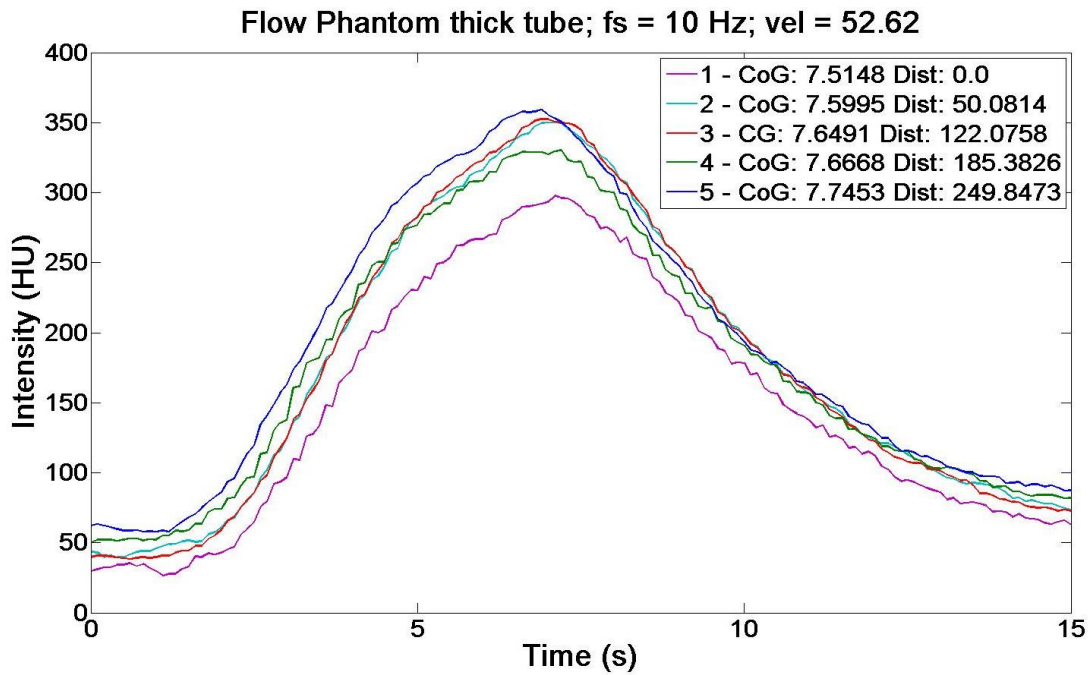


Figure 17. TDCs obtained from ROI in the straight thick tube with a flow of 1.0 l/min and a flow velocity of 52 cm/s. A time delay between TDC and an increasing trend of CoG values were visible. However, the calculated flow velocity was not in accordance with the true flow velocity. The TDC were sampled with 10Hz. CoG indicates center of gravity (s); Dist, distance (mm).

Session 1 showed a calculated flow velocity of 104 cm/s in the straight tube, which was 200% of the true flow velocity. The ROI were separated 25 cm. The maximum amplitude in the straight tube was 359 HU. The calculated flow velocity in the branch after the bifurcation was 55 cm/s, which was 212% of the true flow velocity. The ROI were separated 17 cm. The analysis of the ROI around the bifurcation did not result in clear TDC shape differences. The TDC differed in intensity values at baseline and at peak intensity.

Session 2 showed a calculated flow velocity of 114 cm/s in the straight tube, which was 219% of the true flow velocity. The ROI were separated 65 cm. The maximum amplitude in the straight tube was 398 HU, as shown in figure 18. The calculated flow velocity in the branch after the thin bifurcation was 72 cm/s, which was 232% of the true velocity. The ROI were separated 13 cm. The analysis around the bifurcation did not show large differences in shape of TDC, except for the ROI in the common tube, which has a lower intensity over the complete time coverage, as shown in figure 19.

Table 10. Results of both continuous and pulsating flow for the same parts of the phantom. No differences were found. C indicates continuous; P, pulsating and CoG, center of gravity (s).

Flow method	Tube diameter (cm)	True flow (ml/min; $\times 10^3$)	True mean flow velocity (cm/s)	ROI distance (ROI 1 – ROI 5; cm)	Time delay CoG (s)	Direct-flow principle velocity (cm/s)	Direct-flow principle velocity (% of true velocity)
C	0.635	1,00	52	65	0.57	114	219
C	0.476	0,50	46	13	0.18	72	157
P	0.635	1,00	52	67	0.66	102	196
P	0.476	0,500	46	14	0.18	78	170

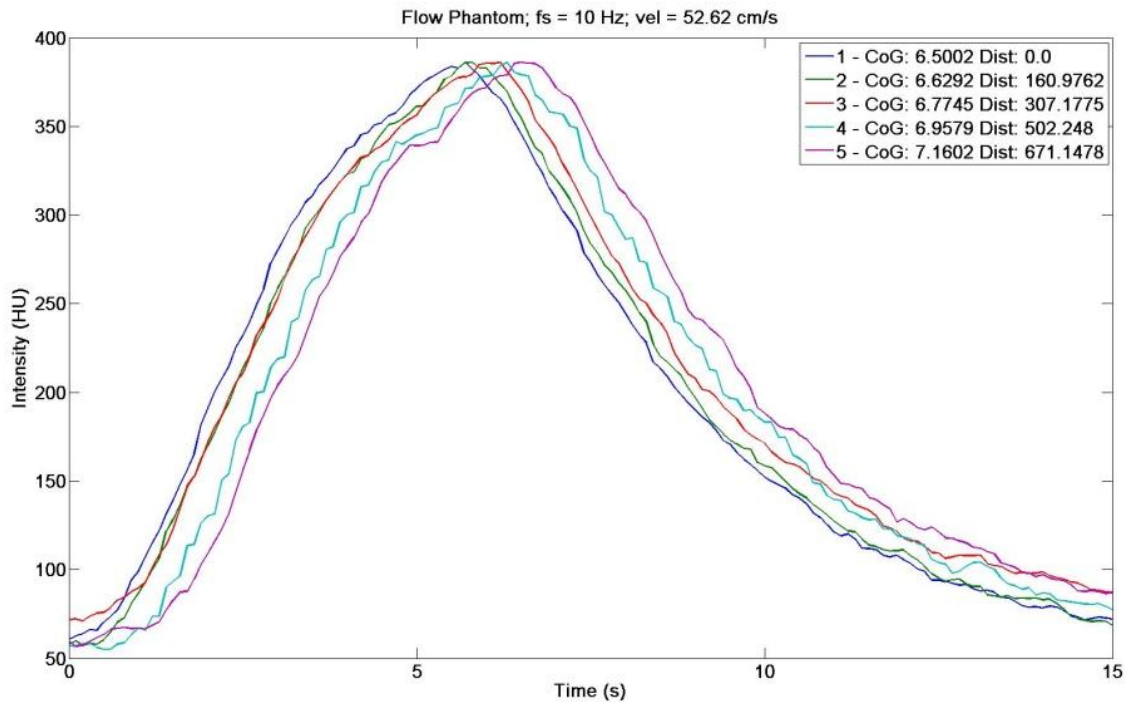


Figure 18. TDC acquired during pulsating flow in the straight thick tube. No clear differences with respect to continuous flow were present. The CoG showed an increasing trend along the vessel and the calculated flow velocity overestimated true velocity. CoG indicates center of gravity (s); Dist, distance (mm).

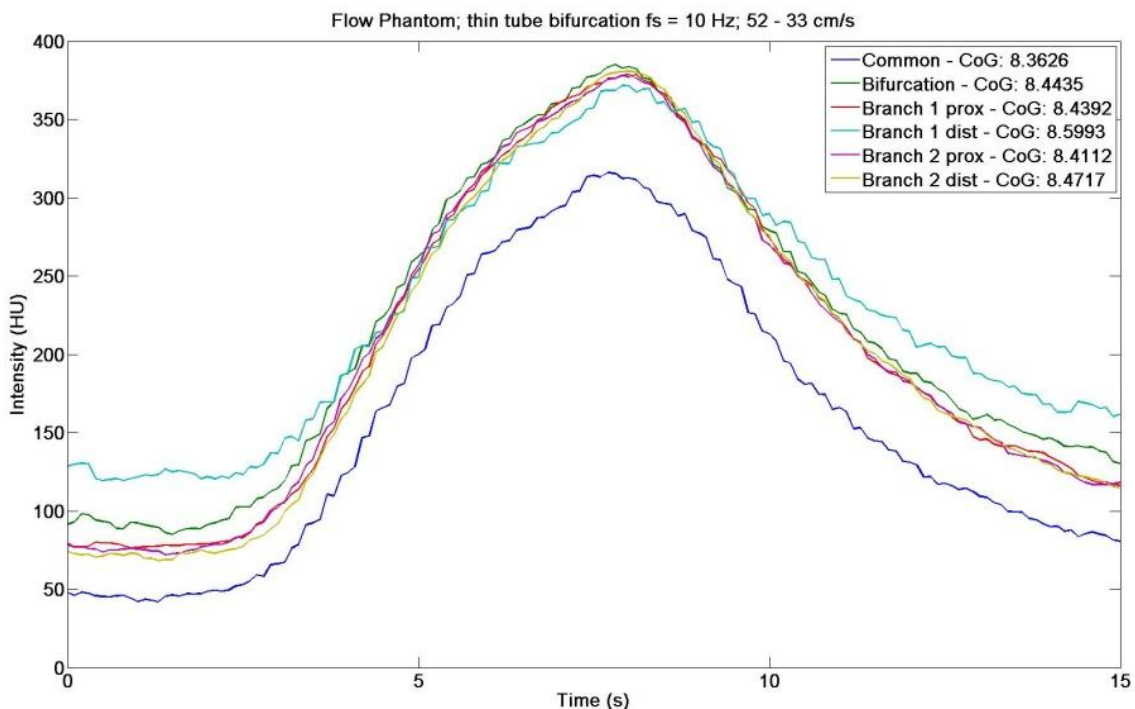


Figure 19. TDC acquired around a bifurcation. ROI 1 and ROI 2 were located in advance to and at the splitting point of the bifurcation, respectively. ROI 3 and 4 and 5 and 6 were located in either of the two branches. CoG indicates center of gravity (s); Dist, distance (mm); prox, proximal; dist, distal.

Session 3 showed a calculated flow velocity of 237 cm/s in the straight tube, which was 226% of the true velocity. The ROI were separated 81 cm. The maximum amplitude in the straight tube was 264 HU. The calculated flow velocity in the branch after the thick bifurcation was 60 cm/s, which was 167% of the true velocity. The ROI were separated 20 cm. The calculated flow velocity in the branch

after the thin bifurcation was 73 cm/s, which was 243% of the true velocity. The ROI were separated 18 cm. The shapes of the TDC showed a plateau zone between contrast inflow and contrast outflow, as shown in figure 20. During the plateau a local minimum occurred. The TDC from the ROI around the thick bifurcation differed in intensity values, but not clearly in shape. The most distal ROI showed lower intensities than the other TDC. The TDC from the ROI around the thin bifurcation showed mainly differences in intensity, but not in shape. One of the ROI in the distal tubes and the ROI in the common tube showed TDC that were lower than the other TDC. No differences regarding the calculated flow velocities were found between a flow from the pump of 1000 ml/min or 2000 ml/min. A difference was found regarding the shape of TDC, the TDC of the higher flow showed a plateau at highest intensity and the TDC of the lower flow showed a peak.

Session 4 showed a calculated flow velocity of 102 cm/s in the straight tube, which was 196% of the true velocity. The ROI were separated 67 cm. The maximum amplitude in the straight tube was 386 HU. The calculated velocity in the branch after the thin bifurcation was 78 cm/s, which was 170% of the true flow velocity. The ROI were separated 14 cm. The ROI around the bifurcation showed TDC that did not reveal a pulsating flow. Further, they showed similar intensity values, except for the ROI in the common tube which showed lower peak intensity. No differences regarding calculated flow velocities and TDC shape were found between continuous flow and pulsating flow.

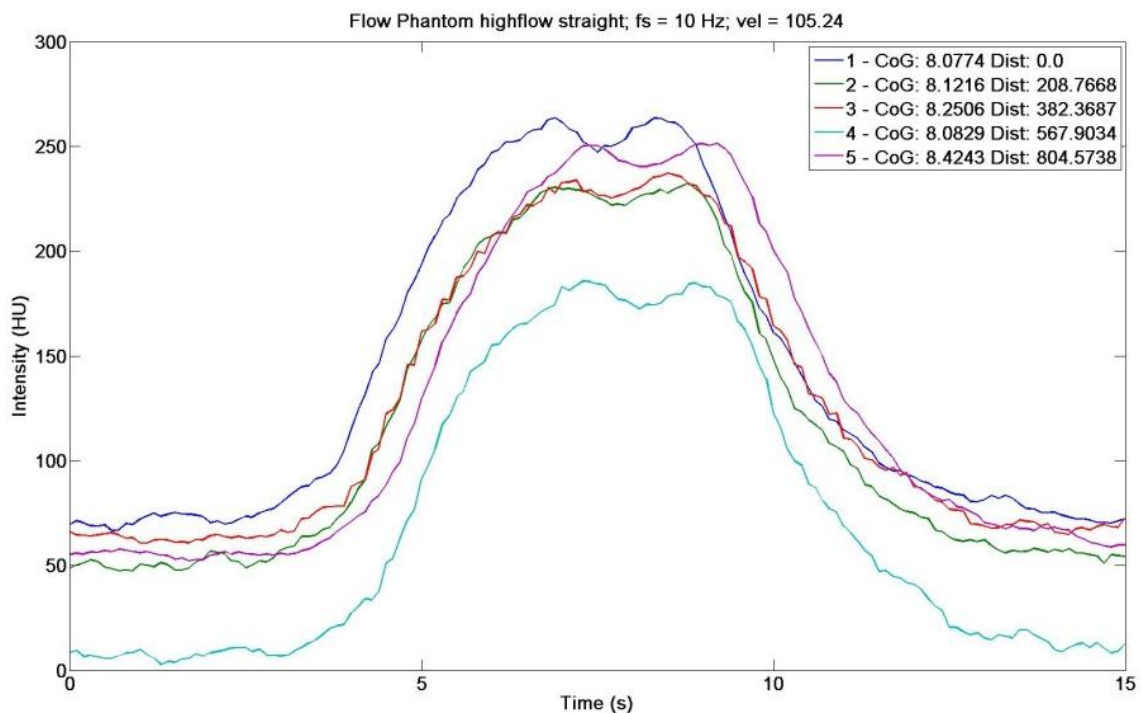
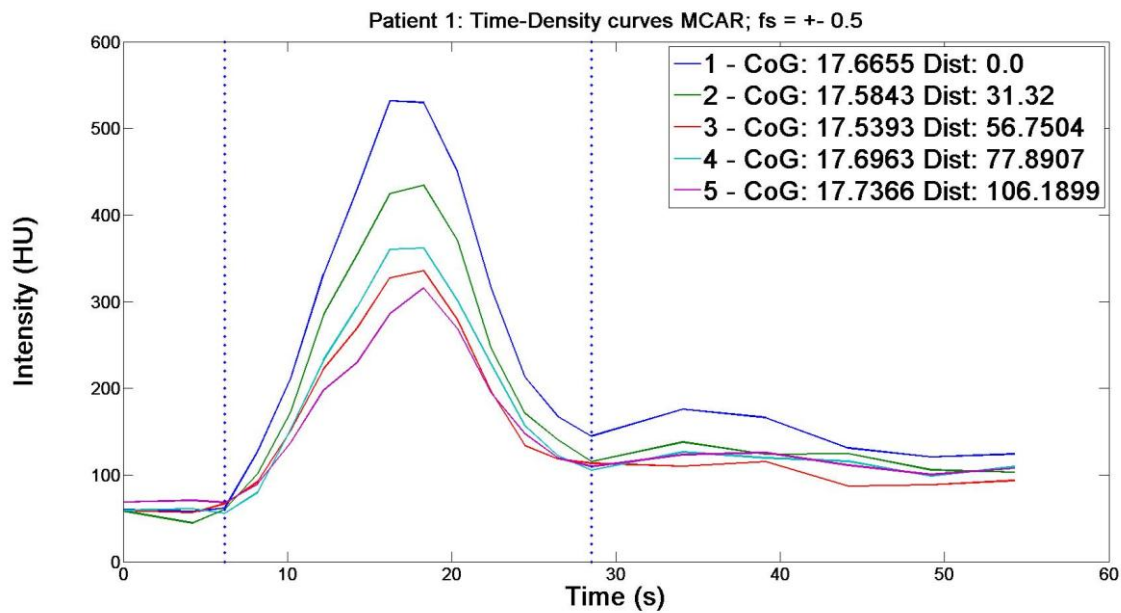


Figure 20. TDC acquired at a doubled flow production by the pump. The TDC showed a plateau with a local minimum instead of an intensity peak. The absolute intensity was decreased in comparison to the low flow measurements. CoG indicates center of gravity (s); Dist, Distance (mm).

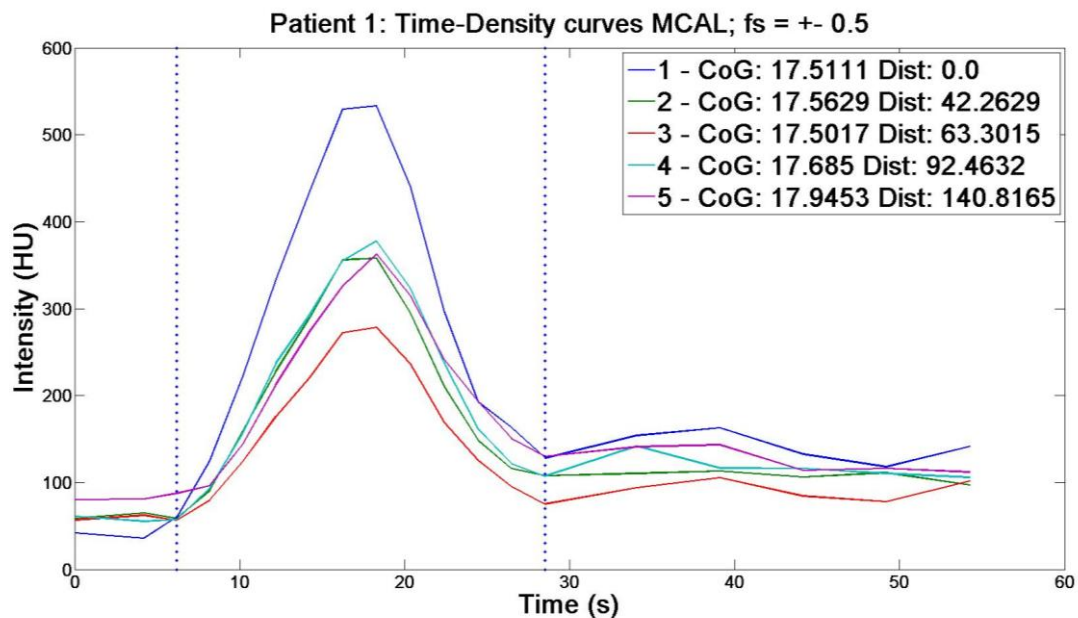
In vivo data

Healthy subjects

The direct-flow model was applied to CTP data of 1 healthy subject. The TDC of the right MCA differed in intensity amplitude, and did visually show a small time delay. The ROI were separated 10.6 cm. The CoG values decreased from the first to the third ROI, but increased from the third towards the fifth ROI, as shown in figure 21a. Therefore the CBFv could not be calculated validly. Though, usage of ROI 1 and ROI 5 resulted in a CBFv of 143 cm/s. The ROI present in the proximal part of the vessel produced TDC with larger amplitudes than the ROI in the distal part. The TDC of the



a)



b)

Figure 21. a) TDCs of the right MCA of a healthy subject. The TDCs showed an amplitude decrease and a time shift between the ROI. No increasing trend was visible in the CoG values. b) TDCs of the left MCA of the same subject. The TDCs showed an amplitude decrease and a clear time shift between ROI. ROI 3 disturbed the increasing trend of CoG. CoG indicates center of gravity (s); Dist, geodesic distance from ROI 1 (mm); MCAR, righter medial cerebral artery and fs, sample frequency (Hz). The vertical blue dotted lines indicate the range in which the CoG was calculated.

left MCA differed in intensity amplitude, and did show a small time delay, as shown in figure 21b. The ROI were separated 14.1 cm. The CoG were comparable in the first three ROI, but was increased in ROI 4 and ROI 5. Usage of ROI 1 and ROI 5 resulted in a CBFv of 33 cm/s.

Time delay between arterial and venous ROI

A time delay between arterial and venous ROIs was visible, as could be seen in figure 22. The time delay between peaks was 6 seconds, but the real time delay might be bigger due to the wiggle at time = 24 seconds. A time delay of 6 seconds represented the time the blood needed to pass through the capillary bed. The peak intensity of the several vessels varied, but the peak intensity of both ICA was the same as yields for the peak intensity of both jugular veins.

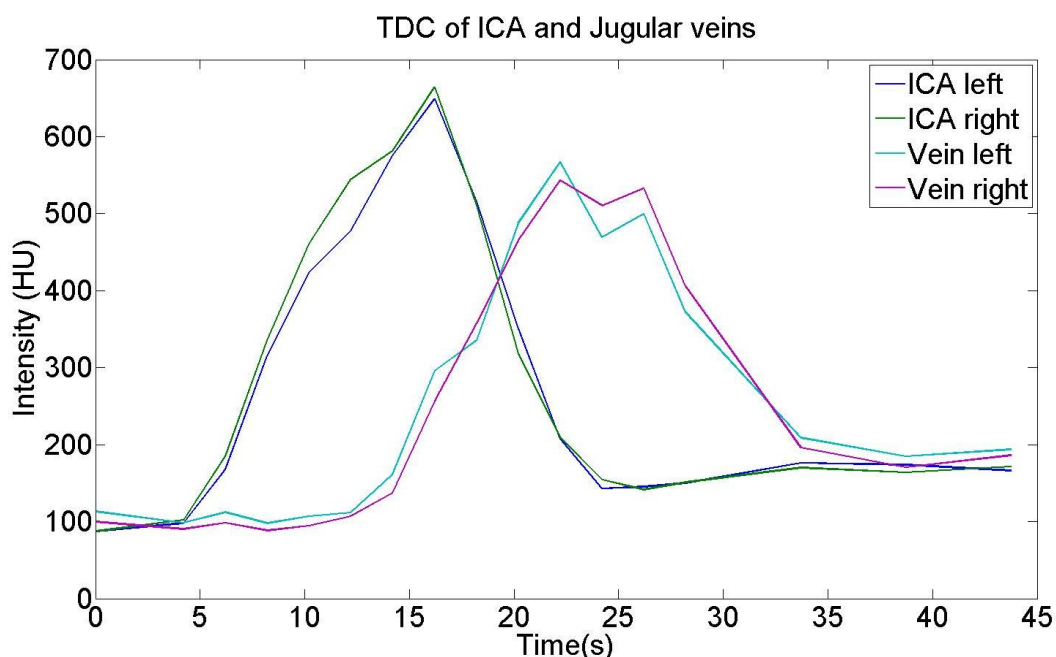


Figure 22. Time delay between ICA and jugular veins. ICA indicates internal carotid artery.

AVM Patients

The data of AVM patients only included the first part of the TDC and was showing the arrival of contrast agent in the arteries until the moment of peak intensity, preventing analysis of the venous contrast outflow. Analysis of the left MCA in AVM-patient 1 showed a decreasing trend of CoG values, corresponding to decreasing amplitudes, as shown in figure 23. Calculation of CBFv from these data would generate negative results. Some noise was visible in the TDC. The TDC of the right MCA and right ACA in patient 1 were comparable (data not shown). However, the CoG values of the right ACA showed an increasing trend, with ROI 3 and ROI 4 as outliers. The CoG values are presented in table 11.

The analysis of the right ACA of AVM-patient 2 showed very low contrast intensity in the distal ROI resulting in TDC that lack a clear peak. The TDC of ROI5 was almost horizontal, causing a low CoG value and this made comparison to ROI1, which has a TDC with a peak, unreliable. Due to the low intensity in the distal regions, distance calculation did not succeed. The CoG of the left and right MCA and the right ACA in patient 2 showed decreasing trends, indicating a negative flow velocity, which is shown for the right MCA in figure 24.

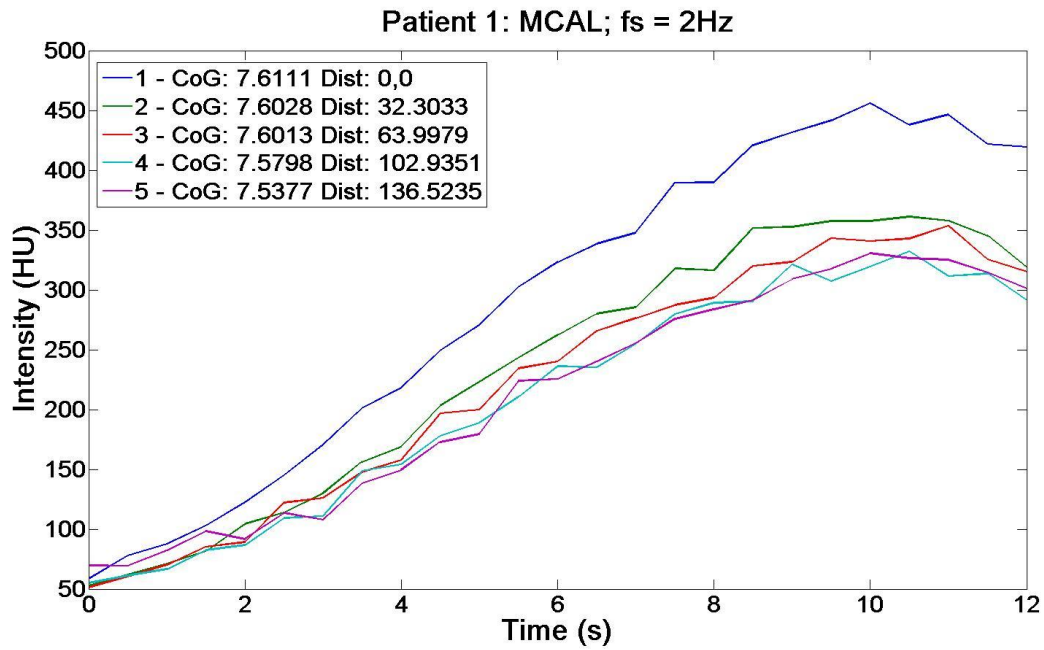


Figure 23. TDCs of the left MCA of patient 1. The CoG of the curves and the distance (mm) from ROI 1 is given in the legend. The CoG showed a decreasing trend. CoG indicates center of gravity (s); fs, sample frequency (Hz); Dist, distance (mm); MCAL, left middle cerebral artery.

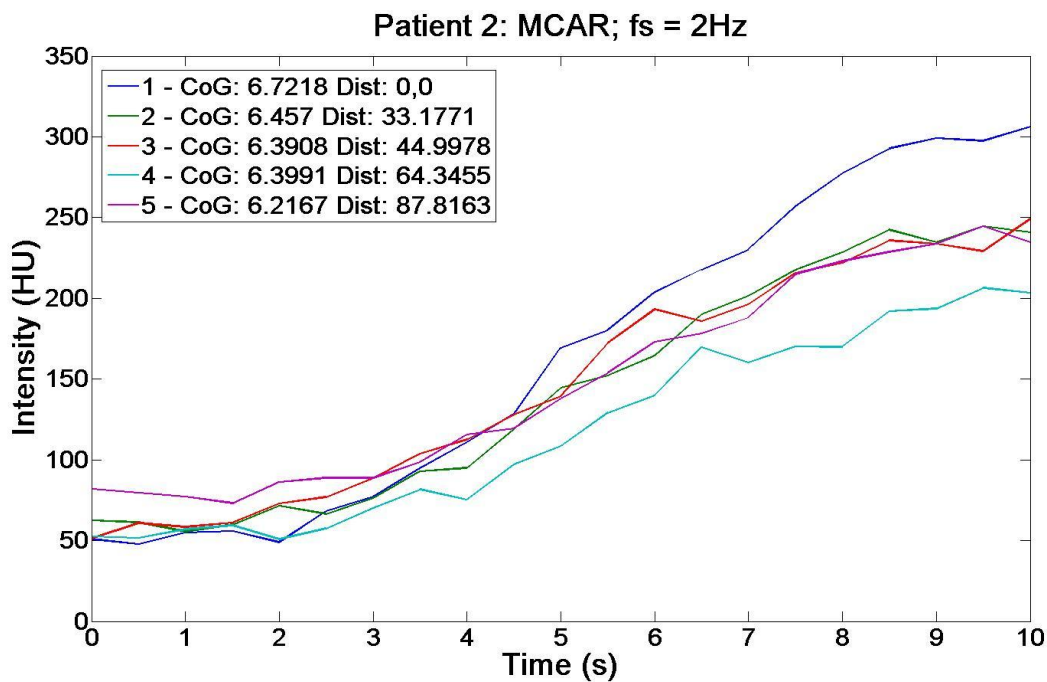


Figure 24. TDCs of the right MCA of patient 2. The CoG of the curves and distances between ROI are given in the legend. The CoG showed a decreasing trend. CoG indicates center of gravity (s); fs, sample frequency (Hz); Dist, distance (mm) and MCAR, right middle cerebral artery.

Table 11. CoG (s) of bilateral MCA and right ACA of both patients. ROI1 and ROI5 were separated approximately 10-14 cm and ROI2, ROI3 and ROI4 were divided homogeneously in between. MCA indicating middle cerebral artery; ACA, anterior cerebral artery; R, right; L, left and ROI, region of interest.

Location	Patient 1			Patient 2		
	MCA R	MCA L	ACA R	MCA R	MCA L	ACA R
ROI 1	7,64	7,61	7,61	6,72	6,72	6,75
ROI 2	7,65	7,60	7,65	6,46	6,37	6,52
ROI 3	7,56	7,60	7,72	6,39	6,17	6,34
ROI 4	7,62	7,58	7,67	6,40	6,41	6,41
ROI 5	7,63	7,54	7,74	6,22	6,34	5,97

Projection data

The calculation of data with a scanning frequency of 10 Hz using projection data was feasible in one AVM patient. The improved scanning frequency was visible in the TDC as more vibrations of the curve. The amplitudes of the TDC decreased with increasing distance from ROI 1, as visible for the left MCA in figure 25. No clear trend in CoG was visible. It was possible to segment and skeletonize 14 cm of the left MCA. In the TDC of ROI 1 a rhythmic noise was present, with a frequency of approximately 1 Hz. The analysis of the right MCA revealed similar results.

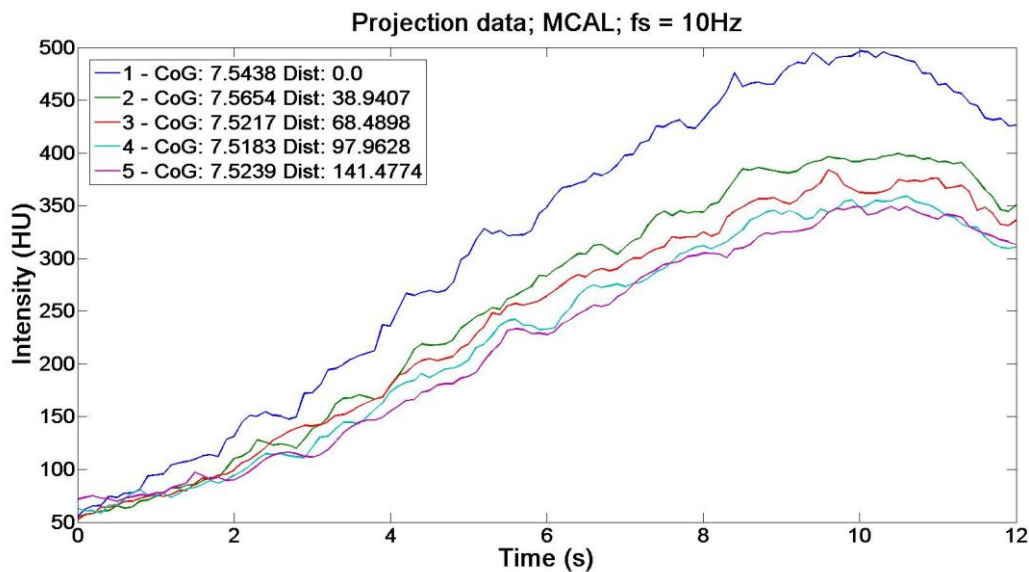


Figure 25. TDCs of ROI selected in the left MCA using projection data of AVM-patient. The data looked jerkier compared to the data with lower frequency. The amplitude of the TDC decreased with increasing distance regarding to ROI 1. CoG indicates Center of Gravity (s); dist, distance (mm); fs, sample frequency (Hz) and MCAL, left middle cerebral artery.

Repeatability

The repeatability of the direct-flow principle was studied using five iterations in the left MCA. The ROI were shifted distally each iteration, as shown in figure 26. The standard deviation (SD) varied from 0.026 to 0.037 seconds and the CoG average of the five attempts showed a decreasing trend, as shown in table 12.

Table 12. Results of repeatability study.

Iteration	Center of Gravity (s)				
	ROI 1	ROI 2	ROI 3	ROI 4	ROI 5
1	7,55	7,53	7,52	7,51	7,54
2	7,54	7,57	7,55	7,49	7,51
3	7,53	7,57	7,54	7,49	7,46
4	7,59	7,60	7,51	7,51	7,49
5	7,62	7,53	7,57	7,57	7,49
Average	7,57	7,56	7,54	7,51	7,50
SD	0,037	0,029	0,026	0,035	0,027

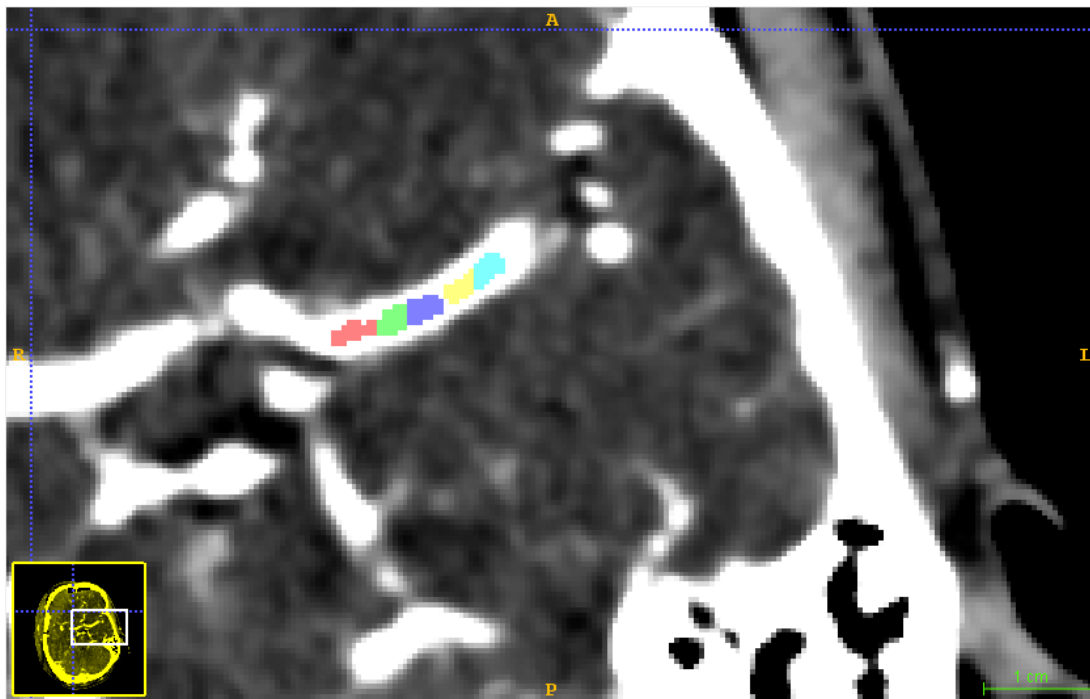


Figure 26. The five iterations of the selection of ROI 1 in the proximal left MCA were presented in different colors.

2.3 Discussion

In this section the results of the first and second study objectives will be discussed. First, an overview of the most important results is given. Next, parameters that may influence the results of the direct flow model are discussed. In addition, limitations of the direct-flow model and the validation method are enumerated. Finally, recommendations for further research are given.

Simulation data showed that it was theoretically possible to calculate reliable CBFv, using a sampling frequency of 10 Hz, a ROI distance of 20 cm and a signal-to-noise ratio of 10% for a CBFv of maximal 100 cm/s. The flow phantom data confirmed that it was possible to measure the flow of contrast through the macrovascular system. Positive time delay was found along the tubes; however the calculated flow velocities overestimated the true velocity significantly in the range of 167-243%. The flow phantom measurements showed no differences between continuous and pulsating flow and showed no large differences in TDC shape at bifurcations. Increase of flow from the pump resulted in a contrast plateau instead of a contrast peak. The correctness of the manual distance calculation used in the direct flow model was confirmed by the results of the flow phantom, in which the known tube lengths corresponded to the measured tube length.

For all included patients it was possible to execute the direct-flow model in the larger cerebral vessels. It was feasible to select the ROIs within the vessels, to extract the TDCs and calculate the CoGs. It was not possible to derive true CBFv from *in vivo* data using the direct-flow model. In *in vivo* data of a healthy subject, flows of 143 cm/s and 33 cm/s were calculated for the right and left MCA, respectively. However, the CoG values did not show a clear trend, indicating that the calculated velocity depended on the ROI that were selected. Therefore, these values were not reliable. Physiologically, the CBFv should have been between 20 and 200 cm/s, but the CoG of our data frequently showed a decreasing trend throughout the vessel, resulting in negative CBFv. This was the case for *in vivo* data of AVM patients, either if it was sampled with a low frequency (2 Hz) or a high frequency (10 Hz). A negative CBFv would have indicated that the arterial flow was directed towards the heart, instead of towards the capillaries. Flow towards the heart was possible in some parts of the circle of Willis due to collateral flow, but our measurement locations were distal from the circle of Willis. We found CBFv values out of the physiological normal range, indicating that the technique is not a reliable measure for the estimation of CBF.

Center of gravity

The use of the CoG to calculate the time delay of bolus arrival between ROI may be the cause of the overestimation of calculated CBFv in the flow phantom data. In figure 18 the CoG approach can be verified using the moment at which the TDC of different ROI reached maximum intensity. The moment of peak intensities differed approximately 1 second between ROI 1 and ROI 5. In contrast, the calculated CoG differed 0.55 seconds. The distance between ROI 1 and ROI 5 was 67 cm and the controlled flow velocity was 53 cm/s, so a time delay of approximately 1 second seemed more reliable. The reason of the deviation of CoG was unclear. The moment of maximum intensity approach was not included to the direct-flow model, because it is very sensitive to noise. It could, however, be used for the flow phantom data, because the flow phantom did not experience much noise.

Scanning frequency

A probable cause of the poor results from *in vivo* data is the low scanning frequency. As concluded from the simulation study a sampling frequency of 10 Hz was required to use the direct-flow model. For the healthy subject a sampling frequency of 0.5 Hz was used, with the consequence that blood that flowed with a velocity of 50 cm/s traveled 100 cm in the time gap between two consecutive scans. Since the vessels in the cerebral vasculature were much shorter than 100 cm, it was impossible to follow and measure the contrast agent bolus and thus to calculate the CBFv. In the other patients, a scanning frequency of 2 Hz was used, resulting in a minimum distance of 25 cm between 2 scans. This distance was still more than the length of blood vessels that could be segmented using the region growing algorithm. Flow phantom data indicated that CBFv was measurable in CTP data sampled at 2 Hz.

The scanning frequency could not be further improved, since it takes the CT scanner 0.275 seconds to do a single rotation. So even if the maximum scanning frequency was used, a blood cell travels $50 \times 0.275 = 13.75$ cm between scans. In order to be able to get a sampling frequency of 10 Hz, projection data using continuous scanning was used, which was, according to the simulation data, enough to find a time delay between TDC of 0.2 seconds. However, using the flow phantom the increase of frequency did not result in more reliable CBFv. The flow velocity was still severely overestimated. Moreover, the CoG of *in vivo* data sampled at 10 Hz showed a decreasing trend, which resulted in negative CBFv values. Therefore, still no reliable CBFv values could be calculated. Concluding, the increase of sample frequency did not improve reliability of CBFv calculation.

Vessel length

The direct flow principle will generally be more accurate for a longer ROI distance. From the simulation, a ROI distance of 20 cm in combination with other satisfying parameters is suitable to perform the direct-flow principle. The MCA and ACA have a length of 20 cm, but the region growing and skeletonization algorithm fails to identify the vessel from the parenchyma with decreasing vessel diameter. Lowering the region growing threshold is undesirable since it leads to the inclusion of many bifurcating vessels and other structures that complicate the distance calculation algorithm. Due to these image analysis limitations a ROI distance of 20 cm may not be possible in every patient. The flow phantom data indicate that the direct-flow principle may work equally well for different vessel lengths if the CBFv is low. Analysis using a combination of vessels that are connected serially could be a solution, but the circle of Willis is always interfering in the connection. The influence of the circle of Willis on the direct-flow principle is unknown, but since the flow may be bidirectional during the cardiac cycle and the flow patterns in the circle are not well understood, it is not included in the current study. In conclusion, the vessel length necessary in order to achieve reliable CBFv results depends mainly on the scanning frequency and the value of CBFv.

Shape of TDC

The presence of bifurcations in a vessel may influence the shape of the TDC. Since the cerebral vasculature does not contain long straight vessel parts without bifurcations, it is important to understand that influence. The bifurcations in the flow phantom did not reveal any influence on the TDC shape. The intensity of the TDC of the common tube was lower, but this was probably caused by the different type of material used for that part of the tube in comparison to the rest of the phantom. The bifurcations of the flow phantom cannot be compared to *in vivo* data, because it only included bifurcations that were designed to guide the flow perfectly with equal sized branches. The

cerebral vessels contain bifurcations varying in angle and radius that may influence the TDC shape more.

The decrease of intensity amplitude along a vessel in *in vivo* data could be caused by a decrease in flow in the vessel caused by bifurcations. Some evidence for that was found during a small experiment to the bifurcation where the ICA splits into the ACA and the MCA (a description of this experiment is included in appendix B). Three ROIs of the same size were drawn just after the entries of the three branches. There the amplitude of intensity was lower in the ACA and MCA compared to the ICA. A second possible cause of the decrease of intensity amplitude is the mixing of contrast agent with contrast-free fluid. This is supported by the fact that the TDCs measured at ROI in the flow phantom that were lower in amplitude if they located more distally from the pump.

The flow velocity changed the shape of the TDC. The absolute intensity decreased at higher circulation flow. This situation could not be explained by a higher flow velocity: circulating flow is measured at the pump, while flow velocity can vary throughout the phantom according to the total cross section of tubes at that part of the phantom. The intensity decrease at a doubled circulating flow may be caused by the fact that the contrast agent is diluted over a doubled amount of fluid. Since the volume of fluid in a voxel remains constant the contrast density per voxel is reduced. Moreover, the contrast borders less contrast-free fluid so it can mix less, which possibly results in the intensity plateau, as shown in figure 20. The effect of velocity on TDC shape may be absent in *in vivo* data, since the contrast was injected in a vein with low flow and at the time travelling a longer distance with more obstacles before reaching the brain. In conclusion, TDC shape variability influences the direct-flow principle result and since the cause of the variability is unknown it may be challenging to invent a correction method.

Measurement duration

The improvement of scanning frequency in *in vivo* data came at the cost of a lower time window coverage that disturbed CoG calculation. The *in vivo* data sampled with 2 or 10 Hz only included the arterial inflow of contrast and stopped a few seconds after peak enhancement was reached. This has significant consequences for time delay calculation. It was assumed that the shape of the TDC would be the same for all ROI distributed in the vessel, but if only a part of the TDC is measured, this is highly unlikely since the time delay shifts increasing parts of the TDC outside the limits of window coverage. Therefore the interrelation between the CoG calculated does not correspond to true time delays of TDC. The simulation of incomplete TDC data shows that the deviation of mean values and SD is very high, even for simulations with low CBFv. So, correct calculation of CBFv is only possible if the complete TDC is available. The data with incomplete TDC is only useful to give an indication of the feasibility of the direct-flow principle, but not to calculate the true CBFv values. In conclusion, a complete TDC is required for adequate estimation of CBFv.

Noise

The repeatability study which was performed in *in vivo* data shows varying CoG results for ROI that were located next to each other and the SD was in the range of 0.02 to 0.04 seconds. A time shift of 0.2 seconds was expected between ROI1 and ROI5, so it seemed unlikely that noise influenced the CoG to the extent that the time delay becomes negative. But the noise can contribute to disturbance of the the signal. Further, the repeatability shows that the exact location of ROI selection is not relevant, provided it is located in the center of a vessel.

The noise may originate from multiple factors. First, the CT scanner introduces a certain amount of noise in the data.¹⁰¹ In addition, several physiological factors such as the cardiac cycle, coughing, swallowing and breathing may cause motion of vessels relative to the skull. The influence of these factors may be large for the neck vessels such as the carotid artery, but will be negligible for the vessels beyond the circle of Willis. An example of noise due to coughing, swallowing or breathing is present in the venous TDC of the analysis of time delay between the cerebral arteries and veins, see figure 22. Principle component analysis of the TDC showed that the wiggle in the top of the venous TDC is caused by lateral motion of the veins. During the shift the average TDC is partly constructed using intensity values of voxels outside the vessel, causing a lower average intensity value. The veins return to their original position after two seconds. Further details regarding the principle component analysis performed are available in appendix B. Wiggles as found in the cerebral veins are not found in cerebral arteries. The cerebral arteries are less susceptible to coughing, swallowing or breathing than veins due to their smaller radius and stronger vessel wall. Patient motion may occur during the CT scan, but that is corrected by the registration process.

Another signal disturbing factor is the pulsatile flow in the arteries. The CBF and CBFv are high during systole and low during diastole. It is assumed that the time delay between the TDC will be smaller during systole and larger during diastole. The flow phantom data with pulsatile flow shows no differences compared to continuous flow. This may indicate that pulsatile flow does not influence the direct-flow model, for instance because the fast rhythm of the cardiac cycle does not disturb the slow rhythm of contrast inflow and outflow. Otherwise, the pulsatile flow of the phantom pump may initiate a pulsed wave that differs from the one that the human heart produces. The pulse wave may be dampened by the phantom, although that is not expected since it is less compliant than the human vascular system. Nevertheless, the 1Hz wave present in the TDC of the 10 Hz *in vivo* projection data may originate from the cardiac cycle. This would indicate that the contrast intensity is higher during systole than during diastole. Moreover, if the cardiac cycle is clearly visible in the signal it could be filtered out. In conclusion, noise is present in CTP data and may influence the results of the direct-flow principle. Most physiologic noise origins do not seem to disturb the arterial flow, so the majority of noise may be introduced by the CT scanner.

Literature

Barfett *et al.*⁹⁷ created a similar method in which they estimated intravascular blood velocity from first-pass contrast bolus profiles. They used a flow phantom and 5 patients for 4D CTA examination. Time delay calculation between ROI was done by time-to-peak (TTP) subtraction after normalizing and fitting the TDC. They found reasonable agreement between calculated intravascular velocity and velocity measured using quantitative MR angiography. Their calculated velocity values correlated better with the true velocities than the current study. This may be explained by the low flow velocities of 2.2 to 12.3 cm/s, that do not represent flow velocities in a human arterial system. In addition, they measured true flow velocities in the ICA of patients in the range of 10.6 to 21.8 cm/s, which significantly lower compared to normal values (table 2)^{33-37,42}. In the current study no measurements were performed with flow velocities in this range. The same authors improved their method four years later. They calculated flow velocity as the slope of the TTP versus path length curve. 8 patients were included to test their method in nine different cerebral values, but again very low CBFv values were found that are not in correspondance with other literature. Similar to our data, Barfett *et al.* concluded that a major limitation of their method is the minimal intravascular distance required, which is often beyond physiological limits. Barfett *et al.*⁹⁵ show that their method is also

applicable to extracranial vessels such as the iliac artery and the pulmonary artery. This is likely also the case for the direct-flow principle, since those vessels are thicker, have a lower blood flow velocity and are longer. However, for those vessels other less complicated techniques such as ultrasound are widely available.

Prevrhal *et al.*⁹⁶ used projection data from CT scans during contrast agent injection to determine flow velocity. They used individual projection images and detector rows to calculate flow velocities. They created a single channel flow phantom to test their method for different flow velocities which corresponded to values found in literature. The results showed a systematic overestimation of the true velocity. Advantage of this method was that a vessel length of a few cm is sufficient. However, the method requires complex technical processing in which a small quantities of noise could disturb the measurement unnoticed. This method is not tested in *in vivo* data yet.

2.4 Limitations

The direct flow model has some challenges and limitations. The algorithms used to perform the model could be improved and probably more steps can be automated or simplified. The main limitations encountered during this study are described below.

The skeletonization result can be complex which may cause errors. The skeleton is better usable when it has as few bifurcations as possible. However, every patient has a unique vessel anatomy and bifurcations at other locations. In order to simplify the skeleton it can be attempted to increase the region growing thresholds. This excludes small vessels from the skeletons, and will frequently reduce skeleton length, which is required for a reliable CBF calculation. A skeleton with many bifurcations is usable at the cost of more manual work and increased risk of errors. The analysis of the skeleton and the calculation of the distance between ROI can probably be automated. Another option is to measure vessel length by clicking the vessel center at all bifurcations manually and calculating the distance between the points. This would be easier, but less accurate.

For the current study subjects have been used with some pathology in the cerebral vascular system. The healthy subject was not entirely healthy; the subject had an indication for a CT perfusion scan based on clinical signs and symptoms of stroke. On the perfusion scan no signs of stroke have been found, the signs and symptoms disappeared and therefore the subject is categorized as healthy. Due to the possibly abnormal physiology in the cerebral vasculature, the results may deviate from results that can be found in truly healthy subjects. The AVM patients have some anatomical abnormalities that may influence the results. However, despite the fact that not the complete anatomy of these patients is known, their flow direction will not be altered, at least not in both the bilateral MCA and the ACA. But the CBFv of these patients may differ from healthy patients.

The direct-flow principle is only applicable if an adequate amount of contrast agent is used and arrives in the cerebral vascularity. The amount of contrast has to be enough to distinguish the vessels of interest from the surrounding tissue, but more importantly from small bifurcating vessels. If the amount of contrast is small the region growing threshold has to be decreased to be able to segment enough vessel length. The decrease of threshold goes at the cost of the inclusion of many small branches of the main artery, which results in a very complex skeleton. The complex skeleton impedes the distance calculation and increases the chance of errors.

Application of the direct-flow principle in the ACA is complicated because the bilateral vessels are located very close to each other or even touch each other. Frequently, the segmentation algorithm could not distinguish both bilateral vessels completely, resulting in a skeleton that had partly two separate ACA and partly one big ACA. This does not represent the true anatomy of the ACA in virtually all subjects and may result in both overestimation of distance between ROI and use of the wrong vessel for distance calculation.

The simulation data and the flow phantom are a simplification of reality in which more variable parameters may exist than included in these systems. For example, the noise added to the simulation data is white noise with amplitude of 5-10%, while it is uncertain if the noise in *in vivo* data is white and if the amplitude is high enough.

2.5 Recommendations

The direct-flow principle is a desired addition for the clinical practice, but before it can be implemented better results should be obtained, for which some recommendations are given. Firstly, a method has to be developed to deal with the incomplete TDC. This can be either a method to measure complete TDC without an increase in radiation dose or a method to correct for TDC shape differences. The latter can maybe be done by a fitting technique as applied by Barfett *et al.*⁹⁷, despite the fact that the TDC shape may be different for every patient and that the fitting procedure introduces a certain error. Next, it is recommended to study the source of the noise present in the TDCs. Once the source is known, the noise can be measured individually and filtered out of the data. Another method to get rid of noise may be subtraction of the first acquisition of the CTP from the acquisitions in which contrast is present. This way only the contrast enhanced regions remain and all other possible noise introducing regions disappear from the image. Furthermore, once the direct-flow principle supplies better results it should be validated using another technique, of which TCD seems the most suitable.

2.6 Conclusion

A model to quantitatively measure CBFv in the macrovascular system using CTP was developed successfully. The model used the principle that velocity could be calculated by the quotient of distance and the time it took to travel that distance. The required information to calculate distance and time delay was extracted from data using local developed algorithms. Validation of the model started with local simulations that revealed the required scanning properties to successfully execute the model. Analysis of flow phantom data resulted in severely overestimated CBFv. Finally, the CBFv calculated from *in vivo* data did not correspond to physiological values mainly due to noise and incomplete TDC coverage. The direct-flow model should be improved to enable introduction in clinical practice.

3. Establishing normal values of perfusion in the *microvascular* system using CT perfusion

3.1 Method

This chapter describes the method, results and discussion of the study objectives related to the second research topic.

RT2) Quantifying normal values of CBF, MTT and CBV in the *microvascular* system

This section will address the methods used for study objectives three and four. First, normal values of CBF, MTT and CBV were derived for several different brain regions (study objective 3). Then, perfusion values of patients with TIA and ischemic stroke were obtained for the same brain regions. Finally, normal values and patient values were compared (study objective 4). The methods for study objective three and four were nearly identical and will not be described separately. Naturally, it will be pointed out when methods did differ.

3.1.1 Population

Patients were identified from a database containing all CTPs performed between January 2014 and June 2015. General indications for a CTP were clinical signs and symptoms of stroke. For the derivation of normal values (study objective 3) only healthy subjects were used. For the comparison of normal values with perfusion values (study objective 4), healthy subjects and TIA and ischemic stroke patients were used.

General inclusion criteria

- CTP of adequate quality for quantitative analysis, without clips, coils or drainage tubes or other imaging artefacts in the region of interest
- CT perfusion within 9 hours after onset of symptoms
- Stable vital signs
- Age > 17 years

Healthy subjects

- No signs compatible with recent ischemia on CT or CT angiography (CTA), and no perfusion defects on CTP
- Other identified, non-vascular cause of the clinical symptoms and signs
- No other concomitant neurological disease, known to compromise cerebral blood flow

TIA patients

- Transient episode of neurologic dysfunction caused by focal brain ischemia, without acute infarctions
- No signs of acute infarction on CT or CTA, and no perfusion defects on CTP

Ischemic stroke patients

- Clinical evidence of brain cell death attributable to ischemia, based on neuropathologic, neuroimaging, and/or clinical evidence of permanent injury
- Signs of acute infarction on CT or CTA, and no perfusion defects on CTP

Exclusion criteria

Patients meeting one or more of the following criteria were excluded from the study:

- Stroke based on or accompanied by hemorrhage
- Presence of tumor lesions, other pathologic malformations in the brain
- Midlineshift > 2 mm
- Unstable vital signs, requiring support by using airway devices, supply of > 5 l O₂/min, or any hemodynamic support.

This study aimed to include at least 50 subjects in the healthy group, based on availability of the CTPs. In addition, a total number of 50 TIA and 50 ischemic stroke patients were included in the analysis. Numbers were based on availability within the database and feasibility of the quantitative analysis.

Allocation of patients to groups

Patients in this database were allocated to a group of healthy subjects, TIA patients or ischemic stroke patients based on clinical information and general (qualitative) CT and CTP data. TIA was defined as a transient episode of neurologic dysfunction caused by focal brain ischemia, without acute infarctions.¹⁰² Ischemic stroke was defined as brain cell death attributable to ischemia, based on neuropathologic, neuroimaging, and/or clinical evidence of permanent injury.¹⁰³ The alternative diagnosis, as documented by the treating physician was recorded. Patients with other major findings on the CT, CTA or CTP (eg tumor, contusion etc) were excluded from the study. The allocation was performed by an intensivist, blinded for the quantitative CTP results.

Demographic data

Demographic information of all groups, including age and sex were recorded. Information regarding the disease, including time to PCT since symptom onset, affected hemisphere, thrombolysis, NIHSS score, mRS score and affected vascular territory were recorded. Clinical parameters, described by the attending doctor, were recorded as shown in table 13. The reason for CTP was classified as clinical suspicion of stroke, clinical suspicion of arteriovenous malformation or other.

Table 13. Overview of clinical parameters that were collected for every patient.

Parameter	unit
Sex	Male/female
Age	year
Time to CT	minute
Affected hemisphere	Left/right/other/unknown
Thrombolysis	Yes/no/unknown
NIHSS	Score 0-42
mRS score	Score 0-6
Affected vascular territory	

3.1.2 Main study endpoint

This section describes the main study endpoints that concretely showed which results were obtained. The main study endpoints belonged to study objective 3, *deriving normal values of CBF, MTT and CBV in healthy subjects for several different brain regions*.

The main study parameters were the values of CBF (ml/100g/min), CBV (ml/100g) and MTT (s) in different regions of the brain in the healthy subject group. The ROI were chosen in the vascular territory supplied by the anterior, medial and posterior cerebral artery in a plane just below the superior margin of the lateral ventricles and in the basal ganglia at the height of the basal ganglia. In addition, values in grey matter were calculated and compared to white matter. The regions of the ROI are shown in figures 27 and 28. Values were expressed in median values (interquartile ranges (IQR)). First, the values of CBF, CBV and MTT of the voxels within a ROI were derived per patient. Subsequently the mean \pm SD or median (IQR) per region were calculated for the total normal group, and were considered as normal values. Every region was compared to the contralateral region to determine left-right differences and to the other regions in the same hemisphere to determine differences per flow region and per tissue type.

3.1.3 Secondary study endpoints

This section describes the secondary study endpoints that concretely showed which results were obtained. The secondary study endpoints belonged to study objective 4, *comparing normal values to perfusion values of patients with TIA and ischemic stroke*.

- Comparison between normal values and values of CBF (ml/100g/min), CBV (ml/100g) and MTT (s) in patients with TIA obtained within the affected vascular territory. Normal values from the ipsilateral sides of the normal brain group were used as a comparison. The affected vascular territory was determined from clinical data by intensivists.
- Comparison between normal values and values of CBF (ml/100g/min), CBV (ml/100g) and MTT (s) in patients with ischemic stroke obtained within the affected vascular territory. Normal values from the ipsilateral sides of the normal brain group were used as a comparison. The affected vascular territory was determined from clinical data by intensivists.
- Comparison between normal values and values of CBF (ml/100g/min), CBV (ml/100g) and MTT (s) in patients with TIA obtained within the unaffected vascular territory. Normal values from the ipsilateral sides of the normal brain group were used as a comparison. The unaffected vascular territory was determined from clinical data by intensivists.
- Comparison between normal values and values of CBF (ml/100g/min), CBV (ml/100g) and MTT (s) in patients with ischemic stroke obtained within the unaffected vascular territory. Normal values from the ipsilateral sides of the normal brain group were used as a comparison. The unaffected vascular territory was determined from clinical data by intensivists.

3.1.4 Study protocol

The CT-scanner used was a Toshiba Aquilion One 320 CT scanner, available at the emergency department of the Radboud UMC. This scanner contained 320 detectors and could therefore produce 320 slices per scanner rotation. Slice thickness was set to 0.5 mm resulting in a scan width of 16 cm. This was enough to include the complete brain without the need of table toggling between scans. The spatial resolution was 512x512x320 voxels, with a voxel size of 0.45x0.45x0.50 mm.

The perfusion measurement was performed according to the standard CT-stroke protocol used in the Radboud UMC. First, 50ml iodinated contrast agent was injected into an antecubital vein. Injection rate was 5 ml/s, thus the total injection was 10 seconds. It took the contrast bolus approximately 20 seconds to reach the carotid arteries, so perfusion CT scanning started 20 seconds after the start of contrast agent injection. The time between contrast injection and perfusion CT scanning was used to make an unenhanced CT scan. At 20 seconds after the start of bolus injection a series of 13 CT scans on 2 second interval was performed which images the arterial inflow of contrast. Next, a series of 5 scans on a 5 second interval was created to view the venous outflow of contrast. In total, 19 scans were performed, leading to 19 separate data files. The measurements were performed by skilled radiology analysts.

3.1.5 Data analysis

First, the data was imported to PMA ASIST, a freely available perfusion CT software tool to create perfusion maps containing values of CBF, CBV and MTT (Acute Stroke Imaging Standardization Group [ASIST], Japan, <http://asist.umin.jp/index-e.htm>)^{58,59}. Subsequently, 5 intra-arterial voxels were depicted as AIF and were localized automatically by PMA ASIST at the voxels with the highest CBF. For this study, AIF were constricted to be located in the ICA or the first part of the MCA of the unaffected side, so AIF that were located outside that range were removed and replaced by a manually selected AIF within that range. Block-circulant SVD (bSVD) deconvolution was used to calculate perfusion values. The slices were downsampled to slabs of 5 mm, reducing the number of slices 10 times to a total of 32. The x- and y-directions were downsampled to a matrix of 256x256. This downsampling was performed to obtain an acceptable and clear amount of data and to reduce computation time. The maps containing perfusion values created in PMA ASIST were saved in the .hdr/.image format combination to be suitable for further analysis.

Next, the maps created in PMA ASIST were imported in MATLAB. Here, vascular pixels were deleted from the perfusion maps using a CBV threshold of 8 ml/100g, of which a result is presented in figure 28.⁶⁹ Next, a midline separating both hemispheres was drawn manually using the CBF map, since the midline was clearly visible on that map. Continuously, ROIs were drawn manually and unilaterally on the CBF map. A ROI was drawn in the basal ganglia at the level of the basal ganglia (figure 27a,c), and in the anterior, medial and posterior flow territory at a height just above the lateral ventricles (figure 27d). As shown in figure 27b, the flow territories of the anterior and posterior artery were rather small at this level and the medial artery covered a big part of the brain at this level. Next, the ROIs drawn were mirrored to the other hemisphere relative to the midline and all ROIs were projected on the CBV and MTT map as well. Finally, the values of the voxels that were included in the ROI were exported and analyzed.

The values of the voxels included in the ROIs were analyzed using MATLAB. The mean and standard deviation of CBF, CBV and MTT was calculated per ROI per patient. The results were exported to a matrix containing the values of all patients. Subsequently, the mean and standard deviation of the ROIs for the patient group was determined. Continuously, the matrix containing the values of all patients was exported to MATLAB for the purpose of statistical analysis.

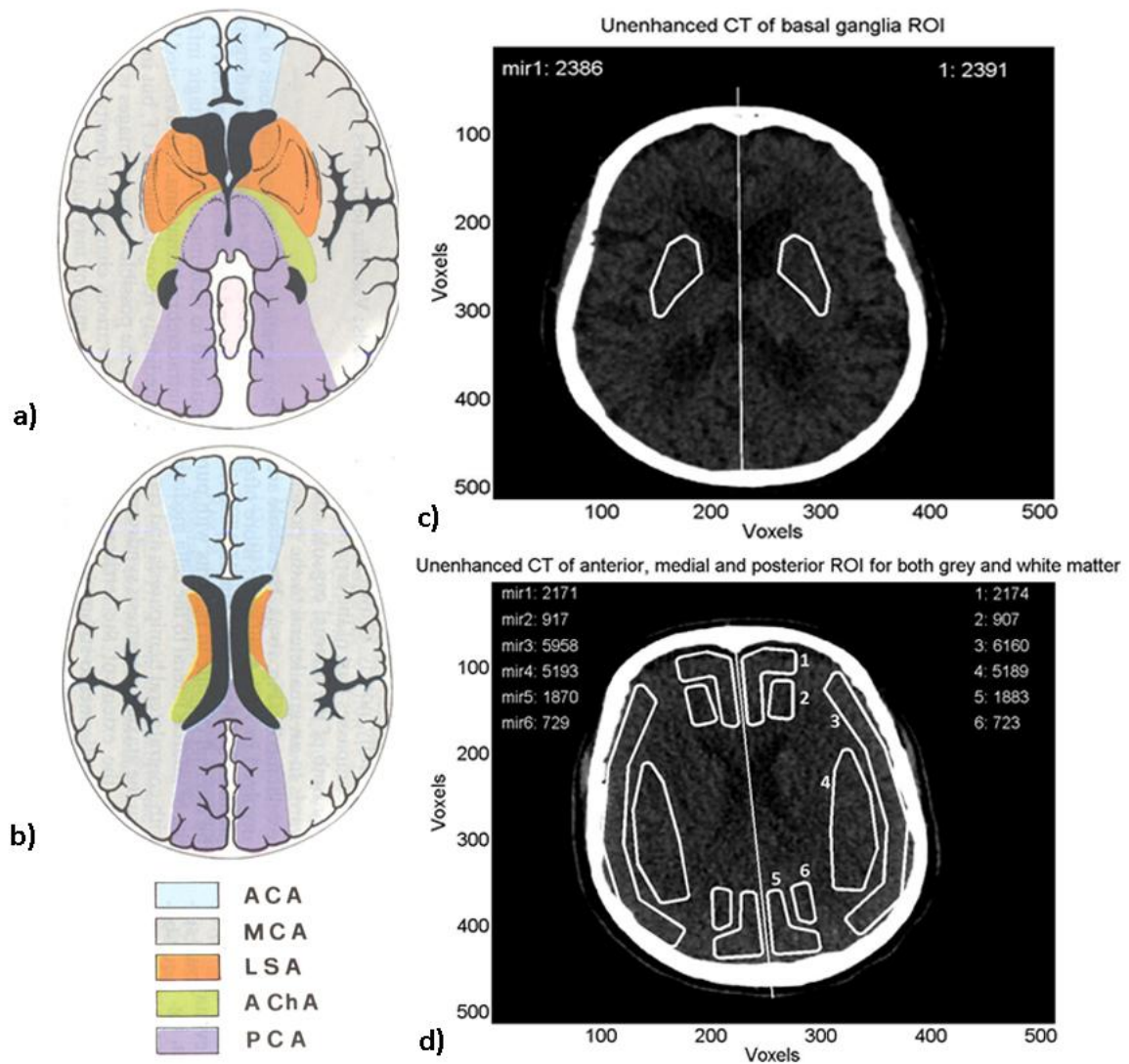


Figure 27. Flow territories at a) the level of the superior basal ganglia and b) the level of the superior lateral ventricles. The flow territory of the lenticulostriate arteries (LSA) at the level of the superior basal ganglia was used for the selection of the ROI in the basal ganglia. The flow territories of the ACA, MCA and PCA at the level of the superior lateral ventricles were used to draw ROI in the anterior, medial and posterior flow territory. c) ROI drawn in basal ganglia on unenhanced CT image. The midline was drawn and separated the two hemispheres. The ROI was mirrored with respect to the midline. d) ROIs drawn in different flow territory and tissue types. ROI 1: anterior grey matter; ROI 2: anterior white matter; ROI 3: middle grey; ROI 4: middle white matter; ROI 5: Posterior grey; ROI 6: Posterior white matter. The ROI were mirrored with respect to the midline. The values in the upper corner represent the number of voxels included in the ROIs before deletion of vascular pixels. Images a) and b) were taken from Savoiaro *et al.*¹⁰⁴. ACA indicates anterior cerebral artery; MCA, middle cerebral artery; LSA, lenticulostriate arteries; A Ch A, anterior choroidal artery and PCA, posterior cerebral artery.

Statistical analysis

Deriving normal values

Demographic data generated qualitative and quantitative data. Quantitative data were presented as mean \pm SD or median (IQR). Values of CBF, CBV and MTT generated quantitative data and were presented as median (IQR). Differences between ROI (left vs right, different vascular territories, grey vs white) were determined by the wilcoxon rank sum test. A $p < 0.025$ was considered to indicate statistical significance.

Comparing normal values to perfusion values

Values of CBF, CBV and MTT generated quantitative data, and were presented as median (IQR). Differences between patient groups were determined for the different ROIs by the Wilcoxon rank sum test. A $p < 0.050$ was considered to indicate statistical significance.

3.1.6 Repeatability of ROI selection

Ten datasets were randomly chosen and were analyzed a second time by the same observer who was blinded for patient number and results of the first analysis. Repeatability was expressed in Coefficient of Variance (CoV), which was calculated as the quotient of SD and mean per couple of observations. Mean CoV was calculated per ROI per perfusion parameter and was also calculated for ROI sizes. A $\text{CoV} < 5\%$ was indicated as repeatable.

3.1.7 Ethical considerations

Since the study was retrospective in nature, had no clinical implications for the individual patients, was not controversial in nature and the data was presented anonymously, there was no need for informed consent.

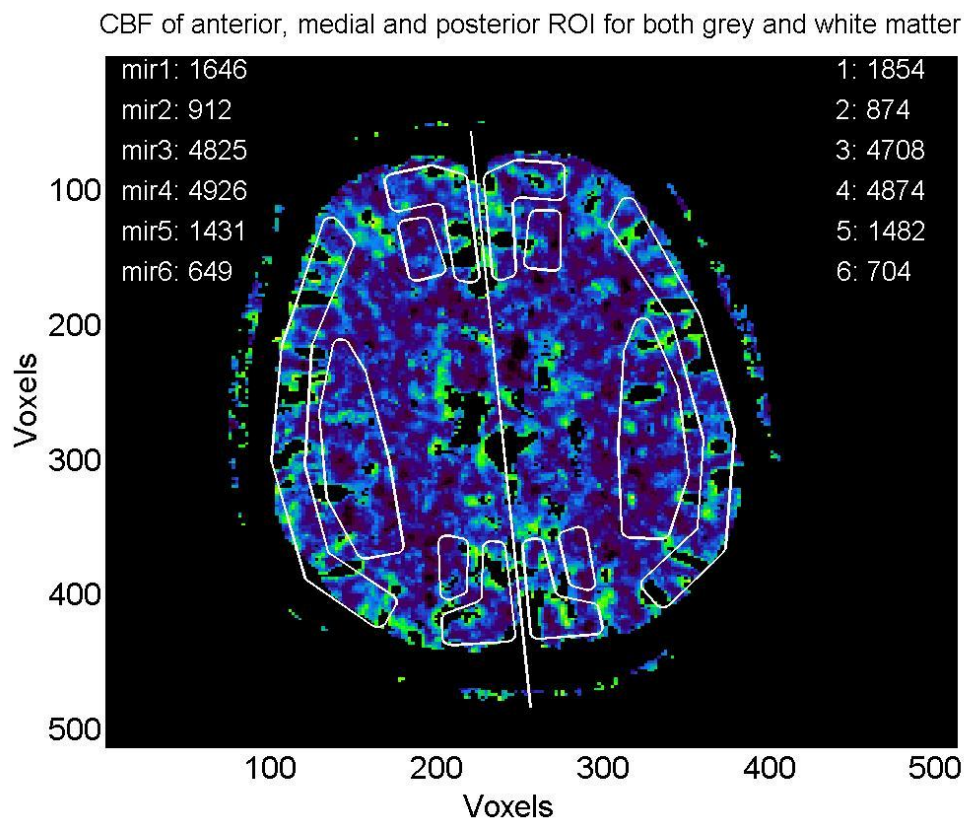


Figure 28. ROIs imaged on CBF map after deletion of vascular pixels. The values shown in the upper corners of the image represent the number of voxels included in the ROIs after deletion of vascular pixels.

3.2 Results

3.2.1 Population

CTP data of 87 patients was available, of which 27 could not be included in any group. Five patients were excluded because of coils or clips; 3 had large artefacts with unknown cause; data of 6 patients showed repeatedly errors in the PMA Asist, 1 had a CTP without contrast, and 11 patients could not be included because they had severe additional conditions. One TIA patient could not be included because the patient report was not available. Finally, 13 patients were included in the normal group, 8 in the TIA group and 39 in the ischemic stroke group. For 2 TIA patients and 10 ischemic stroke patients the affected hemisphere was not clear, so these patients could not be used for perfusion value analysis. Patient characteristics are presented in table 14.

Table 14. Characteristics of normal, TIA and CVA patients. Values are given as mean (SD), median (IQR) or absolute numbers (%). Not all variables were available for all patients. NIHSS indicates National Institute of Health Stroke Scale; mRS, modified Rankin Scale at hospital discharge; ACM, medial cerebral artery; ACP, posterior cerebral artery; Basilar, Basilar artery; Vertebral, vertebral artery.

Variable	Normal	TIA	Ischemic stroke
N	13	8	39
Sex, male/female	5/8	3/5	33/6
Age , years (mean)	57 (9)	58 (13)	64 (11)
Time to CT, min (mean)	132 (56) (N = 3)	179 (103) (N = 7)	163 (85)(N = 28)
Hemisphere, L/R/other/unknown		3/3/2/0	14/15/8/2
Thrombolysis	2 (15)	2 (25)	24 (62)
NIHSS (median)		0.5 (0 – 1.25)	4 (2 – 7.25) (N = 36)
mRS (median)	0 (0 – 0) (N = 8)	0 (0 – 1)	2 (0.5 – 4) (N = 36)
Vascular territory			
ACM		5	23
ACP		1	4
ACM-ACP			2
ACM-ACA			2
Basilar			5
Vertebral		1	1
Thalamus-pons			1
Diffuse		1	1

3.2.2 Deriving normal values of CBF, MTT and CBV in healthy subjects per brain region

This section presents the results of the third study objective: *Deriving normal values of CBF, MTT and CBV in healthy subjects for several different brain regions.*

Values of CBF, CBV and MTT for the normal patient group were derived and presented in table 15. CBF values of grey matter varied between 55 and 141 ml/100g/min with median values between 77 and 87 ml/100g/min. CBF values of white matter varied between 37 and 131 ml/100g/min with median values between 57 and 77 ml/100g/min. An overview of the variability of CBF values is given in figure 29. Within the left hemisphere significant differences were found between CBF in total grey matter (ROIs 1, 3 and 5) and CBF in basal ganglia (ROI 7) and CBF in total white matter (ROIs 2, 4 and 6) with the CBF in grey matter ($Z = 3.408$, $p < 0.001$) and in basal ganglia ($Z = -3.5291$, $p < 0.001$) showing higher CBF than in white matter. A significant difference was found between CBF in grey matter and CBF in white matter for the anterior flow territory, with grey matter showing higher CBF; $Z = 3.077$, $p = 0.002$. No significant differences were found between CBF in the anterior, medial and

Table 15. Perfusion values of normal subjects. Values are presented as median (IQR). CBF in ml/100g/min; CBV, ml/100g and MTT, s.

N = 13	Anterior		Medial		Posterior		Basal g.
	Grey	White	Grey	White	Grey	White	
CBF l	87 (70-100)	57 (47-66)	77 (71-89)	76 (61-87)	85 (70-93)	68 (56-84)	95 (80-108)
CBF r	84 (74-87)	59 (48-68)	82 (74-89)	71 (67-78)	87 (75-100)	77 (56-86)	85 (76-99)
CBV l	4.6 (4.0-5.3)	3.1 (2.7-4.0)	4.5 (4.2-4.8)	4.2 (3.5-4.8)	4.6 (4.2-5.3)	4.0 (3.2-4.7)	5.0 (4.5-5.8)
CBV r	4.5 (4.2-5.1)	3.6 (3.0-4.1)	4.5 (4.1-5.0)	4.0 (3.9-4.3)	4.6 (4.5-5.3)	4.5 (3.4-5.3)	4.8 (4.4-5.5)
MTT l	7.3 (6.9-7.7)	8.0 (7.6-8.3)	7.7 (7.5-8.1)	7.7 (7.5-8.0)	7.6 (7.4-8.1)	7.8 (7.5-8.1)	7.3 (7.0-7.6)
MTT r	7.7 (7.1-8.0)	8.2 (7.9-8.6)	7.5 (7.3-7.9)	7.8 (7.6-8.0)	7.5 (7.2-8.1)	8.2 (7.6-8.3)	7.4 (7.2-8.0)

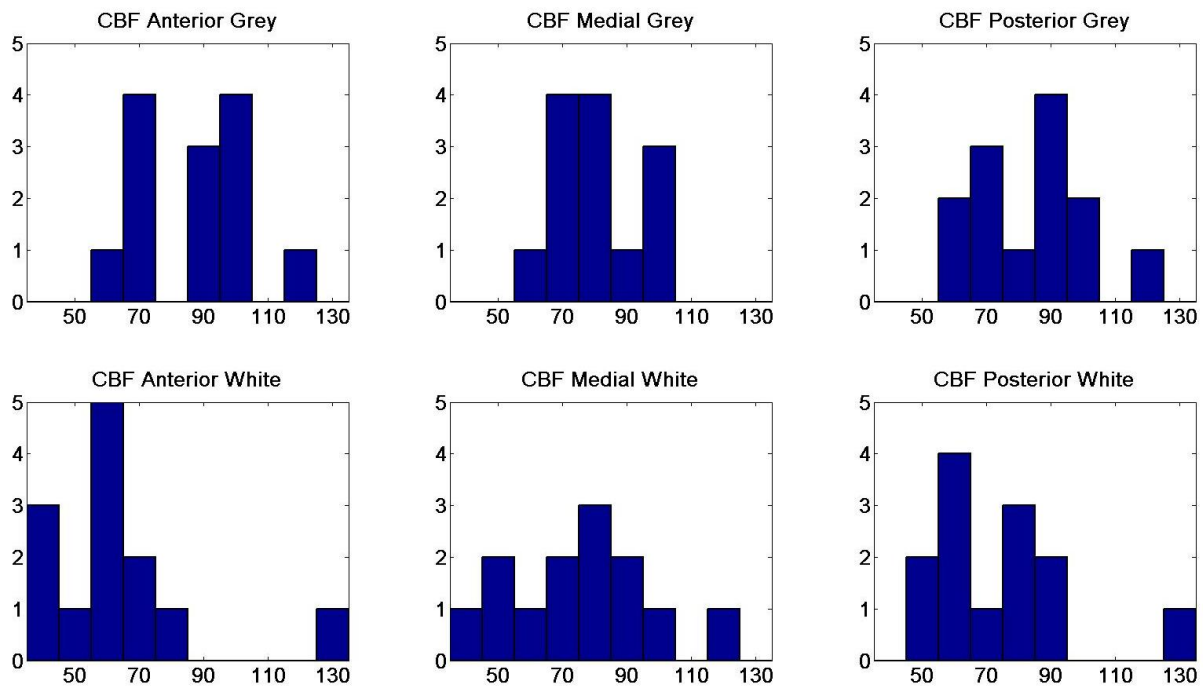


Figure 29. Histograms presenting the number of patients with CBF value per bin in the six ROIs of the left hemisphere of normal subjects. The ROI in grey matter showed higher CBF than the ROI in white matter. CBF in ml/100g/min.

posterior flow territories and no significant differences were found between the left and right hemisphere.

CBV values of grey matter varied between 3.6 and 7.5 ml/100g with median values between 4.5 and 4.6 ml/100g. CBV values of white matter varied between 2.0 and 7.0 ml/100g with median values between 3.1 and 4.5 ml/100g. Within the left hemisphere significant differences were found between CBV in total grey matter (ROIs 1, 3 and 5) and CBV in basal ganglia (ROI 7) and CBV in total white matter (ROIs 2, 4 and 6) with the CBV in grey matter ($Z = 3.428, p < 0.001$) and in basal ganglia ($Z = -3.487, p < 0.001$) showing higher CBV than in white matter. A significant difference was found between CBV in grey matter and CBV in white matter for the anterior flow territory, with grey matter showing higher CBV; $Z = 3.026, p = 0.003$. No significant differences were found between CBV in the anterior, medial and posterior flow territories and no significant differences were found between the left and right hemisphere.

MTT values of grey matter varied between 6.6 and 9.6 s with median values between 7.3 and 7.7 s. MTT values of white matter varied between 6.3 and 9.9 s with median values between 7.7 and 8.2 s.

Within the left hemisphere significant differences were found between MTT in total grey matter (ROIs 1, 3 and 5) and MTT in basal ganglia (ROI 7) and MTT in total white matter (ROIs 2, 4 and 6) with the MTT in grey matter ($Z = -3.168$, $p = 0.001$) and in basal ganglia ($Z = -2.980$, $p = 0.003$) showing lower MTT than in white matter. A significant difference was found between MTT in grey matter and MTT in white matter for the right anterior flow territory, with grey matter showing lower MTT; $Z = -2.308$, $p = 0.021$. The differences found in the right hemisphere were not significant in the left hemisphere. No significant differences were found between MTT in the anterior, medial and posterior flow territories and no significant differences were found between the left and right hemisphere.

3.2.3 Comparing normal values to perfusion values in TIA and ischemic stroke patients

This section presents the results of the fourth study objective: *Comparison of normal values to perfusion values of patients with TIA and ischemic stroke.*

Special attention should be drawn to the fact that complete hemispheres have been used for the comparison instead of affected flow territories. For example, the comparison using the affected hemispheres of ischemic stroke patients included patients with MCA deficits, patients with PCA deficits and patients with other deficits. A single exception was figure 30, which was created using separated groups for patients with a deficit of the MCA flow territory and patients with a deficit of the posterior flow territory.

The most striking findings in the comparison using the groups that are created according to the affected flow region were the MTT differences within the ischemic stroke group. The MTT was increased in the affected flow region for both the patients with a medial and with a posterior flow deficit, as shown in figure 30.

Comparison to the affected hemisphere of TIA patients

Values of CBF, CBV and MTT for the affected hemisphere of the TIA patients group were derived and presented in table 16. CBF values of grey matter varied between 69 and 110 ml/100g/min with median values between 80 and 91 ml/100g/min. CBF values of white matter varied between 40 and 113 ml/100g/min with median values between 65 and 73 ml/100g/min. No significant CBF differences between the hemispheres of the normal patient group and the affected hemisphere of the TIA patients group were found. CBV values of grey matter varied between 3.7 and 6.2 ml/100g with median values between 4.6 and 5.0 ml/100g. CBV values of white matter varied between 2.2 and 6.1 ml/100g with median values between 3.8 and 4.2 ml/100g. No significant differences with the normal patient group were found. MTT values of grey matter varied between 6.9 and 7.3 s with median values between 7.4 and 7.5 s. MTT values of white matter varied between 7.1 and 9.0 s with median values between 7.6 and 7.8 s. No significant differences with the normal patient group were found.

Table 16. Perfusion values of the affected hemisphere of TIA patients. Values are presented as median (IQR). CBF in ml/100g/min; CBV, ml/100g and MTT, s.

N = 6	Anterior		Medial		Posterior		Basal g.
	Grey	White	Grey	White	Grey	White	
CBF	91 (89-94)	65 (54-77)	80 (76-94)	65 (57-83)	90 (82-96)	73 (54-88)	92 (80-100)
CBV	4.9 (4.7-5.4)	3.9 (3.1-5.1)	4.6 (4.1-5.3)	3.8 (3.3-4.8)	5.0 (4.5-5.3)	4.2 (3.1-5.0)	5.0 (4.2-5.7)
MTT	7.4 (7.0-7.9)	7.8 (7.8-8.3)	7.5 (7.4-7.7)	7.8 (7.5-7.9)	7.4 (7.2-7.6)	7.6 (7.4-7.8)	7.3 (7.0-7.6)

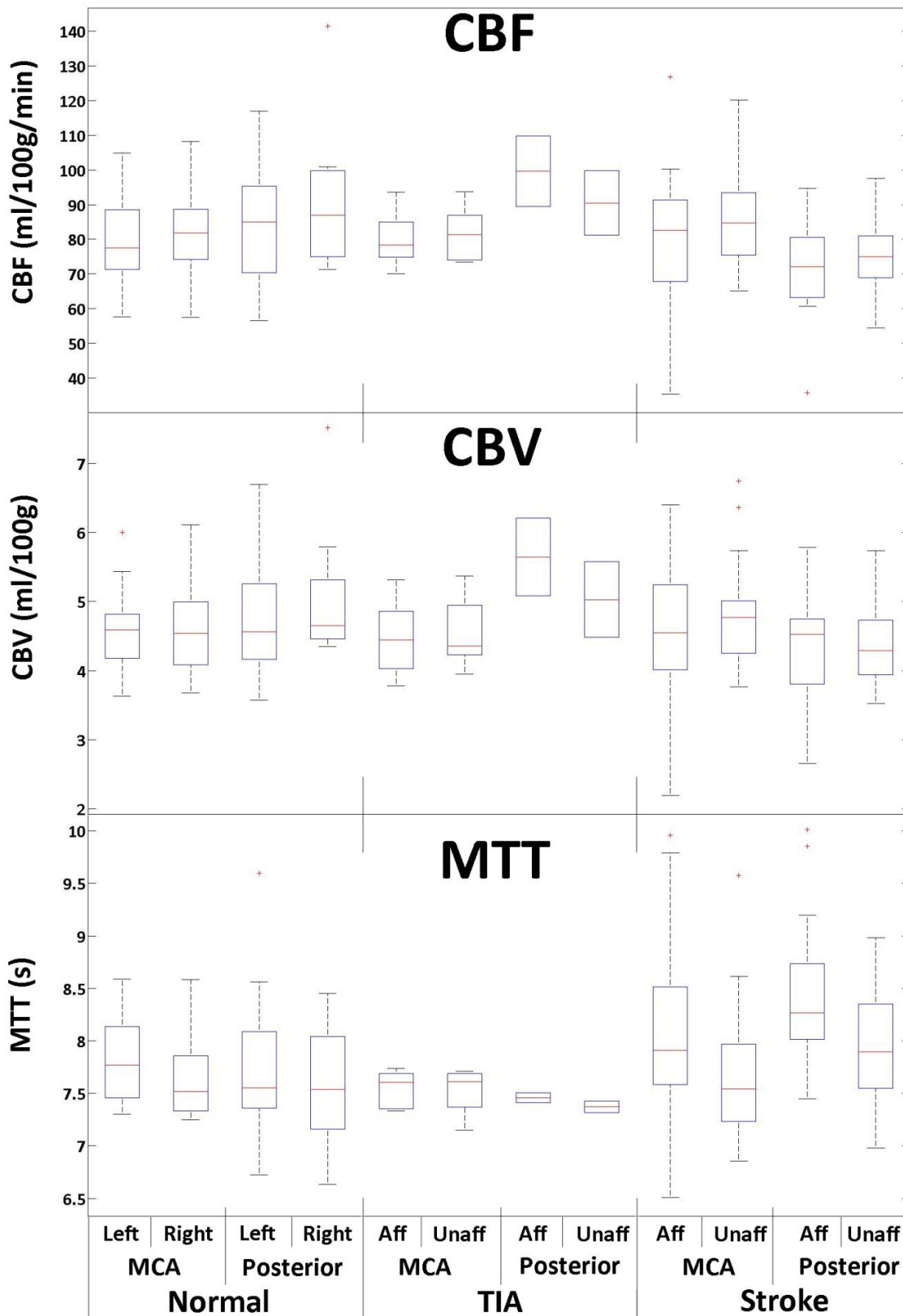


Figure 30. Boxplots presenting CBF, CBV and MTT obtained from the grey matter of normal subjects, TIA patients and ischemic stroke patients. For the normal subjects boxplots of the medial and posterior flow territories in the right and left hemisphere were included. TIA patients and ischemic stroke patients were divided over a medial and posterior group according to the affected flow territory. In the patient groups the affected flow territory was compared to the contralateral unaffected flow territory. For patients that had a central posterior deficit the mean of the perfusion values of the left and right hemisphere was used and was compared to the unaffected medial flow territory. (eg patients with a basilar artery deficit). Aff indicates affected; Unaff, unaffected.

Comparison to the affected hemisphere of ischemic stroke patients

Values of CBF, CBV and MTT for the affected hemisphere of the ischemic stroke patients group were derived and presented in table 17. CBF values of grey matter varied between 33 and 151 ml/100g/min with median values between 76 and 88 ml/100g/min. CBF values of white matter varied between 31 and 119 ml/100g/min with median values between 55 and 71 ml/100g/min. No significant CBF differences between the hemispheres of the normal patient group and the affected hemisphere of the TIA patients group were found. CBV values of grey matter varied between 2.1 and 7.0 ml/100g with median values between 4.5 and 4.8 ml/100g. CBV values of white matter varied between 1.9 and 6.8 ml/100g with median values between 3.4 and 4.1 ml/100g. No significant differences with the normal patient group were found. MTT values of grey matter varied between 5.9 and 11.3 s with median values between 7.6 and 7.9 s. MTT values of white matter varied between 7.0 and 10.6 s with median values between 8.0 and 8.2 s. The MTT of grey matter in the medial flow territory showed a significant increase with respect to the MTT of the same region in the right hemisphere of normal subjects; $Z = -1.986$, $p = 0.047$. Further, the MTT of white matter in the medial flow territory showed a significant increase with respect to the MTT of the same region in the left hemisphere of normal subjects; $Z = -2.013$, $p = 0.044$.

Table 17. Perfusion values of the affected hemisphere of ischemic stroke patients. Values are presented as median (IQR). CBF in ml/100g/min; CBV, ml/100g and MTT, s.

N = 29	Anterior		Medial		Posterior		Basal g.
	Grey	White	Grey	White	Grey	White	
CBF	78 (66-96)	55 (50-73)	76 (68-90)	61 (54-73)	88 (74-96)	71 (56-83)	90 (81-110)
CBV	4.5 (3.8-5.3)	3.4 (2.8-4.1)	4.5 (4.1-5.1)	3.9 (3.3-4.7)	4.8 (4.5-5.4)	4.1 (3.6-4.9)	51 (47-58)
MTT	7.6 (7.1-8.2)	8.0 (7.6-8.6)	7.9 (7.6-8.4)	8.2 (7.6-9.0)	7.6 (7.3-8.2)	8.1 (7.6-8.5)	7.4 (6.9-7.8)

Comparison to the unaffected hemisphere of TIA patients

Values of CBF, CBV and MTT of the unaffected hemisphere of the TIA patients group were derived and presented in table 18. CBF values of grey matter varied between 70 and 111 ml/100g/min with median values between 51 and 84 ml/100g/min. CBF values of white matter varied between 43 and 96 ml/100g/min with median values between 65 and 75 ml/100g/min. No significant CBF differences between the hemispheres of the normal patient group and the affected hemisphere of the TIA patients group were found. CBV values of grey matter varied between 3.9 and 6.2 ml/100g with median values between 4.5 and 4.6 ml/100g. CBV values of white matter varied between 2.5 and 5.5 ml/100g with median values between 3.8 and 4.4 ml/100g. No significant differences with the normal patient group were found. MTT values of grey matter varied between 6.6 and 7.9 s with median values between 7.0 and 7.5 s. MTT values of white matter varied between 7.2 and 8.7 s with median values between 7.6 and 7.9 s. No significant differences with the normal patient group were found.

Table 18. Perfusion values of the unaffected hemisphere of TIA patients. Values are presented as median (IQR). CBF in ml/100g/min; CBV, ml/100g and MTT, s.

N = 6	Anterior		Medial		Posterior		Basal g.
	Grey	White	Grey	White	Grey	White	
CBF	84 (76-100)	65 (48-86)	83 (74-94)	75 (59-81)	51 (73-86)	71 (67-81)	94 (83-102)
CBV	4.6 (4.0-5.7)	3.8 (2.9-4.7)	4.6 (4.3-5.4)	4.4 (3.3-4.7)	4.5 (4.0-5.0)	4.2 (3.6-4.5)	5.1 (4.6-5.7)
MTT	7.0 (7.2-7.9)	7.9 (7.9-8.1)	7.5 (7.4-7.7)	7.6 (7.8-8.1)	7.4 (7.3-7.8)	7.9 (7.4-8.2)	7.2 (7.0-7.5)

Comparison to the unaffected hemisphere of ischemic stroke patients

Values of CBF, CBV and MTT of the unaffected hemisphere of the ischemic stroke patients group were derived and presented in table 19. CBF values of grey matter varied between 57 and 137 ml/100g/min with median values between 80 and 87 ml/100g/min. CBF values of white matter varied between 37 and 121 ml/100g/min with median values between 61 and 73 ml/100g/min. No significant CBF differences between the hemispheres of the normal patient group and the affected hemisphere of the TIA patients group were found. CBV values of grey matter varied between 3.2 and 7.3 ml/100g with median values of 4.8 ml/100g. CBV values of white matter varied between 2.4 and 8.0 ml/100g with median values between 3.6 and 4.3 ml/100g. No significant differences with the normal patient group were found. MTT values of grey matter varied between 6.5 and 10.1 s with median values between 7.6 and 7.7 s. MTT values of white matter varied between 6.9 and 9.9 s with median values between 7.8 and 8.0 s. No significant differences with the normal patient group were found.

Table 19. Perfusion values of the unaffected hemisphere of ischemic stroke patients. Values are presented as median (IQR). CBF in ml/100g/min; CBV, ml/100g and MTT, s.

N = 36	Anterior		Medial		Posterior		Basal g.
	Grey	White	Grey	White	Grey	White	
CBF	82 (74-100)	61 (48-69)	80 (75-93)	67 (56-77)	87 (77-93)	73 (63-84)	80 (86-107)
CBV	4.8 (4.2-5.3)	3.6 (2.9-4.1)	4.8 (4.2-5.0)	3.7(3.2-4.3)	4.8 (4.5-5.2)	4.3 (3.8-4.9)	4.9 (4.6-5.7)
MTT	7.6 (7.2-8.0)	8.0 (7.7-8.6)	7.7 (7.2-7.9)	7.9 (7.7-8.1)	7.6 (7.1-7.9)	7.8 (7.4-8.6)	7.5 (7.0-7.9)

3.2.4 Intraobserver repeatability

The repeatability was highest for MTT and comparably lower for CBF and CBV, as shown in table 20.. The size of the ROI varied most between the attempts. The posterior flow territory had lower repeatability than the anterior, medial and basal ganglia flow territories. The CoV of the posterior flow territory exceeded 5% for the CBF and CBV.

Table 20. Intraobserver repeatability. Values represent average CoV, which was calculated as the quotient of the SD and the mean of the repeated analysis results in a patient. CoV indicates coefficient of variance (%); L, left; R, right; Bg, basal ganglia.

ROI	1L	1R	2L	2R	3L	3R	4L	4R	5L	5R	6L	6R	Bg l	Bg r
Size	9	9	12	12	10	11	13	13	9	9	20	20	16	15
CBF	2	3	4	5	2	1	2	4	2	4	7	8	3	3
CBV	2	3	3	4	1	1	3	3	2	4	5	6	3	2
MTT	1	1	2	3	1	1	1	1	2	2	2	2	2	2

3.3 Discussion

3.3.1 Deriving normal values

This section discusses the results of the third study objective: *Deriving normal values of CBF, MTT and CBV in healthy subjects for several different brain regions.*

This study found normal perfusion values of CBF, CBV and MTT with medians in the range of, respectively, 77-87 ml/100g/min, 4.5-4.6 ml/100g and 7.3-7.7 s for grey matter, 57-77 ml/100g/min, 3.1-4.5 ml/100g and 7.7-8.2 s for white matter and 85-95 ml/100g/min, 4.8-5.0 ml/100g and 7.3-7.4 s for the basal ganglia. The CBF and CBV were significantly higher and the MTT correspondingly significantly lower in the grey matter and basal ganglia compared to the white matter. The CBF and CBV in the anterior flow territory were significantly higher in grey matter than in white matter. The MTT in the anterior flow territory was significantly lower in grey matter than in white matter for the right hemisphere. No differences were found between flow territories or between hemispheres.

The normal values found differ with other perfusion values in healthy subjects found in literature. These studies all used different processing steps which may have influenced the results; for example all studies used a dated CT scanner with a smaller detector width. An older study by Wintermark *et al.*⁶⁸ found lower values compared to our data. They used standard SVD (sSVD) CTP in 9 subjects to derive CBF values in healthy patients and found a CBF of 68 ± 13 ml/100g/min in grey matter and 26 ± 10 ml/100g/min in white matter. Their method mainly differs from the current one in that they define all ROIs at the level of the basal ganglia, they let software automatically select AIF, and they use the sSVD deconvolution method, which may explain the differences. Another study is performed by Kudo *et al.*⁶⁹ in 2003, which was the first to use a vascular pixel elimination method. They found a CBF of 52.75 ml/100g/min in grey matter and of 30.38 ml/100g/min in white matter, which is significantly lower compared to the values found in this study. Their study differed to the current one in that they only used 5 healthy volunteers, that they took a scanning plane caudal of the basal ganglia and that they used basic deconvolution. Furthermore, a study performed by Grüner *et al.*⁷⁶ in 2011 found mean CBF values for the basal ganglia between 69 and 74 ml/100g/min and mean CBF values of grey and white matter between 67 and 75 ml/100g/min and between 18 and 24 ml/100g/min, respectively. All mean CBF values they found were lower than the values found in the current study. The authors did not specify the deconvolution method and used an imaging plane at the level of the basal ganglia. The most recent study was performed by Wang *et al.*⁷⁷ in 2014. They used the same areas for ROI selection and found mean grey matter CBF of 44-50 ml/100g/min and mean white matter CBF of 23-29 ml/100g/min, which are lower than the values found in the current study. Their method differed from the current one in that they used a venous output function for scaling, and automatic AIF selection. In conclusion, compared to the small number of studies that have been published previously, the current results show a higher CBF value for grey and white matter and the basal ganglia. This may be related to other processing methods.

The normal values derived in this study can be used as a guide to the management of patients with ABI. Quantitative perfusion values indicate the location and severity of perfusion deficits. They are an improvement of the currently available qualitative perfusion maps, because the maps only reflect whether flow is homogeneously distributed throughout the brain or not. A lower flow in a flow region can indicate a perfusion deficit in that particular region, or it can indicate that the flow in other regions is increased. It is very important to distinguish flow increase from flow decrease, since

it has contrary consequences for patient treatment. In conclusion, the type and severity of the perfusion deficit may assist the physician to choose an optimal treatment method and timing.

Furthermore, the normal values derived from this study may be used as a reference for future studies using CTP or other modalities to measure perfusion values quantitatively. No golden standard is present that may function as a true reference for perfusion values, since all previous studies have compared this technique with different imaging modalities. This study using CTP may function as a reference, because it uses one of the most recent CT scanners and used the currently best processing steps. The normal values found in this study may become more reliable by including more subjects.

It was expected that the perfusion values would be higher in grey matter and basal ganglia than in white matter, as these regions have a higher metabolic demand and therefore a higher CBF. However, the difference between grey and white matter was only present with the three ROIs per tissue type combined. This may be caused by the sample size, since the values for the three ROIs within a tissue type had almost the same perfusion values and therefore the absolute difference between grey and white matter did not increase when the ROIs were grouped. The flow territories did not have significant perfusion value differences, as was in agreement with previously found by other groups.^{76,77} Finally, as expected in normal subjects the CBF in the left and right hemisphere was comparable.

3.3.2 Comparison to perfusion values of TIA patients and ischemic stroke patients

This section discusses the results of the fourth study objective: *Comparison of normal values to perfusion values of patients with TIA and ischemic stroke.*

This study found differences in the MTT of the medial flow territory between grey matter in the affected hemisphere of ischemic stroke patients and the right hemisphere of normal subjects and between white matter in the affected hemisphere of ischemic stroke patients and the left hemisphere of normal subjects. The affected hemisphere of ischemic stroke patients had mainly lower CBF and CBV and higher MTT compared to normal subjects, although this did not reach statistical significance, possibly due to a low sample size. No differences in CBF between healthy patients and patients after TIA or in the unaffected hemisphere of ischemic stroke patients were found.

The normal values found in this study can be used to distinguish ischemic stroke patients from normal subjects. However, the groups do overlap, so a very low specificity and sensitivity is expected. A significant difference in CBF between stroke and non-stroke patients was expected. A significant difference in MTT of the medial flow territory between these groups was present. This difference was expected, because the majority of the ischemic stroke patients had medial flow territory deficits. The data suggests that MTT may be the perfusion value that is most severely affected in ischemic stroke patients. This is confirmed by table 5 in section 1.2.5 which shows that MTT deteriorates proportionally to perfusion pressure during mild to severe impairment, while CBF is initially kept constant and CBV initially increases. The lack of significance in the remaining differences between ischemic stroke patients and normal values may have had several causes. First, no patients with anterior flow deficits and only a few patients with posterior flow deficits were included. Significant differences between the ischemic stroke group and the normal group in the anterior and posterior flow territory were therefore unlikely. Second, the method of group selection could have influenced the results. The total group of ischemic stroke patients was categorized according to the affected

hemisphere: left, right or other. However, patients groups were not further divided as ischemic stroke in the ACA, MCA and PCA region. Therefore, changes in the perfusion in a specific region may be balanced out by patients that have normal perfusion values in that region, but worsened perfusion in another region.

The normal values found in this study cannot be used to distinguish normal subjects from TIA patients. That is as expected, since a TIA patient may have normal perfusion by the time the CTP is performed. We did not find changes in the perfusion of the unaffected side in a stroke patient compared to normal controls.

3.3.3 Repeatability

The repeatability study showed that the calculation of CBF, CBV and MTT in different flow territories and tissue types is reliable. The perfusion values of CBF and CBV showed a CoV between 1% and 8% and 1% and 6%, respectively. For MTT this was better: between 1% and 3%. Though, the sizes of the ROIs showed larger CoV: between 9% and 20%. These results indicate that the exact size of the ROI does not influence the perfusion values. In comparison to the study of Sanelli *et al.*⁷³ the repeatability is moderate. They used observers with varying levels of experience to draw ROI on patient data. They found CoV between 0.33 and 8.38% for CBF, CBV and MTT and concluded that the selection of ROI could be done by observers with different levels of experience. The observer of the current study is less experienced than the observers of that study, but at least 2 of 6 observers achieved worse results in that study indicating that the current method of ROI selection has a good repeatability. As the differences between the patient groups are low, the variance of the technique must be low to generate adequate sensitivity for detection of ischemia.

3.4 Limitations

The first limitation is that the subjects treated as ‘healthy subjects’ may not be truly healthy. They had an indication for CTP based on signs and symptoms of stroke, so they may have had a perfusion deficit. The deficit may have resolved by the time the CTP was performed, but still the perfusion values may be influenced by this temporary deficit. On the other hand, we were able to identify stroke patients from non-stroke patients which was a clinically relevant result. Values from non-stroke patients may differ from normal values, but this has limited clinical relevance.

Second, a large limitation is the small sample size, especially of the normal and TIA group. The data of a large group of patients is saved in the databases of the RadboudUMC. For the data to be available for calculation, they need to be transferred to another database, causing a very high burden on the digital network of the hospital and was therefore not available for the current study; but will become available soon.

The midline and all ROI were drawn manually. The advantage of this method is that the observer can handle every individual different patient. But, it may increase the chance of errors. For example, a midline which is not truly drawn on the midline may cause discrepancies regarding the left-to-right comparison. Moreover, the ROI are drawn with different shapes and sizes, which may for example result in the selective inclusion of cortices with a higher metabolic demand.

The identification of tissue type or flow territory is based on schematic atlases. Differences in anatomy between subjects may result in misclassification of tissue (For example, that a ROI is selected in the white matter, while it was destined to be selected in grey matter).

Finally, as mentioned earlier all processing steps that are incorporated in the analysis of CTP data influence the final result. The one and only best processing algorithm does not exist, so the results are partly based on hardware properties and choices made by the researchers. The extent of variance of each individual step is moderate, but the total variance of all processing steps may be significant.

3.5 Recommendations

First, as mentioned earlier, it is recommended to increase the size of the patient groups, especially the normal group and the TIA group. A larger group will give more confidence that the normal values give a true representation of healthy subjects. To compare the subjects to patient groups, that groups have to be of a satisfying size as well. A group size of at least 50 patients per group is recommended.

In addition, a review should be performed to the CTP processing factors. In this study the combination of processing settings was chosen according to literature, availability and experience of the authors. However, an objective review per processing factor would further optimize CTP acquisition. Consequently, the quantitative results would be more reliable and would be better applicable in clinical practice.

Further, it is recommended to perform a study to identify the best method to determine an individual threshold for the deletion of vascular pixels. The vascular pixel deletion algorithm of the current study used a constant threshold for all patients. However, the correctness of the value of the threshold can be questioned. The results of the deletion differed per patient: in some patients only vessel like structures were deleted, while in others also bigger structures were deleted. This finding suggests that each patient may require an individual deletion threshold. Some possible solutions are manual setting of the individual threshold, or the threshold can be set to a certain percentage of the maximum intensity values or the vessels can be segmented and deleted in the source data.

Next, it is recommended to find a method to improve the identification of anatomical structures. During this study a large number of anatomical varieties of the brain were encountered. These varieties make the recognition of the anatomical structures difficult and may have led to incorrect placement of ROIs. The recognition of the anatomical structures could be improved by an MRI scan of the patients, which is available for some patients in the database. Otherwise an experienced radiologist may perform better on distinguishing anatomical structures and therefore ROI selection.

Furthermore, it is recommended to select patient groups according to a specific affected flow territory, instead of an affected hemisphere. In this study, comparison of flow territories was performed using a group of patients with a heterogeneous division of affected hemispheres. Therefore, potential perfusion differences in a certain flow territory were balanced out by patients with a perfusion deficit in another flow territory. More reliable differences would be found with specifically selected groups.

Finally, it is recommended to perform a study in which patient groups are selected according to severity of ischemic stroke. In the current study patients with mild, moderate and severe stroke are combined. The differences in perfusion values may be reduced by patients with a mild and small impairment. Division of patients can be performed according to the NIHSS. Using the subdivision

perfusion values per group can be determined. These values could be used as a guide for assessing severity of stroke.

3.6 Conclusion

This study found normal perfusion values of CBF, CBV and MTT with medians in the range of, respectively, 77-87 ml/100g/min, 4.5-4.6 ml/100g and 7.3-7.7 s for grey matter, 57-77 ml/100g/min, 3.1-4.5 ml/100g and 7.7-8.2 s for white matter and 85-95 ml/100g/min, 4.8-5.0 ml/100g and 7.3-7.4 s for the basal ganglia. Small differences were found between the affected side in stroke patients compared to other groups. Increase in sample size, improvement of the vascular pixel deletion method and optimization of recognition of anatomical structures for ROI selection is required before introduction into clinical practice.

References

1. Nationaal Kompas Volksgezondheid. Beroerte: prevalentie, incidentie en sterfte naar leeftijd en geslacht. 2014. Available at: <http://www.nationaalkompas.nl/gezondheid-en-ziekte/ziekten-en-aandoeningen/hartvaatstelsel/beroerte/omvang/>. Accessed August 10, 2015.
2. Kim D, Dunn I, Ellegala D, Fox J. Principles of cerebral oxygenation and blood flow in the neurological critical care unit. *Neurocrit Care*. 2006;77–82. doi:10.1385/Neurocrit.
3. Smith BA, Clayton EW, Robertson D. Experimental Arrest of Cerebral Blood Flow in Human Subjects: the Red Wing studies revisited. *Perspect Biol Med*. 2013;54(2). doi:10.1353/pbm.2011.0018.Experimental.
4. Dagal A, Lam AM. Cerebral blood flow and the injured brain: how should we monitor and manipulate it? *Curr Opin Anaesthesiol*. 2011;24(2):131–7. doi:10.1097/ACO.0b013e3283445898.
5. Boron WF, Boulpaep EL. Section III: The nervous system. In: *Medical Physiology: a cellular and molecular approach*. Elsevier Health Sciences; 2007.
6. Kontos H, Wei E, Navari R. Responses of cerebral arteries and arterioles to acute hypotension and hypertension. *Am J Physiol*. 1978;234(4):371–383.
7. Willie CK, Tzeng Y-C, Fisher J a, Ainslie PN. Integrative regulation of human brain blood flow. *J Physiol*. 2014;592(Pt 5):841–59. doi:10.1113/jphysiol.2013.268953.
8. Grotta J, Ackerman R, Correia J, Fallick G, Chang J. Whole blood viscosity parameters and cerebral blood flow. *Stroke*. 1982;13(3):296.
9. Bisschops LL a, Pop G a M, Teerenstra S, Struijk PC, van der Hoeven JG, Hoedemaekers CWE. Effects of viscosity on cerebral blood flow after cardiac arrest. *Crit Care Med*. 2014;42(3):632–7. doi:10.1097/CCM.0000000000000027.
10. Irace C, Tripolino C, Scavelli F, et al. Blood viscosity but not shear stress associates with delayed flow-mediated dilation. *Eur J Appl Physiol*. 2014. doi:10.1007/s00421-014-3058-8.
11. Lassen NA. Cerebral blood flow and oxygen consumption in man. *Physiol Rev*. 1959;39:183–283.
12. Numan T, Bain AR, Hoiland RL, Smirl JD, Lewis NC, Ainslie PN. Static autoregulation in humans: a review and reanalysis. *Med Eng Phys*. 2014;36(11):1487–95. doi:10.1016/j.medengphy.2014.08.001.
13. Willie CK, Macleod DB, Shaw a D, et al. Regional brain blood flow in man during acute changes in arterial blood gases. *J Physiol*. 2012;590(14):3261–75. doi:10.1113/jphysiol.2012.228551.

14. Sato K, Sadamoto T, Hirasawa A, et al. Differential blood flow responses to CO₂ in human internal and external carotid and vertebral arteries. *J Physiol*. 2012;590(14):3277–90. doi:10.1113/jphysiol.2012.230425.
15. Ainslie PN, Ashmead JC, Ide K, Morgan BJ, Poulin MJ. Differential responses to CO₂ and sympathetic stimulation in the cerebral and femoral circulations in humans. *J Physiol*. 2005;566(2):613–24. doi:10.1113/jphysiol.2005.087320.
16. Battisti-Charbonney a, Fisher J, Duffin J. The cerebrovascular response to carbon dioxide in humans. *J Physiol*. 2011;589(12):3039–48. doi:10.1113/jphysiol.2011.206052.
17. Kass IS. Physiology and Metabolism of the Brain and Spinal Cord. In: Newfield P, Cottrell JE, eds. *Handbook of Neuroanesthesia*. 4th ed. Lippincott Williams & Wilkins; 2007:3–22.
18. Mardimae A. The interaction of carbon dioxide and hypoxia in the control of cerebral blood flow. *Pflugers Arch Eur J Physiol*. 2012;464:345–351.
19. Obermeier B, Daneman R, Ransohoff R. Development, maintenance and disruption of the blood-brain barrier. *Nat Med*. 2013;19(12):1584–1596. doi:10.1038/nm.3407.Development.
20. Hamner JW, Tan CO, Tzeng Y-C, Taylor JA. Cholinergic control of the cerebral vasculature in humans. *J Physiol*. 2012;590(Pt 24):6343–52. doi:10.1113/jphysiol.2012.245100.
21. Fox P, Raichle M. Focal physiological uncoupling of cerebral blood flow and oxidative metabolism during somatosensory stimulation in human subjects. ... *Natl Acad Sci*. 1986;83:1140–1144.
22. Rosengarten B, Aldinger C, Kaufmann A, Kaps M. Comparison of visually evoked peak systolic and end diastolic blood flow velocity using a control system approach. *Ultrasound Med Biol*. 2001;27:1499–1503.
23. Peterson EC, Wang Z, Britz G. Regulation of cerebral blood flow. *Int J Vasc Med*. 2011;2011:1–8. doi:10.1155/2011/823525.
24. Marchal G, Beaudouin, V. Rioux P, de la Sayette V, et al. Prolonged Persistence of Substantial Volumes of Potentially Viable Brain Tissue After Stroke. *Stroke*. 1996;27:599–606.
25. Hoeffner EG, Case I, Jain R, et al. Cerebral perfusion CT: technique and clinical applications. *Radiology*. 2004;231:632–644.
26. Wintermark M, Dillon WP, Smith WS, et al. Visual grading system for vasospasm based on perfusion CT imaging: comparisons with conventional angiography and quantitative perfusion CT. *Cerebrovasc Dis*. 2008;26(2):163–70. doi:10.1159/000139664.
27. Steiner L a, Andrews PJD. Monitoring the injured brain: ICP and CBF. *Br J Anaesth*. 2006;97(1):26–38. doi:10.1093/bja/ael110.
28. Cianfoni A, Colosimo C, Basile M, Wintermark M, Bonomo L. Brain perfusion CT: principles, technique and clinical applications. *Radiol Med*. 2007;112(8):1225–43. doi:10.1007/s11547-007-0219-4.

29. Fieselmann A, Kowarschik M, Ganguly A, Hornegger J, Fahrig R. Deconvolution-Based CT and MR Brain Perfusion Measurement: Theoretical Model Revisited and Practical Implementation Details. *Int J Biomed Imaging*. 2011;2011:467563. doi:10.1155/2011/467563.
30. Brauer P, Kochs E, Werner C. Correlation of transcranial Doppler sonography mean flow velocity with cerebral blood flow in patients with intracranial pathology. *J Neurosurg Anesthesiol*. 1998;10(2):80–85. Available at: http://journals.lww.com/jnsa/abstract/1998/04000/correlation_of_transcranial_doppler_sonography.3.aspx. Accessed December 9, 2014.
31. Boulpaep E, Lederer W, Segal S. The Cardiovascular System. In: Boron WF, Boulpaep EL, eds. *Medical Physiology: a cellular and molecular approach.*; 2005:421–590.
32. White H, Venkatesh B. Applications of transcranial Doppler in the ICU: a review. *Intensive Care Med*. 2006;32(7):981–94. doi:10.1007/s00134-006-0173-y.
33. Aaslid R, Markwalder T, Nornes H. Noninvasive transcranial Doppler ultrasound recording of flow velocity in basal cerebral arteries. *J Neurosurg*. 1982;57:769–774. Available at: <http://thejns.org/doi/abs/10.3171/jns.1982.57.6.0769>. Accessed April 20, 2015.
34. Kelley R, Chang J, Scheinman N. Transcranial Doppler assessment of cerebral flow velocity during cognitive tasks. *Stroke*. 1992. Available at: <http://stroke.ahajournals.org/content/23/1/9.short>. Accessed April 20, 2015.
35. Newell D, Aaslid R, Lam A, Mayberg T, Winn H. Comparison of flow and velocity during dynamic autoregulation testing in humans. *Stroke*. 1994:793–798. Available at: <http://stroke.ahajournals.org/content/25/4/793.short>. Accessed April 20, 2015.
36. Ferrara L, Mancini M, Iannuzzi R, et al. Carotid Diameter and Blood Flow Velocities in Cerebral Circulation in Hypertensive Patients. *Stroke*. 1995;26:418–421.
37. Nakae R, Yokota H, Yoshida D, Teramoto A. Transcranial Doppler ultrasonography for diagnosis of cerebral vasospasm after aneurysmal subarachnoid hemorrhage: mean blood flow velocity ratio of the ipsilateral and contralateral middle cerebral arteries. *Neurosurgery*. 2011;69(4):876–83; discussion 883. doi:10.1227/NEU.0b013e318222dc4c.
38. Pase MP, Grima N a, Stough CK, Scholey A, Pipingas A. Cardiovascular disease risk and cerebral blood flow velocity. *Stroke*. 2012;43(10):2803–5. doi:10.1161/STROKEAHA.112.666727.
39. Haubrich C, Steiner L, Diehl RR. Doppler Flow Velocity and Intra-cranial Pressure: Responses to Short-Term Mild Hypocapnia Help to Assess the Pressure-Volume Relationship After Head. *Ultrasound Med* 2013. Available at: <http://www.sciencedirect.com/science/article/pii/S0301562913006212>. Accessed August 14, 2015.
40. Pase MP, Grima N a, Stough C, Scholey A, Pipingas A. Association of pulsatile and mean cerebral blood flow velocity with age and neuropsychological performance. *Physiol Behav*. 2014;130:23–7. doi:10.1016/j.physbeh.2014.03.015.

41. Droste DW, Iliescu C, Vaillant M, et al. Advice on lifestyle changes (diet, red wine and physical activity) does not affect internal carotid and middle cerebral artery blood flow velocity in patients with carotid arteriosclerosis in a randomized controlled trial. *Cerebrovasc Dis*. 2014;37(5):368–75. doi:10.1159/000362535.
42. Serber SL, Rinsky B, Kumar R, Macey PM, Fonarow GC, Harper RM. Cerebral blood flow velocity and vasomotor reactivity during autonomic challenges in heart failure. *Nurs Res*. 2014;63(3):194–202. doi:10.1097/NNR.000000000000027.
43. Oosterom A, Oostendorp TF. Afbeeldingstechnieken. In: *Medische Fysica*.; 1997:111–130.
44. Endo M, Mori S, Tsunoo T, et al. Development and Performance Evaluation of the First Model of 4-D CT-Scanner. *IEEE Trans Nucl Sci*. 2003;50(5):1667–1671.
45. Eastwood JD, Lev MH, Provenzale MP. Perfusion CT with Iodinated Contrast Material. *Am J Roentgenol*. 2003;180(1):3–12.
46. Miles KA. Image acquisition and contrast enhancement protocols for perfusion CT. In: *Multidetector Computed Tomography in Cerebrovascular Disease - CT perfusion*.; 2007:47–55.
47. Wintermark M, Smith W. Dynamic perfusion CT: optimizing the temporal resolution and contrast volume for calculation of perfusion CT parameters in stroke patients. *Am J Neuroradiol*. 2004;25:720–729.
48. Dankbaar JW, Hom J, Schneider T, et al. Dynamic perfusion CT assessment of the blood-brain barrier permeability: first pass versus delayed acquisition. *Am J Neuroradiol*. 2008;29(9):1671–6. doi:10.3174/ajnr.A1203.
49. Radiation Dose in X-Ray and CT Exams. *Am Radiol Soc North Radiol Am Coll*. 2014. Available at: www.radiologyinfo.org/en/safety/?pg=sfty_xray.
50. Manniesing R, Oei M, Ginneken B van, Prokop M. Quantitative Dose Dependency Analysis of Whole-Brain CT Perfusion Imaging. *Radiology*. 2015:1–8. Available at: <http://pubs.rsna.org/doi/abs/10.1148/radiol.2015142230>. Accessed July 9, 2015.
51. Aquilion ONE family. Available at: medical.toshiba.com/products/ct/aquilion-one-family/scalable-technology.php.
52. Lin C, Wu T, Lin C. Can iterative reconstruction improve imaging quality for lower radiation CT perfusion? Initial experience. *Am J ...*. 2013:1–6. Available at: <http://www.ajnr.org/content/34/8/1516.short>. Accessed August 19, 2015.
53. Martínez-de-alegría A, García-figueiras R, Baleato-gonzález S, Rodríguez-alvarez MJ, Martínez-souto I, Villalba-martín C. Effect of Slice Thickness Reconstruction on Quantitative Vascular Parameters in Perfusion CT. 2014;(March):53–59.
54. Lee TY, Murphy B. Implementing deconvolution analysis for perfusion CT. In: *Multidetector Computed Tomography in cerebral disease CT Perfusion Imaging*.; 2007.

55. Mendrik AM, Vonken E, van Ginneken B, et al. TIPS bilateral noise reduction in 4D CT perfusion scans produces high-quality cerebral blood flow maps. *Phys Med Biol*. 2011;56(13):3857–72. doi:10.1088/0031-9155/56/13/008.
56. Fahmi F, Riordan A, Beenen L, et al. The effect of head movement on CT perfusion summary maps: simulations with CT hybrid phantom data. *Med Biol Eng Comput*. 2014;52:141–147. doi:10.1007/s11517-013-1125-7.
57. Fahmi F, Marquering H, Borst J, et al. 3D movement correction of CT brain perfusion image data of patients with acute ischemic stroke. *Neuroradiology*. 2014;56:445–452. doi:10.1007/s00234-014-1358-7.
58. Kudo K, Sasaki M, Ogasawara K, Terae S. Difference in Tracer Delay–induced Effect among Deconvolution Algorithms in CT Perfusion Analysis: Quantitative Evaluation with Digital Phantoms 1. *Radiology*. 2009;251(1):241–249. Available at: <http://pubs.rsna.org/doi/abs/10.1148/radiol.2511080983>. Accessed August 15, 2015.
59. Kudo K, Sasaki M, Yamada K. Differences in CT Perfusion Maps Generated by Different Commercial Software: Quantitative Analysis by Using Identical Source Data of Acute Stroke Patients 1. *Radiology*. 2009;254(1). doi:10.1148/radiol.254082000/-/DC1.
60. Niesten J, Schaaf I van der, Riordan A, Jong W de, Mali W, Velthuis B. Optimisation of vascular input and output functions in CT-perfusion imaging using 256 (or more)-slice multidetector CT. *Eur Radiol*. 2013;23:1242–1249. doi:10.1007/s00330-012-2731-8.
61. Zaro-Weber O, Moeller-Hartmann W. input function on absolute and relative perfusion-weighted imaging penumbral flow detection a validation with 15O-water positron emission tomography. *Stroke*. 2012;43:378–385. doi:10.1161/STROKEAHA.111.635458.
62. Soares BP, Dankbaar JW, Bredno J, et al. Automated versus manual post-processing of perfusion-CT data in patients with acute cerebral ischemia: influence on interobserver variability. *Neuroradiology*. 2009;51(7):445–51. doi:10.1007/s00234-009-0516-9.
63. Wintermark M, Lau BC, Chien J, Arora S. The anterior cerebral artery is an appropriate arterial input function for perfusion-CT processing in patients with acute stroke. *Neuroradiology*. 2008;50(3):227–36. doi:10.1007/s00234-007-0336-8.
64. Manniesing R. Expert Opinion. 2015.
65. Abels B, Klotz E, Tomandl BF, Kloska SP, Lell MM. Perfusion CT in acute ischemic stroke: a qualitative and quantitative comparison of deconvolution and maximum slope approach. *AJNR Am J Neuroradiol*. 2010;31(9):1690–8. doi:10.3174/ajnr.A2151.
66. Schneider T, Hom J, Bredno J, Dankbaar JW, Cheng S-C, Wintermark M. Delay correction for the assessment of blood-brain barrier permeability using first-pass dynamic perfusion CT. *Am J Neuroradiol*. 2011;32(7):134–8. doi:10.3174/ajnr.A2152.
67. Boutelier T, Kudo K, Pautot F, Sasaki M. Bayesian hemodynamic parameter estimation by bolus tracking perfusion weighted imaging. *IEEE Trans Med Imaging*. 2012;31(7):1381–95. doi:10.1109/TMI.2012.2189890.

68. Wintermark M, Thiran J. Simultaneous measurement of regional cerebral blood flow by perfusion CT and stable xenon CT: a validation study. *Am J Neuroradiol*. 2001;22:905–914.
69. Kudo K, Terae S, Katoh C. Quantitative cerebral blood flow measurement with dynamic perfusion CT using the vascular-pixel elimination method: comparison with H215O positron emission. *Am J Neuroradiol*. 2003;24:419–426.
70. Sase S, Honda M. Comparison of cerebral blood flow between perfusion computed tomography and xenon-enhanced computed tomography for normal subjects: territorial analysis. *J Comput ...*. 2005;29(2):270–277. Available at: http://journals.lww.com/jcat/Abstract/2005/03000/Comparison_of_Cerebral_Blood_Flow_Between.23.aspx. Accessed April 8, 2015.
71. Kudo K, Christensen S, Sasaki M. Accuracy and reliability assessment of CT and MR perfusion analysis software using a digital phantom. *Radiology*. 2013;267(1):201–211. doi:10.1148/radiol.12112618/-/DC1.
72. Fahmi F, Marquering HA, Streekstra G, et al. Differences in CT perfusion summary maps for patients with acute ischemic stroke generated by 2 software packages. *Am J Neuroradiol*. 2012;33:2074–2080. Available at: <http://www.ajnr.org/content/33/11/2074.short>. Accessed July 9, 2015.
73. Sanelli P, Nicola G, Johnson R, et al. Effect of training and experience on qualitative and quantitative CT perfusion data. *Am J Neuroradiol*. 2007;28:428–432. Available at: <http://www.ajnr.org/content/28/3/428.short>. Accessed July 9, 2015.
74. Waaijer A, Schaaf IC, Velthuis BK, et al. Reproducibility of quantitative CT brain perfusion measurements in patients with symptomatic unilateral carotid artery stenosis. *Am J Neuroradiol*. 2007;28:927–932. Available at: <http://www.ajnr.org/content/28/5/927.short>. Accessed April 20, 2015.
75. Ziegelitz D, Starck G, Mikkelsen IK, et al. Absolute quantification of cerebral blood flow in neurologically normal volunteers: Dynamic-susceptibility contrast MRI-perfusion compared with computed tomography (CT)-perfusion. *Magn Reson Med*. 2009;62(1):56–65. doi:10.1002/mrm.21975.
76. Grüner J, Paamand R, Højgaard L, Law I. Brain perfusion CT compared with 15O-H2O-PET in healthy subjects. *EJNMMI Res*. 2011;1(1):28. doi:10.1186/2191-219X-1-28.
77. Wang Y, Zhang H, Tang S, et al. Assessing regional cerebral blood flow in depression using 320-slice computed tomography. *PLoS One*. 2014;9(9):e107735. doi:10.1371/journal.pone.0107735.
78. Böck JC, Henrikson O, Götze AH, Wlodarczyk W, Sander B, Felix R. Magnetic resonance perfusion imaging with gadolinium-DTPA. A quantitative approach for the kinetic analysis of first-pass residue curves. *Invest Radiol*. 1995;30(12):693–699.
79. Leiva-Salinas C, Provenzale JM, Kudo K, Sasaki M, Wintermark M. The alphabet soup of perfusion CT and MR imaging: terminology revisited and clarified in five questions. *Neuroradiology*. 2012;54(9):907–18. doi:10.1007/s00234-012-1028-6.

80. Calamante F, Gadian DG, Conolly A. Delay and dispersion effects in dynamic susceptibility contrast MRI: simulations using singular value decomposition. *Proc Intl Soc Mag Reson Med*. 2000;8:745.
81. Grüner JM, Paamand R, Kosteljanetz M, Broholm H, Højgaard L, Law I. Brain perfusion CT compared with 15O-H₂O PET in patients with primary brain tumours. *Eur J Nucl Med Mol Imaging*. 2012;39(11):1691–1701. doi:10.1007/s00259-012-2173-1.
82. Bisdas S, Donnerstag F, Berding G, Vogl TJ, Thng CH, Koh TS. Computed tomography assessment of cerebral perfusion using a distributed parameter tracer kinetics model: validation with H(2)((15))O positron emission tomography measurements and initial clinical experience in patients with acute stroke. *J Cereb blood flow Metab*. 2008;28(2):402–11. doi:10.1038/sj.jcbfm.9600522.
83. Koenig M, Klotz E, Luka B, Venderink DJ, Spittler JF, Heuser L. Perfusion CT of the brain: diagnostic approach for early detection of ischemic stroke. *Radiology*. 1998;209:85–93.
84. Furukawa M, Kashiwagi S. Evaluation of cerebral perfusion parameters measured by perfusion CT in chronic cerebral ischemia: comparison with xenon CT. *J Comput Assist Tomogr*. 2002;26(2):272–278.
85. Cenic A, Nabavi D. Dynamic CT measurement of cerebral blood flow: a validation study. *Am J ...* 1999;(January):63–73. Available at: <http://www.ajnr.org/content/20/1/63.short>. Accessed April 8, 2015.
86. Bisdas S, Hartel M, Cheong LH, Koh TS, Vogl TJ. Prediction of subsequent hemorrhage in acute ischemic stroke using permeability CT imaging and a distributed parameter tracer kinetic model. *J Neuroradiol*. 2007;34(2):101–108.
87. Van der Hoeven EJRJ, Dankbaar JW, Algra A, et al. Additional diagnostic value of computed tomography perfusion for detection of acute ischemic stroke in the posterior circulation. *Stroke*. 2015;46(4):1113–5. doi:10.1161/STROKEAHA.115.008718.
88. Miles KA, Menon DK. Cerebrovascular physiology and pathophysiology. In: *Multidetector Computed Tomography in Cerebrovascular Disease - CT perfusion.*; 2006:71–82.
89. Wintermark M, Melle G Van, Schnyder P. Admission Perfusion CT: Prognostic Value in Patients with Severe Head Trauma. *Radiology*. 2004;232:211–220. Available at: <http://pubs.rsna.org/doi/abs/10.1148/radiol.2321030824>. Accessed January 20, 2015.
90. Wintermark M, Chiolerio R. Cerebral vascular autoregulation assessed by perfusion-CT in severe head trauma patients. *J Neuroradiol*. 2006;33:27–37. Available at: <http://www.sciencedirect.com/science/article/pii/S015098610677225X>. Accessed January 20, 2015.
91. Bendinelli C, Bivard A, Nebauer S, Parsons MW, Balogh ZJ. Brain CT perfusion provides additional useful information in severe traumatic brain injury. *Injury*. 2013;44(9):1208–1212.
92. Nabavi D, LeBlanc L, Baxter B, Lee D. Monitoring cerebral perfusion after subarachnoid hemorrhage using CT. *Neuroradiology*. 2001;43:7–16.

93. Lui YW, Tang ER, Allmendinger a M, Spektor V. Evaluation of CT perfusion in the setting of cerebral ischemia: patterns and pitfalls. *AJNR Am J Neuroradiol*. 2010;31(9):1552–63. doi:10.3174/ajnr.A2026.
94. Cremers CHP, Vos PC, van der Schaaf IC, et al. CT perfusion during delayed cerebral ischemia after subarachnoid hemorrhage: distinction between reversible ischemia and ischemia progressing to infarction. *Neuroradiology*. 2015. doi:10.1007/s00234-015-1543-3.
95. Barfett JJ, Velauthapillai N, Fierstra J, et al. Intra-vascular blood velocity and volumetric flow rate calculated from dynamic 4D CT angiography using a time of flight technique. *Int J Cardiovasc Imaging*. 2014;30(7):1383–92. doi:10.1007/s10554-014-0471-3.
96. Prevrhal S, Forsythe C, Harnish R. CT angiographic measurement of vascular blood flow velocity by using projection data. *Radiology*. 2011;261(3):923–929. Available at: <http://pubs.rsna.org/doi/abs/10.1148/radiol.11110617>. Accessed August 7, 2015.
97. Barfett J, Fierstra J, Mikulis D, Krings T. Blood velocity calculated from volumetric dynamic computed tomography angiography. *Invest Radiol*. 2010;45(12):778–781. Available at: http://journals.lww.com/investigativeradiology/Abstract/2010/12000/Blood_Velocity_Calculated_From_Volumetric_Dynamic.3.aspx. Accessed April 20, 2015.
98. König M. Diagnosis of acute stroke. In: *Multidetector Computed Tomography in cerebral disease CT Perfusion Imaging.*; 2007:83–.
99. Yushkevich PA, Piven J, Hazlett HC, et al. User-guided 3D active contour segmentation of anatomical structures: Significantly improved efficiency and reliability. *Neuroimage*. 2006;31(3):1116–1128.
100. Atkinson R, Awad I, Batjer H. Reporting terminology for brain arteriovenous malformation clinical and radiographic features for use in clinical trials. *Stroke*. 2001;32:1430–1442. Available at: <http://europepmc.org/abstract/med/11387510>. Accessed August 19, 2015.
101. Hanson KM. Noise and contrast discrimination in computed tomography. In: Newton TH, Potts DG, eds. *Radiology of the Skull and Brain*. Vol 5. 5th ed.; 1981:3941–3955.
102. Easton JD, Saver JL, Albers GW, et al. Definition and evaluation of transient ischemic attack: a scientific statement for healthcare professionals from the American Heart Association/American Stroke Association Stroke Council; Council on Cardiovascular Surgery and Anesthesia; Council on Cardio. *Stroke*. 2009;40(6):2276–93. doi:10.1161/STROKEAHA.108.192218.
103. Sacco RL, Kasner SE, Broderick JP, et al. An updated definition of stroke for the 21st century: a statement for healthcare professionals from the American Heart Association/American Stroke Association. *Stroke*. 2013;44(7):2064–89. doi:10.1161/STR.0b013e318296aeca.
104. Savoiardo M. The vascular territories of the carotid and vertebrobasilar systems. Diagrams based on CT studies of infarcts. *Ital J Neurol Sci*. 1986;7:405–409. Available at: <http://link.springer.com/article/10.1007/BF02283018>. Accessed July 9, 2015.

Appendix

A. Effect of bifurcation in in vivo data

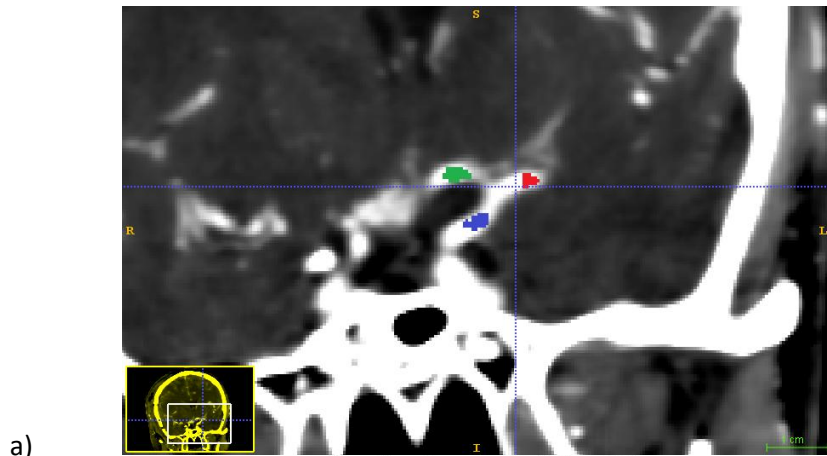
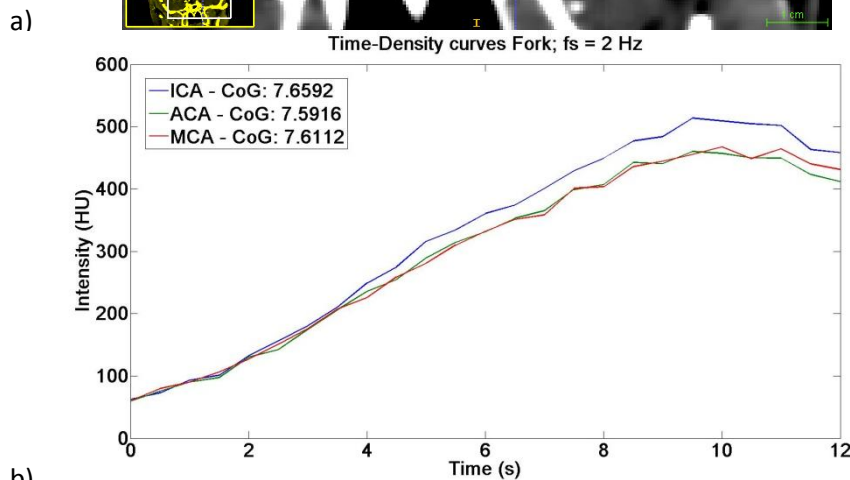


Figure 31 Comparison of TDCs at a bifurcation. In this case the distal end of the left ICA of patient 1 is analyzed. a) The ICA (ROI1; blue) splits up in the left ACA (ROI2; green) and MCA (ROI3; blue). b) TDCs of the ROI at a bifurcation.



b) To study the effect of a bifurcation on TDC amplitude ROIs are selected right before and right after a bifurcation. ROI1 was selected in the ICA, just before it splits in the MCA and the ACA, in which ROI2 and ROI3 are located, respectively (figure 31a). Results were analyzed with both equally sized large ROIs and with single-voxel ROIs. The analyses resulted in comparable TDCs, with a decrease in amplitude for the ROIs located in the bifurcated vessels, as shown in figure 31b. The cause of the decrease is not entirely understood. It seems likely that the intensity of a single voxel in a larger vessel such as the ICA should be the same as in a smaller directly connected vessel such as the ACA, but the current results suggest otherwise. Other possible causes of the amplitude decrease could be the change in CBFv, a change in blood or contrast density, an increase in turbulence and artifacts such as scattering from surrounding voxels, which a larger vessel will experience more.

B. The source of a wiggle in a TDC

In the investigation of the time delay between arterial and venous ROI a remarkable wiggle is present in the TDCs of the venous ROI at time = 24 seconds. The cause of the wiggle becomes clear after principal component analysis (PCA; figure 32). The not-averaged TDCs of the venous ROI show two types of TDCs, one with a wiggle and one without. The origin in the vessel of the alternative curve type can be investigated using PCA. It becomes clear that the wiggle is caused by the TDCs of the medial voxels of the vein, suggesting motion of the vein. Visual inspection of the image data shows indeed motion of both jugular veins at time = 24 seconds. This bilaterally synchronous motion may

be caused by swallowing. Since veins have a higher compliance than arteries, the effects of swallowing and other physiological motions will be mainly present in veins. The main goal of this study is to calculate the CBF in the arteries; therefore it is not expected to experience many troubles with this phenomenon.

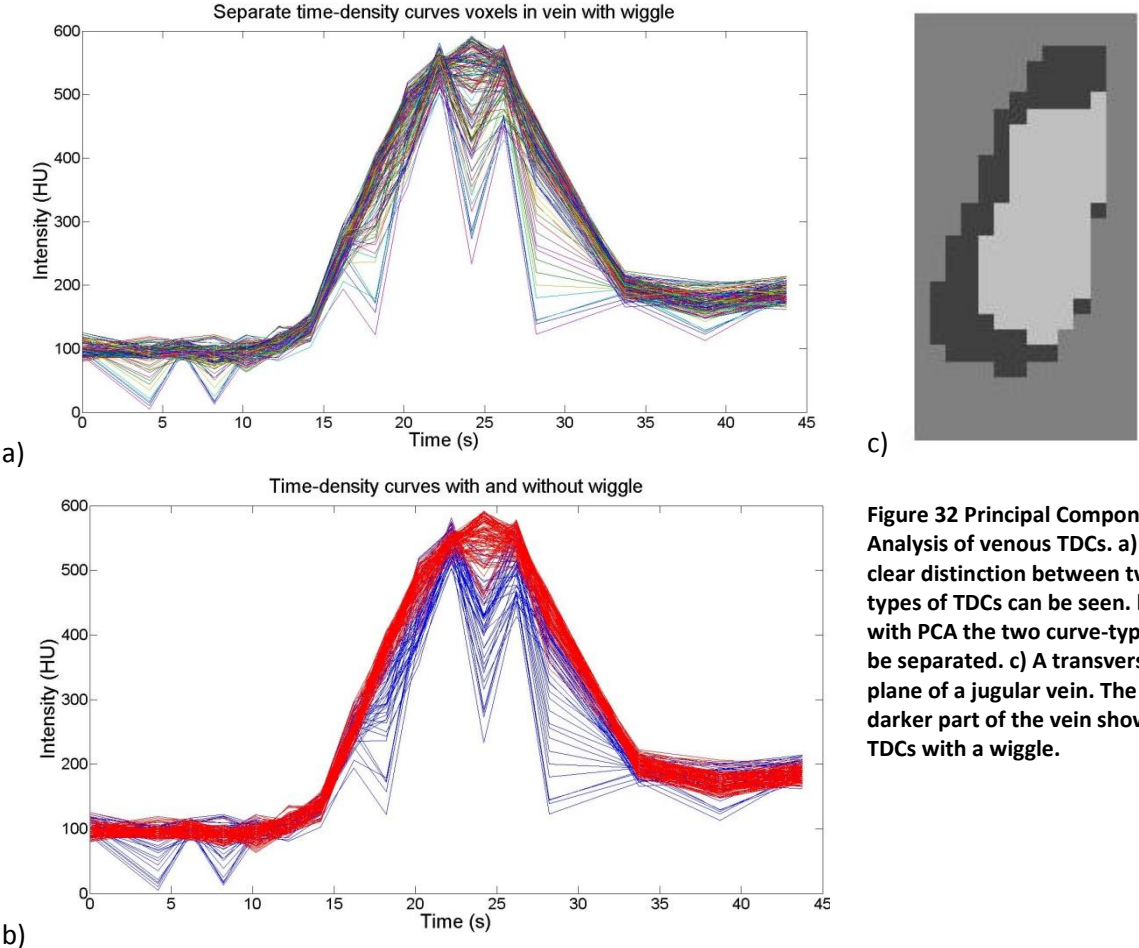


Figure 32 Principal Component Analysis of venous TDCs. a) A clear distinction between two types of TDCs can be seen. b) with PCA the two curve-types can be separated. c) A transverse plane of a jugular vein. The darker part of the vein shows TDCs with a wiggle.

C. ROI sizes

The ROI sizes are presented as the number of voxels included in a ROI in table 21. The ROI in the grey matter were larger than the ROI in white matter for all flow territories. For most flow territories, the ROI in the left hemisphere were larger than the ROI in right hemisphere. Without statistical analysis no clear differences were present between the patient groups.

Table 21. ROI sizes indicating number of voxels included after deletion of vascular pixels. Values are presented as median (IQR). un indicates unaffected side; af, affected side; norm, normal subjects; Tia, transient ischemic attack; Str, ischemic stroke; l, left; r, right and basal g., basal ganglia.

Group	Anterior		Medial		Posterior		Basal g.
	Grey	White	Grey	White	Grey	White	
All l N = 60	1498 (1128-1780)	934 (739-1098)	4430 (3155-5324)	2876 (1982-3433)	1513 (1228-1832)	684 (487-907)	1812 (1339-2229)
All r N = 60	1353 (1036-1673)	895 (718-1063)	4168 (3003-5171)	2925 (2057-3612)	1453 (1073-1715)	669 (467-900)	1803 (1384-2187)
norm l N = 13	1448 (1049-1565)	910 (835-1106)	4427 (3065-5060)	2418 (1991-3323)	1485 (1205-1853)	645 (457-937)	1812 (1563-2145)
norm r N = 13	1427 (1076-1601)	919 (805-1082)	3326 (2604-4993)	2020 (1783-3175)	1326 (1110-1656)	626 (446-860)	1821 (1485-2198)
Tia af N = 6	1209 (922-1558)	757 (624-925)	3667 (3195-5228)	2918 (1547-3842)	1475 (1006-1813)	507 (405-924)	1595 (1251-1958)
Tia un N = 6	1408 (976-1591)	834 (635-1147)	4015 (3034-5634)	2466 (2265-3421)	1517 (1335-1913)	579 (450-929)	1646 (1272-1944)
Str af N = 29	1551 (1245-1758)	895 (732-1078)	4168 (3255-5408)	3012 (2520-3343)	1500 (1214-1677)	665 (475-881)	1828 (1498-2252)
Str un N = 36	1579 (1234-1765)	882 (769-1095)	4622 (3191-5356)	3036 (2663-3592)	1554 (1186-1836)	729 (634-925)	1856 (1269-2268)